UNIVERSITÀ DEGLI STUDI DI PADOVA
DIPARTIMENTO DI INGEGNERIA CIVILE, EDILE E AMBIENTALE
Department Of Civil, Environmental and Architectural Engineering

Master's degree in Environmental Engineering
Soil Protection and Water Management

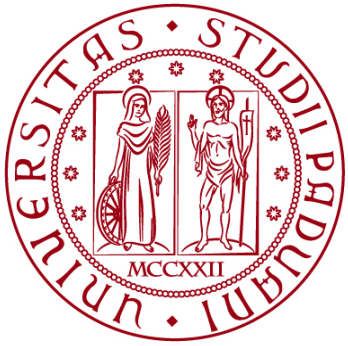

Master's Thesis

Monitoring and management strategies for a Double Arch Dam using FEM modelling: the case study of the Ponte Cola Dam

***Supervisor*:**
Dr. Eng. Ph.D. LORENZO BREZZI

***Candidate*:**
FEDERICO MARCHIORI
n. 2090553

Academic Year 2023-2024

Abstract

Nowadays, the monitoring of large-scale structures is essential to ensure their proper functioning and the public safety. In this thesis, the use and functioning of FEM modeling software will be initially discussed, and later applied to build the model of the Ponte Cola dam, located in the municipality of Gargnano (BS). The effects of the temperature and the levels of filling of the reservoir have on the displacements of the dam are studied, also considering the stability contributions given by the surrounding terrain. Having as a final objective the study of the behavior of the dam, in order to optimize the factors involved in the model for a correct operation in accordance with the environmental variables and the determination of conditions that would lead to the development of critical issues in the structure.

Index

Introduction

In this paper, the preliminary studies and the creation of a Finite Element Model are addressed, allowing to study the complex case of Ponte Cola Dam (BS). The dam, built for hydropower production purposes, is being monitored due to an unexpected increase in piezometric pressure at the base of the dam in 2004, which led to request a lowering of the water level in the reservoir, that has negatively affected the energy production.
The displacements are mainly a function of the water level in the reservoir and of the heat transfer mechanisms between water, air, and the surrounding environment. Thanks to a huge monitoring campaign it was possible to use the necessary data to create a FEM model thanks to the use of the software Midas FEA NX.
The goal of the thesis is to create a model true to reality, that responds correctly both thermally and mechanically, with the final aim to individuate the limit cases that could lead to the development of critical conditions.

The paper is subdivided into five chapters, summarized as follows:

I. The first chapter provides a general overview of the structures for hydropower production, comparing different types of plants and classifying them according to various characteristics.

II. The second chapter describes the Ponte Cola dam, providing a detailed description of the structure in each of its components, describing also the monitoring strategies applied to the structure and the studies conducted in the past.

III. In the third chapter, the Finite Element modelling is introduced, studying the thermal influence on simple domains, such as cubes or parallelepipeds, in order to define the dependence of results on thermal parameters. In the last part of the chapter, a simple model with realistic dimensions, similar to the studied dam, is built in order to give a physical meaning to the results.

IV. The fourth chapter represents the central body of the study, in which the construction of the dam model is described, starting from preliminary elaboration of the data through the use of different software, such as AutoCAD, QGIS and MATLAB, to then use this data in the creation of the Midas model. Once built, the model is calibrated thermally and mechanically, to show, in the end, the best results in terms of temperature and displacements obtained through calibrations.

V. In the fifth and last chapter, the calibrated model is used in the analysis of a critical case, such as the maintenance of a constat high water level in the reservoir for a period of one year. This allows us to identify the critical conditions of the structure and to hypothesize management strategies to limit the displacements.

1. Dams

A dam is defined as an artificial structure that blocks or regulates the flow of a watercourse, protects a stretch of coast or a port, or creates a basin or reservoir for a hydroelectric power plant.

Focusing on retention dams, they can be classified in three main categories:

- Gravity dams: made in concrete and designed to resist overturning and sliding forces by their own weight. In modern construction, the base profile is a triangle with the vertex at the level of the maximum retention, and with a crown superimposed on it, which can be the site of a road. The planimetric layout is preferably rectilinear. Advantages are given by a greater resistance to difficult environmental conditions and the oversizing of the structure, which could be lightened in the central part (Figure 1.1).

Figure 1.1: Gravity dam of Hachisu (Japan)

- Arch dams: made in concrete, exploit the arched structure to redistribute water pressure to the lateral sides of the valley. They require less material, especially at the top, where the acting pressure is lower. To be used, they need more restrictive conditions than gravity dams; the lateral rocky sides must meet compactness, stability and resistance requirements (Figure 1.2).

Figure 1.2: Arch dam of Hoover (USA)

- Earth dams: made with natural materials such as clay, gravel and earth, by adding an impermeable core or lining to prevent the water seepage. Due to the huge necessity of materials, they are built only when the availability does not represent a limitation. The top of the dam cannot be overpassed by water to avoid the erosion of materials and the quick collapse of the dam (Figure 1.3).

Figure 1.3: Earth dam of Arkun (Türkiye)

Detention dams are structures built in a valley gorge with the purpose of creating a basin by constructing a barrage. Strategic management and sustainability are two of the most important topics. They are used for hydropower production, irrigation of agricultural fields and as freshwater reservoir. Acting as storage, a dam is able to store water during rainy periods and release it gradually over time, mitigating the possible flood events downstream of the dam. The last application highlights the sustainability concept, due to the fact that the variabilities in flow rate are completely different when comparing natural and human regulation, following a cyclic pattern that reflects the typical human habits and the economic interests (Figure1.4).

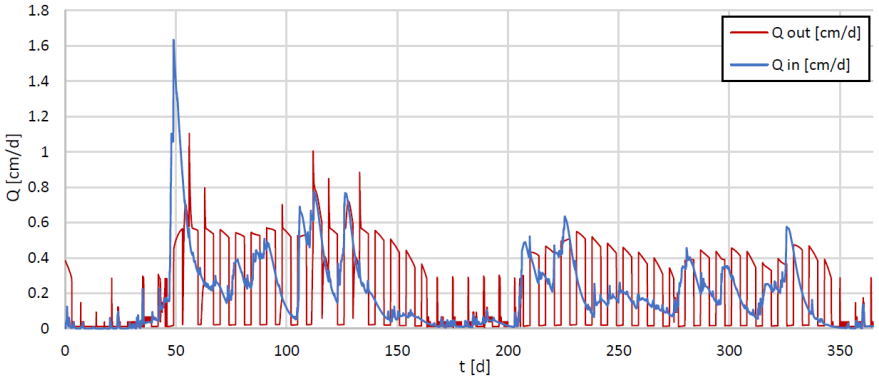

Figure 1.4.: Simulated comparison between natural and regulated discharge

Stored water can also infiltrate into the ground and contribute to the recharge of groundwater, maintaining groundwater levels and providing a source for wells and springs.

The Italian Legislation classifies dams according to the height of the structure or a certain storage capacity. Starting from the 1994, with " *Decreto Legge 8 Agosto 1994, n. 507* ", dams are described as those structures that exceed 15 *m* in height (between the level of the crowning plane and that of the most depressed point of the facings) or with a storage capacity higher than 1.000.000 m^3 (capacity of the tank between the highest level of the overflow thresholds, or the top of any gates, and the level of the most depressed point of the upstream face). Structures classified under these categories are subjected to more stringent measures to protect the population, especially those residing downstream of the dam, as well as the surrounding environment. Structures that do not fall into this classification are defined as barrages and are used only as storage for deposits or for industrial residue washing.

The construction of the dam is usually done downstream of a flat portion of valley and where the two sides of the valley become closer, in order to reduce the length of the dam and create a V-shape valley groove. To perform the evaluation of the construction, various aspects must be studied: from the stability point of view, topography plays a crucial role in determining the best location to build the dam. Geological tests provide information about the soil's nature and geotechnical stability. Hydrology is fundamental to categorize

maximum flow, floods, sedimentation and water quality. Additionally, climatic characteristics that can influence the processes in the reservoir's mass balance, such as evapotranspiration, must be considered when evaluating a possible construction of the dam.

1.1. Hydropower Plants

From a global point of view, hydropower is the largest single source of renewable energy, and pumped storage hydropower provides more than 90% of all stored energy in the world. It plays a crucial role in the renewable sector, being flexible and allowing the production of energy when other sources, such as sun or wind, are not available. Looking at the different sources of energy, the use of coal in the last years has decreased in US and China but is increasing in the rest of the world. Actually, China has become the world leader in hydropower production with an installed capacity of $\approx 250\ GW$.

Hydropower plants are usually associated with the presence of a dam, through which they convert the potential, pressure and kinetic energy of the water into mechanical energy and then into electric power.
The process on which hydropower production is based relies on the movement of the water from higher to lower potential energy levels. First of all, the water is stored in the reservoir through the presence of the dam, which works as a barrage. When energy production is required, the spillways are opened, allowing the water to flow towards the turbines.

The production is proportional to the head (the difference between upstream and downstream specific energy) and to the flow rate processed by the plant. Efficiency plays a crucial role and in case of hydropower plants, can be considered as the product of three specific efficiencies:

- Pipe efficiency η_p (0.90 – 0.95), it takes into account distributed and local energy losses along pipes (function of the velocity and type of tube);

- Turbine efficiency η_T (0.80 – 0.90), internal efficiency of the turbine in turning the hydraulic energy into mechanical energy;
- Intrinsic efficiency η_O (~ 1), it takes into account losses due to power unit, auxiliary plants maintenance.

Hydropower plants can be classified into small, medium and large plants according to:

	Small Plants	Medium Plants	Large Plants
Streamflow *[m^3/s]*	< 10	10 – 100	>100
Head *[m]*	< 50	50 – 250	>250
Power *[MW]*	< 5	5 – 200	>200

Table 1.1.1: Hydropower Plants classification.

2. Case Study

2.1. Reservoir Description

The dam studied in this work is the Ponte Cola dam, situated in the valley of the Toscolano stream in the locality of S. Maria di Valvestino (BS), 9 *km* from its outlet into Lake Garda. The dam was built with the aim of regulating the storable energy in the Toscolano and S. Michele streams, with a pumping system from Lake Garda, during night and weekend days, capable of generating a capacity of $45 \cdot 10^6$ *kWh*.

Valvestino dam was constructed between 1962 and 1966, taking approximately four years to complete. Currently, the dam is managed by Enel Green Power, a company that is part of the Enel Group and specializes in renewable energy sources, including hydroelectric infrastructures.

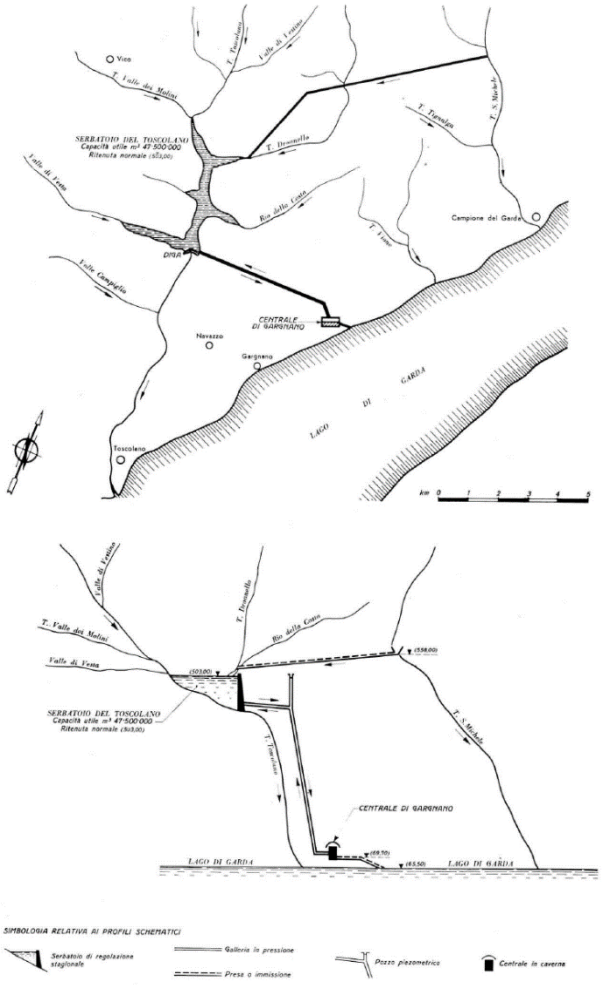

Figure 2.1: Hydroelectric plants of Sarca-Mincio.

The following section lists the main data relating to the reservoir:

Normal water level	503.00 *m a.s.l.*
Maximum water level	504.00 *m a.s.l.*
Minimum normal water level	438.00 *m a.s.l.*

Storage Capacity:

Total	52.25 *M cu. m*
Effective	47.50 *M cu. m*

Catchment Area:

Natural	97.25 *sq. km*
Diverted (S. Michele Torrent)	24.58 *sq. km*
Total	121.83 *sq. km*

2.2. Dam Characteristics

The dam is a double-curvature arch standing on pulvinus and foundation plug, with a symmetrical structure in respect of the centerline vertical plane, coinciding with the plane of the arch curvature centers.

Main geometric data:

Height of the crest (at El. 505):	
above lowest point of plug	124.00 *m*
above downstream riverbed	115.00 *m*
Free height of the crest:	
above normal water level	2.00 *m*
above maximum water level	1.00 *m*
Length of crest at extrados	282.45 *m*
Chord of crest at extrados	246.00 *m*
Horizontal radius:	
crest arch at El. 505 (intrados)	161.507 *m*
crest arch at El. 505 (extrados)	164.907 *m*
arch at El. 390 (intrados)	38.629 *m*
arch at El. 390 (extrados)	62.268 *m*
Thickness at crown:	
on top, at El. 505	3.40 *m*
at base, at El. 390	23.64 *m*
Dam foundation excavation	106.000 *cu. M*
Concrete volume of dam (equal to 1 cu. m of pour per 198 cu. m of effective storage)	239.000 *cu. m*
Steel reinforcement for dam (equal to 2.9 Kg/cu. m of concrete poured)	688.000 *kg*

The dam is placed in the gorge, along the cradle-shaped surface of the perimetral joint, by means of a foundation pad, which is 6 *m* thick in the upper section and increases to 11.5 *m* in the lower part. A continuous perimetral gallery runs along the whole pulvinus.

The latter rests, in its turn, on a foundation plug, deeply built into the rock, through a second continuous perimetral joint, built by separating the pours with sheets of paper and designed further to reduce the torsional stresses transmitted to the foundation plug by the underlying curved plate.

The structure is subdivided by radial joints into 21 blocks, 12 *m* long at the extrados. The radial and perimetral joints were partially grouted in the lower part after shrinkage. The dam is made of concrete with 250 *kg* of cement per *cu. m*; faces and pulvinus are provided with a light reinforcement to absorb surface stresses, there is also reinforcing armature at the pulvinus support base.

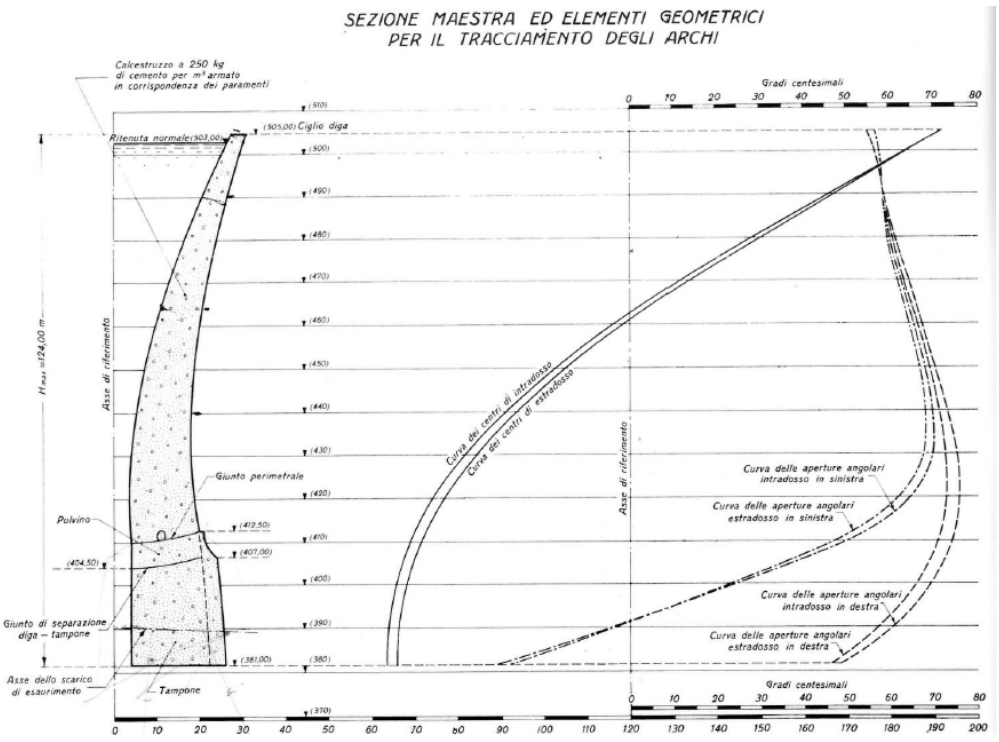

Figure 2.2.1: Master section and geometric elements for tracing the arches.

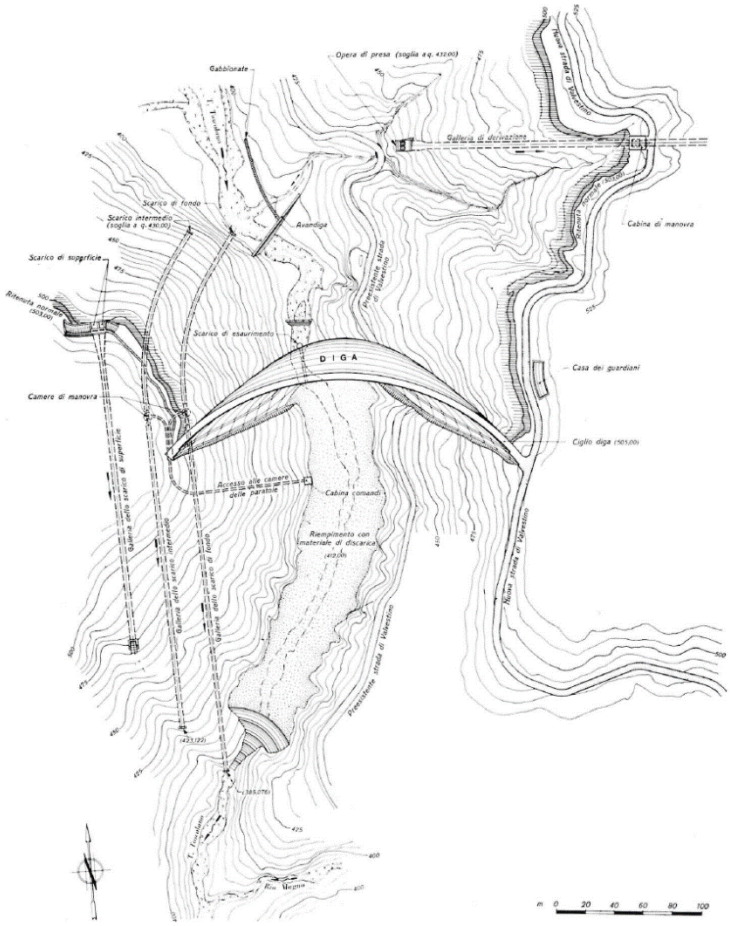

Figure 2.2.2: General plan of the valley with contour lines;
works constituting the hydroelectric plant and their positioning

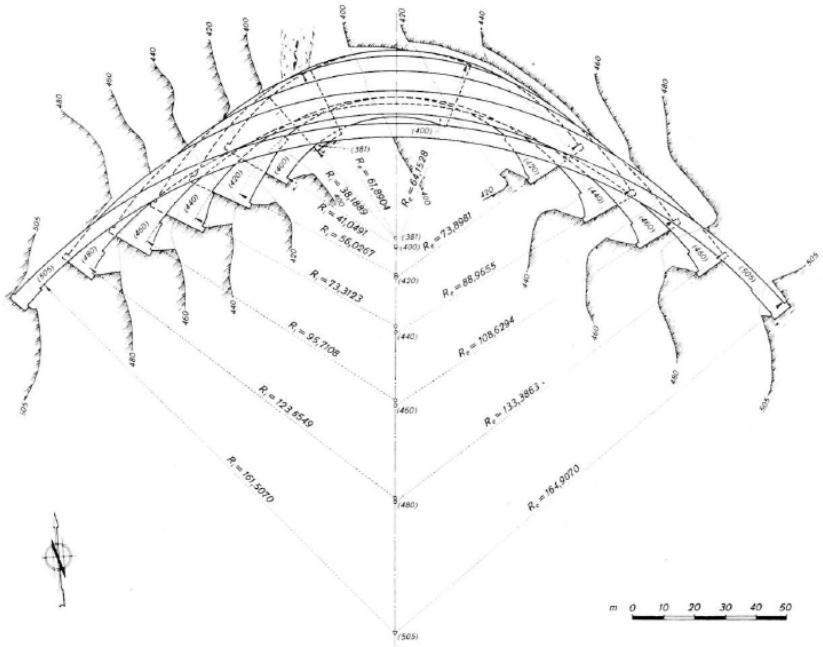

Figure 2.2.3: Superimposed arch plan.

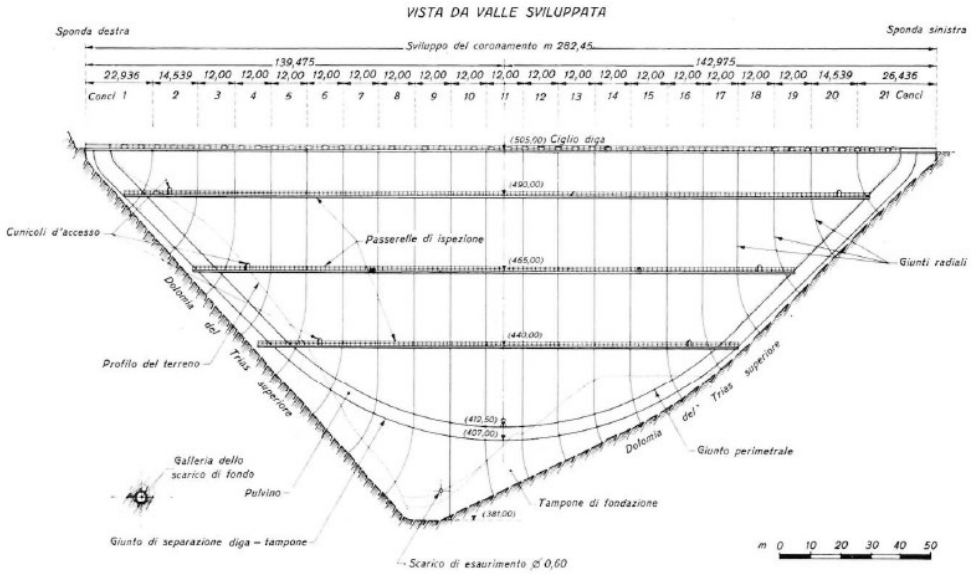

Figure 2.2.4: Valley view developed by the arches.

2.3. Concrete mixture

The concrete mixture used for the construction of the dam was made with aggregates extracted from a specially cultivated stepped quarry located on the right bank of the Toscolano stream, about 4 *km* upstream from the dam. The quarry consisted of a large wall of compact limestone, with an average specific weight of 2850 kg/m^3 and an average absorption coefficient of 0.34%. The cement used had a strength of 600 kg/m^3 for normal dam concrete and contained an active Roman pozzolana content between 40% and 50%, with a heat of hydration below 65 *cal/g* of cement (after 20 days of curing in a calorimeter).

The concrete made had an average setting time ranging between 2 hours 35 minutes and 5 hours 30 minutes, with average compressive strengths after 7 and 28 days of curing of 502.6 kg/cm^2 and 687 kg/cm^2, respectively. The average tensile strengths at the same intervals were 30.8 kg/cm^2 and *39* kg/cm^2, determined through 7800 laboratory tests. The aggregate gradation was designed according to a cubic curve, with a maximum diameter of 75 *mm*, and no additives were used. The water-to-cement ratio was 0.5, with a consistent cement dosage of 250 kg/m^3 and mixing times in the concrete mixer lasting 2 hours and 30 minutes. The composition of the concrete was progressively adjusted

according to the performance characteristics of the mixes, as indicated in the following table:

Components	Dimensions [*mm*]	From 18/5/61 to 30/10/61 [kg/m^3]	From 30/10/61 to the end [kg/m^3]
Cements	0 ÷ 0.2	250	250
Sand	0 ÷ 4	700	682
Small Gravel	4 ÷ 15	440	546
Gravel	15 ÷ 45	590	609
Gravel	45 ÷ 75	465	388
Total Solid Part	--	2445	2475
Water (A/C = 0.5)	--	125	125
Weight of Concrete [kg/m^3]		2570	2600

Table 2.3.1: Concrete composition.

For the concrete used in the dam, the average specific weight was found to be 2580 kg/m^3. The permeability coefficient K, evaluated using Darcy's law, ranges between 0 and 1, and the elastic modulus E is 300000 kg/cm^2. The concrete also exhibits the following average compressive strength characteristics:

Time *[days]*	7	28	90	180	360
Elastic Modulus $[kg/cm^3]$	215	345	406	429	431

Table 2.3.2: Resistance to Compression.

Periodic control tests conducted at official laboratories consistently provided values slightly higher than the average values mentioned above. The concrete pours were carried out in staggered sections using metal formwork, with a maximum of three 50 *cm* layers per day. The concrete was carefully vibrated using 140 *mm* diameter vibrators operating at a frequency of 12000 vibrations per minute. The formwork was removed 48 hours after the completion of the pours.

2.4. Structural components of the dam

The structure is equipped with a surface spillway, a drain outlet and two deep spillways situated at different elevations and independent of each other.

The surface spillway is located on the right bank of the reservoir, outside the dam body and consists of a reinforced concrete structure containing two sluices with inlet at 499 *m a.s.l.*. The opening is controlled by sluice gates with simultaneous oil-pressure and emergency manual operation, gates can be overflowed for a maximum height of 1 *m*. It connects at its terminal part to a polycentric section tunnel operating at free surface with radius $r = 3.90$ *m* and bottom slope $i = 5\ \%$.

The intermediate outlet is located on the right bank of the reservoir and consists of a circular section, of dimensions 130.63 *m* long and 2.50 *m* in diameter, arched in plan and with 2% gradient in the section upstream of the gates. The second part is made by a tunnel 218.25 *m* long and 2.60 *m* in diameter, with the same gradient of before. The tunnel inlet is at an elevation of 430 *m a.s.l.* and is controlled by two $1.60 \cdot 2.30$ *m* slide gates in series, operated by an independent oil-pressure servomotor and manually in case of emergency.

The bottom outlet is also located on the right bank of the reservoir and consists of a 2.00 *m* of diameter and 132.77 *m* long circular section tunnel, arched in plan with 2% gradient in the stretch upstream of the gates. The inlet is at an elevation of 392.50 *m a.s.l.*. At 132.77 *m* from the inlet, the tunnel is controlled by two $1.40 \cdot 2.00$ *m* slide-gates, operated by an independent oil-pressure device and manually at site in case of emergency.

The drain outlet consists of two steel pipe segments, each with a diameter of 0.80 *m*, positioned at an elevation of 390.30 *m a.s.l.*. The first segment is controlled by an upstream slide gate, operated from a deck extending over the upstream face. This pipe leads into a chamber at the base of a control and aeration shaft, where it is sealed with a plug. The second segment is closed upstream by a sluice gate, operated from a gallery within the dam structure at an elevation of 402.50 *m a.s.l.*, and it discharges into the Toscolano Torrent.

In the following Table are summarized the different discharge capacities of each part of the dam (referred to a maximum water level of 504 *m a.s.l.*):

Spillway	192 m^3/sec
Intermediate Outlet	113 m^3/sec
Bottom Outlet	106 m^3/sec
Total	411 m^3/sec
Per sq. km of natural drainage Area	4.22 m^3/sec

Table 2.4: Spillways and outlets discharge capacities.

The maximum exceptional flood flow coming into the reservoir has been evaluated in 300 m^3/sec, equal to 3.14 m^3/sec *per sq. km.*. This can be discharged with exceptional rise of storage level by 1 *m* (at the elevation of 504 *m a.s.l.*) through the spillway and intermediate outlet, without taking into account the effect of flattening of wave flood in the reservoir, which corresponds to a flow of 50 m^3/sec, and of the bottom outlet.

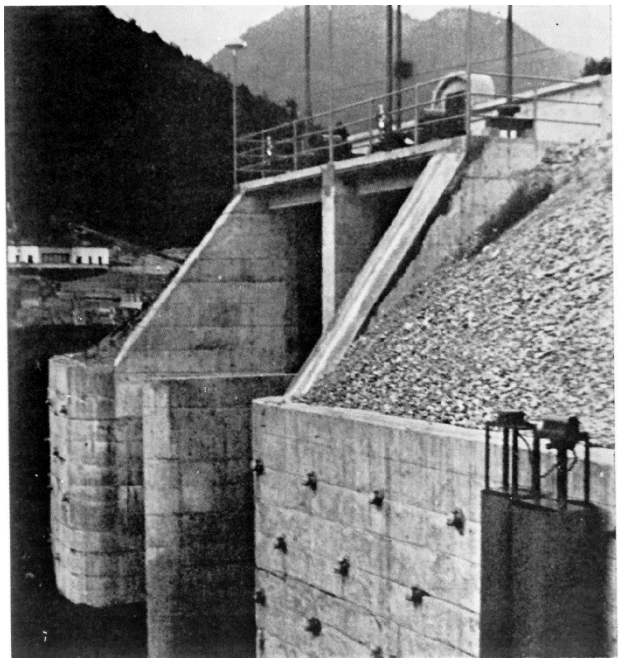

Figure 2.4.1: Spillway inlet.

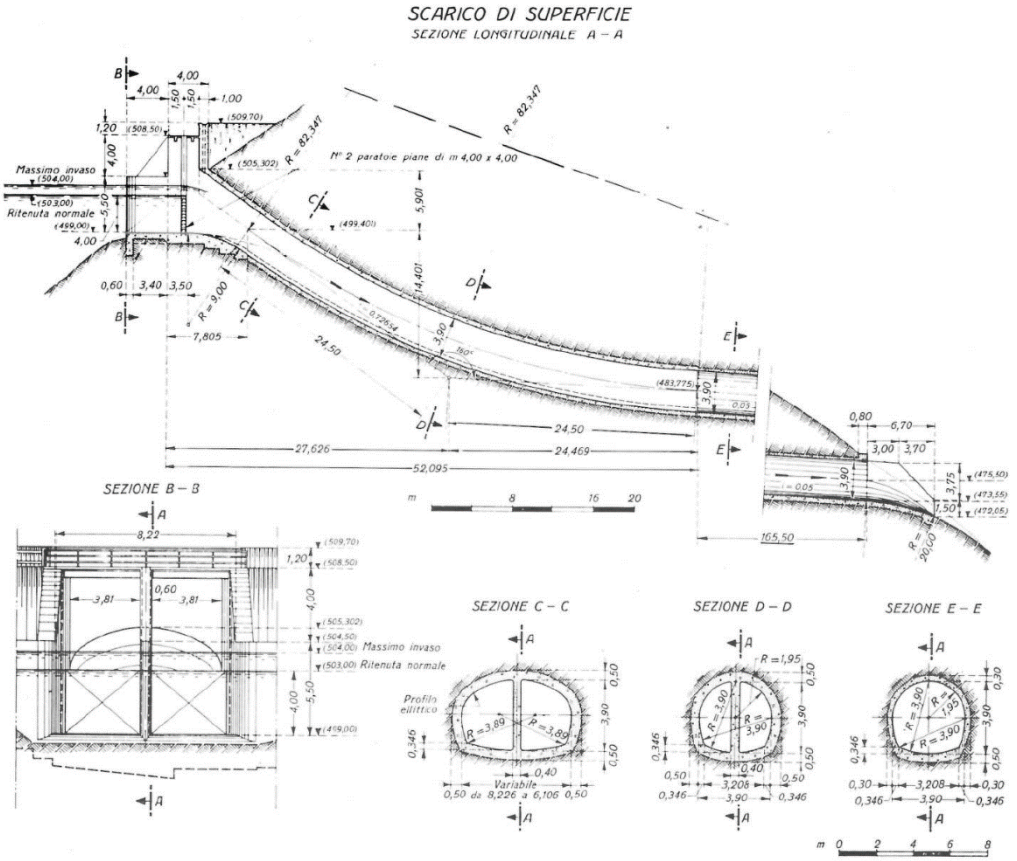

Figure 2.4.2: Surface spillway.

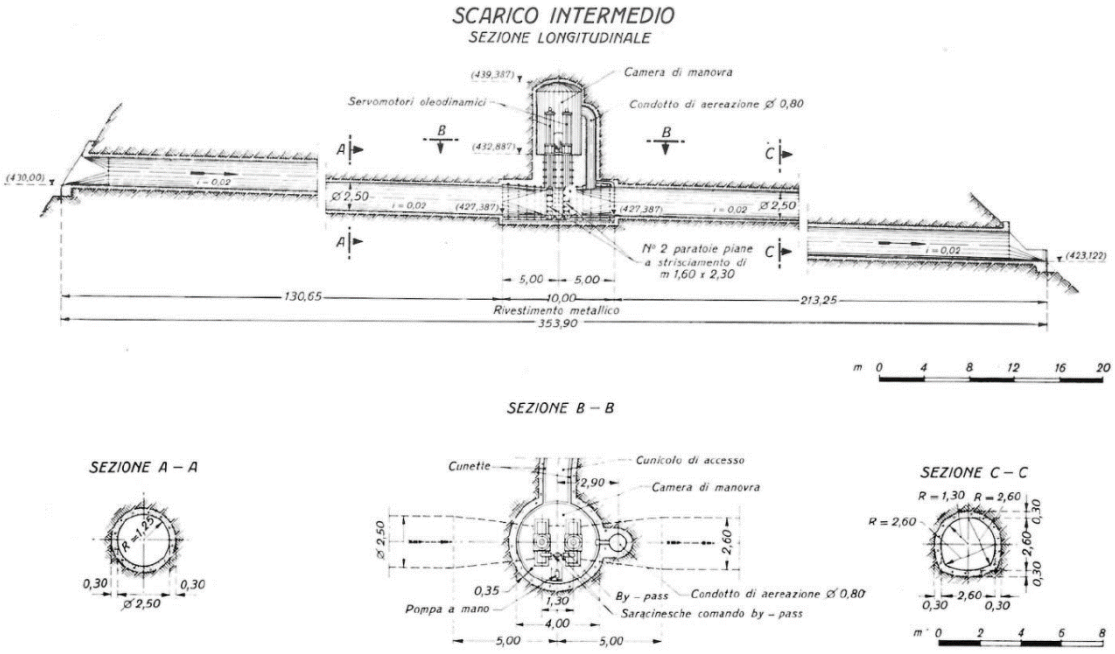

Figure 2.4.3: Intermediate spillway.

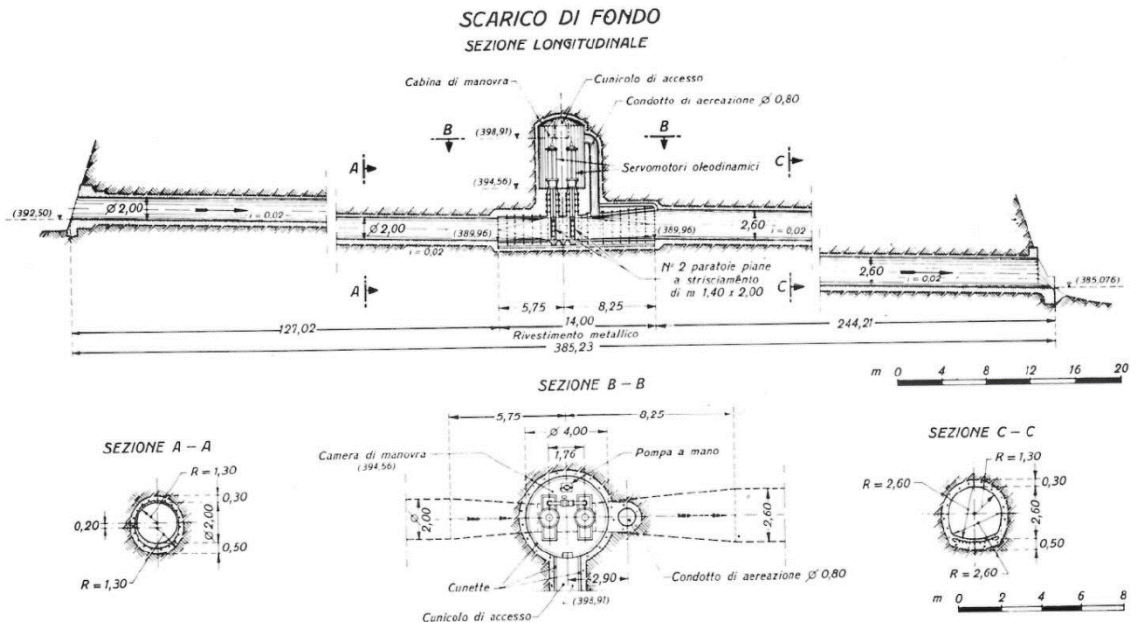

Figure 2.4.4: Deep spillway.

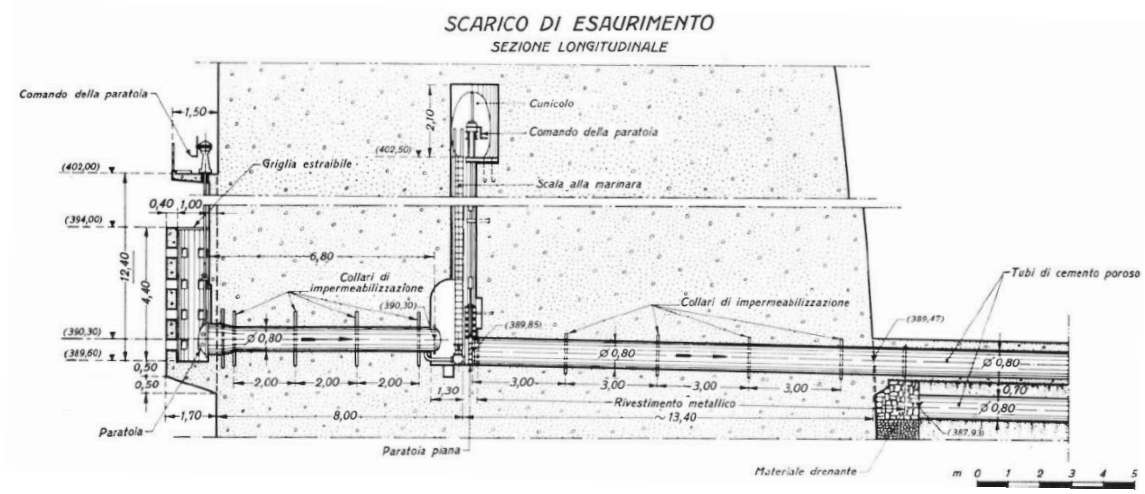

Figure 2.4.5: Drain outlet.

The intake structure is located on the left bank of the reservoir and is separated from the main dam body. It consists of a reinforced concrete entrance and a tapered section that connects to the circular section of the diversion tunnel, which has a diameter of 4.20 *m*. The entrance is positioned with its threshold at an elevation of 432 *m a.s.l.* and is equipped with a flat metal grid measuring 6.20 *m* by 10.00 *m*.

The tapered section extends for a length of 23.87 *m*. At a distance of 166.72 *m* from the entrance, a sluice gate is installed with a clear opening of 3.00 *m* by 4.20 *m* and a threshold at an elevation of 431.86 *m a.s.l.*. This sluice gate is a roller type, operated by a hydraulic actuator controlled directly on-site from an operating cabin located at an elevation of 514.10 *m a.s.l.*. The cabin houses an electric pump for the hydraulic actuator and a hand-operated auxiliary pump for emergency use. The sluice gate is equipped with upstream and downstream metallic connections, each with a 4.20 *m* section of the diversion tunnel. The downstream connection includes a vertical metallic ventilation pipe with a diameter of 0.80 *m* that vents directly to the outside to prevent water hammer effects.

During the construction of the dam, the Toscolano Torrent was blocked by a cofferdam with a crest elevation of 397.50 *m a.s.l.*, diverting the torrent's waters into the bottom outlet tunnel. Under these conditions, the tunnel was capable of handling a flow rate of 20 m^3/s, more than sufficient to manage the waters under normal seasonal conditions.

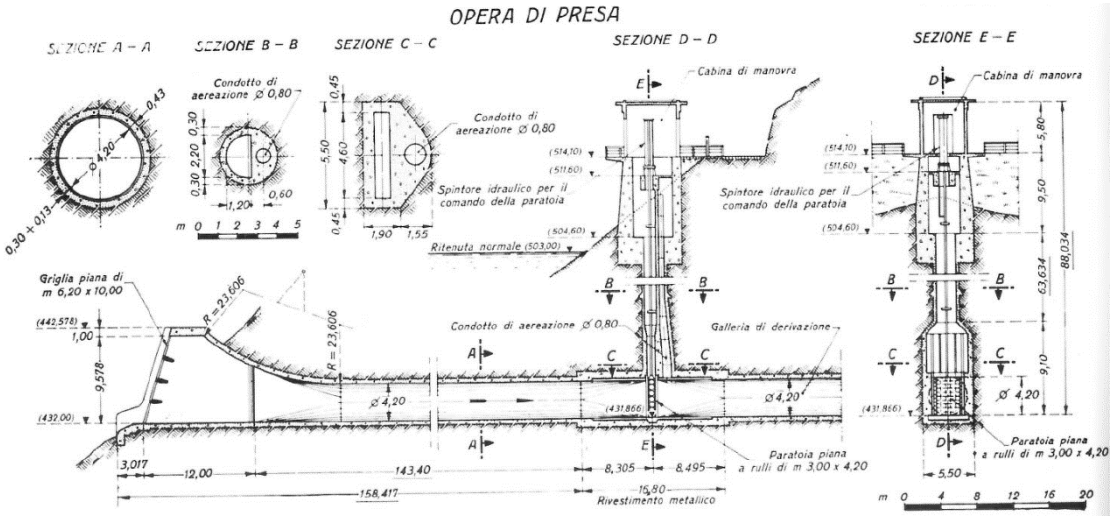

Figure 2.4.6: Intake structure.

2.5. Site Analysis and Geological Stratigraphy

2.5.1. July 1975 results

In July 1975, a study was conducted to analyze the mechanical properties of the dam's foundation rock and to assess the structure's performance during the flood that occurred in 1974. The research stated that the dolomitic formation, which serves as the foundation rock for the dam and significantly influences its behavior, is characterized by intense fracturing. At greater depths, these fractures are tightly closed, resulting in rock properties that can be deemed satisfactory, exhibiting high strength, low deformability, and low permeability. Along the slopes of the valley incision, the rock near the surface is observed to be loosened and decompressed, with the thickness of this loosened zone appearing to increase with elevation. It is considered that the rocks underlying the dolomitic formation do not exert a significant influence on the structure's behavior, as they possess favorable in-situ characteristics.

Foundation Rocks			
In Situ Elastic Modulus *[kg/cm²]*	Surface		Near the crown
	100 - 150		20 - 30
Extensometer – Math. Elastic Modulus *[kg/cm²]*	at 440 *m a.s.l.*	at 465 *m a.s.l.*	25
	60	45	

Table 2.5.1.1: Elastic Modulus values from 1975's research.

During the 1974 -1975 reservoir filling cycles, the rock extensometers exhibited behavior typical of a fractured rock mass: the displacement-reservoir level curves describe closed loops with a noticeable hysteresis area but without any residual permanent deformations.

In 2001 a study was carried out relating to a numerical and experimental modal analysis, with the aim of describing the modal characteristics and own ways of vibrating.

2.5.2. 2009 Geological – Geotechnical analysis

During the 2008-2009 period, an extensive campaign of in-situ and laboratory investigations was conducted to update the geological, hydrogeological and geotechnical characterization and to deepen the understanding of the area at the base and downstream of the dam, particularly to identify, based on objective data, any potential uplift pressures in the downstream area of the dam's foundation.

This enhanced understanding of the hydrogeological conditions at the base and immediately downstream of the dam became necessary following an event in 2004. This event revealed unexpected conditions of hydraulic load at the base of the dam, correlated with the reservoir level and thermal phenomena, when the reservoir reached its maximum level of 500 *m a.s.l.*.

Specifically, when the reservoir, after years of management at generally higher levels compared to the previous period, reached its peak level of 500.04 *m a.s.l.*, the piezometric instruments at the base of the central cantilever of the dam (SP2 piezometers) recorded a significant rise in piezometric levels. This rise, which was already detected at the beginning of the annual measurements (April 2004), prior to the start of the filling phases, persisted until the reservoir level reached 500.04 *m a.s.l.* (August 9, 2004).

The on-site investigations consisted of the following activities:

- Verification of instruments within the dam body through televised inspections;
- Execution of direct boreholes immediately downstream of the dam, including:
    - Lugeon tests;
    - Sampling of materials encountered;
    - Installation of piezometers to monitor piezometric pressure above and below the thrust fault separating the Dolomia Principale formation from the underlying Scaglia Rossa formation (refer to the geological section B-B' along the valley axis in Table 3). The piezometers were located approximately 12 to 55 *m* from the downstream face of the dam;

- Specific boreholes included:
  - 3 continuous core boreholes (S1/08-DH, S2/08-DH, S3/08-DH), where "down-hole" tests were conducted;
  - 3 non-core boreholes (S1/08-PZ2, S2/08-PZ1, S3/08-PZ2) with open-tube piezometers installed to monitor piezometric levels within the Dolomia Principale;
  - 2 non-core boreholes (S1/08-PZ1, S3/08-PZ1) with open-tube piezometers installed to monitor piezometric levels within the Scaglia Rossa;
  - 1 non-core borehole (S3/08-CH) for "cross-hole" testing.
- Topographic survey of the tunnels on both the right and left banks;
- Execution of indirect geophysical investigations:
  - Within boreholes, using "down-hole," "cross-hole," and sonic coring tests;
  - Along the valley axis (downstream of the dam) using surface seismic and geoelectric surveys;
  - Along the dam's foundation (transversely to the valley axis) using surface and tunnel seismic surveys and sonic tomography between pairs of tunnels.

In the following Tables are summarized all the stratigraphy results.

	From *[m]*	To *[m]*	Description
S1/08-DH	0	9.4	Alluvial material (gravel, sand, with calcareous and sometimes silty presence)
	9.4	37.5	Dolomites, moderately to intensely fractured
	37.5	48.4	Calcareous breccia, moderately to intensely fractured
**	46.5	47.1	Marly-argillaceous layer
	48.4	81.8	Compact or slightly fractured calcareous marl

	From *[m]*	To *[m]*	Description
S2/08-DH	0	7.2	Alluvial material (gravel, sand, with calcareous and sometimes silty presence)
	7.2	34.1	Dolomites, moderately to intensely fractured
	34.1	46	Calcareous breccia, moderately fractured
**	45.3	45.7	Argillaceous layer
	46	82	Slightly fractured calcareous marl

	From *[m]*	To *[m]*	Description
S3/08-DH	0	6.1	Alluvial material (gravel, sand, calcareous and sometimes silty presence)
	6.1	28.2	Intensely fractured dolomite
	28.2	40.1	Intensely fractured calcareous breccia
**	38.15	39.2	Argillitic level
	40.1	81.3	Partially fractured calcareous marl

Table 2.5.2.1: Stratigraphy from boreholes analysis.

In particular, these data are not used in the study of the dam, since they represent points located downstream and do not represent the stability contribution from the interaction between rock and pulvinus.

2.6. Monitoring Data

The Ponte Cola Dam is equipped with monitoring systems that are essential for continuously assessing the safety and conservation status of the dam. The dam is equipped with several monitoring devices that allow for the constant detection of structural and environmental data, including temperature, displacements, water flows and pressures, basin level and movements of adjacent areas.
Some of the monitoring devices were installed when the design and monitoring of dams was still based on a set of national and international regulations, founded on past experiences, civil engineering studies and concepts learned from significant accidents.
The monitoring systems used initially were installed during construction or shortly after the completion of the dam. Some, such as the thermometers, automatically transmit information to a control unit located in the keeper's house, others, such as the strain gauges, are manually detected at regular intervals by personnel in charge of monitoring.

From the official documents about the construction and description of the dam, can be found the following monitoring systems:

- Temperature: for measuring temperatures in air, water and concrete are installed 10 thermometers in the downstream side, 4 thermometers in the upstream side and 18 thermometers inside the concrete (with a measuring range - 30 °*C* and + 60 °*C*);

- Elastic deformations: are measured using 65 removable strain gauges, 29 tele-extensometers and 124 thermo-strain gauges, of which 61 downstream and 63 upstream;

- Global displacements and rotations: displacements are detected by 5 collimation stations through the collimation of 3 targets placed on the dam crest. The rotations are monitored using clinometers (10 clinometers bases on the downstream face) and 22 clinometers bases in the access galleries, the latter were installed in 1966.

In 2020, ENEL decided to install a new dam control system, consisting of new sensors capable of autonomously measuring the desired parameters. The system consists of 5 long-base strain gauges starting from a niche created in the dam body, just above the pulvinus. The 5 instruments pass through the foundation of the dam and the various layers of the underlying soil, with the aim of identifying the individual displacements of each component.

In the same period, a new dam control system has been installed in collaboration with the ICEA department of the University of Padua, and in particular fiber optic sensors able to increase the acquirable measurements, improving at the same time both precision and velocity in acquiring data. For technical characteristics of the optical fiber, two different types of optic fibers were used, one to measure the deformations and one to measure the temperature. The thermal sensing fiber is not very sensitive to mechanical stresses and is crucial to understanding the behavior of the structure. It also allows to understand the thermal effects on the fiber, isolating and correcting the deformation component caused only by thermal variations, guaranteeing that the deformation measurements are not influenced by thermal changes. The optical fiber used to measure the strain, is built in order to deform according to the structure at which is constrained.

Both types of fibers are installed at two different locations: one in a niche, where the fibers are placed parallel to the extensometers, reaching a depth of 90 *m*, and the other along the crest of the dam at an elevation of 503 *m a.s.l.*.

In 2020, ENEL installed an automatic displacement measurement system for the downstream face of the dam using a total station. The topographic measurements focus on 19 targets located on the downstream side, distributed as follows: 7 targets at the crest, at an elevation of 505 *m a.s.l.*, 4 targets at 490 *m a.s.l.*, 4 targets at 456 *m a.s.l.*, 3 targets at 440 *m a.s.l.*, and the final target at 410 *m a.s.l.*.

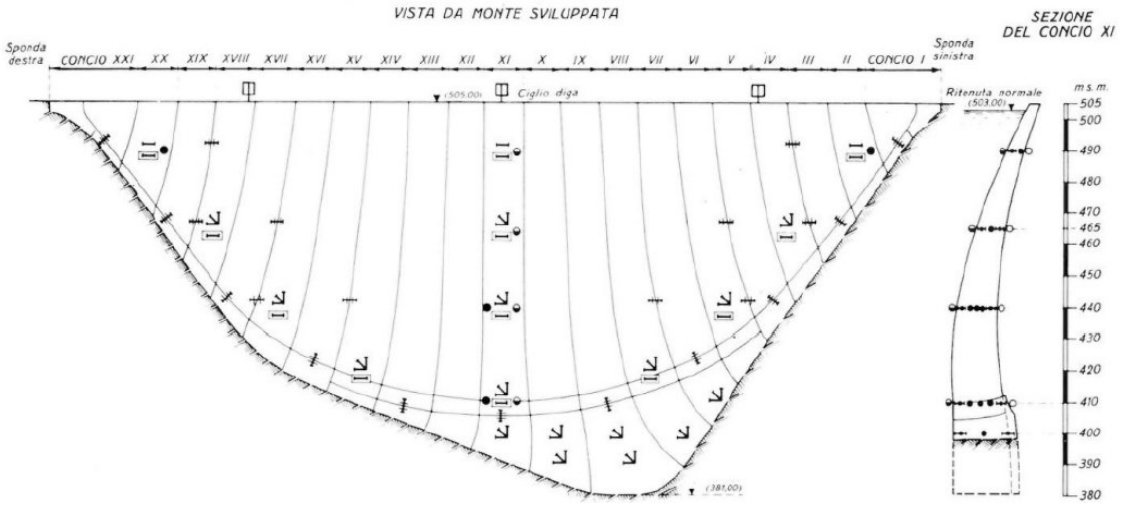

Figure 2.6.1: Monitoring instruments upstream side

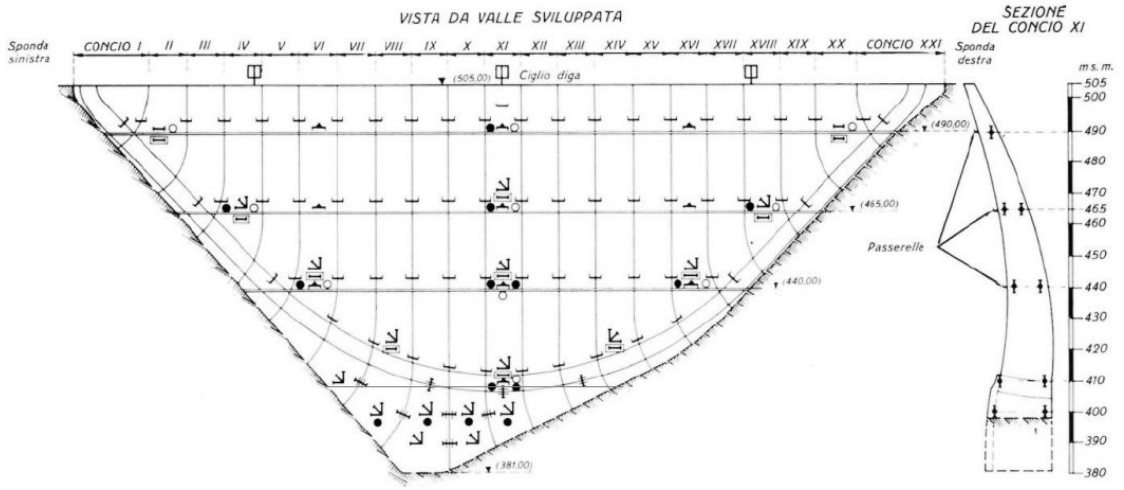

Figure 2.6.2: Monitoring instruments downstream side

These interests regarding monitoring derive from what happened in 2004 when, due to factors related to water levels and climatic conditions, unexpected conditions regarding the hydraulic load at the base of the dam occurred. In particular, after several years in which the level in the reservoir has been maintained higher on average than the past period. The level increased reaching the maximum level allowed of 500.04 m a.s.l., causing a piezometric increment at the base of the central shelf of the dam and registered by piezometer SP2.

This event must still consider that:

- Since 2004 decreases in a significant way the difference between the upstream piezometric level (SP2-4) and the one downstream (SP2-1). In the period following 2004, the negative pressures at the base of the dam recover, after some time, to a triangular distribution.
- For several years before 2004, there has been a trend of rising piezometric levels at the base of the dam, leading to a gradual reduction in the difference between these levels and the reservoir elevation. This trend may also be correlated with the increase in the average operating level of the reservoir.

In the following figures are shown the behavior of temperatures of concrete at an altitude of 440 *m a.s.l.* and *490 m a.s.l.* compared with the level of the water in the reservoir and the behavior of water and air temperatures in the year 2021.

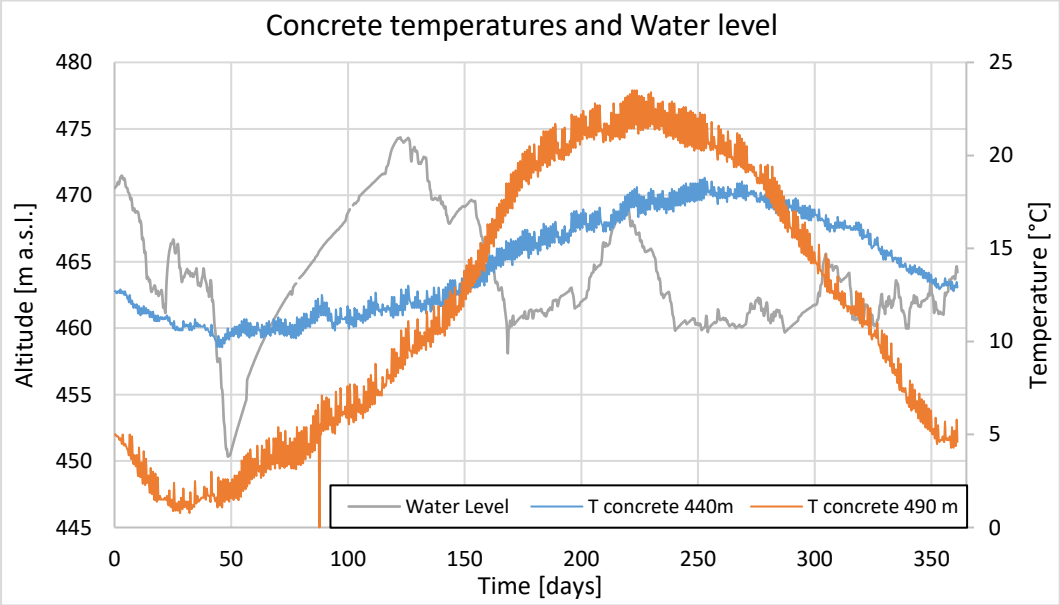

Figure 2.6.2: Concrete temperatures and water level

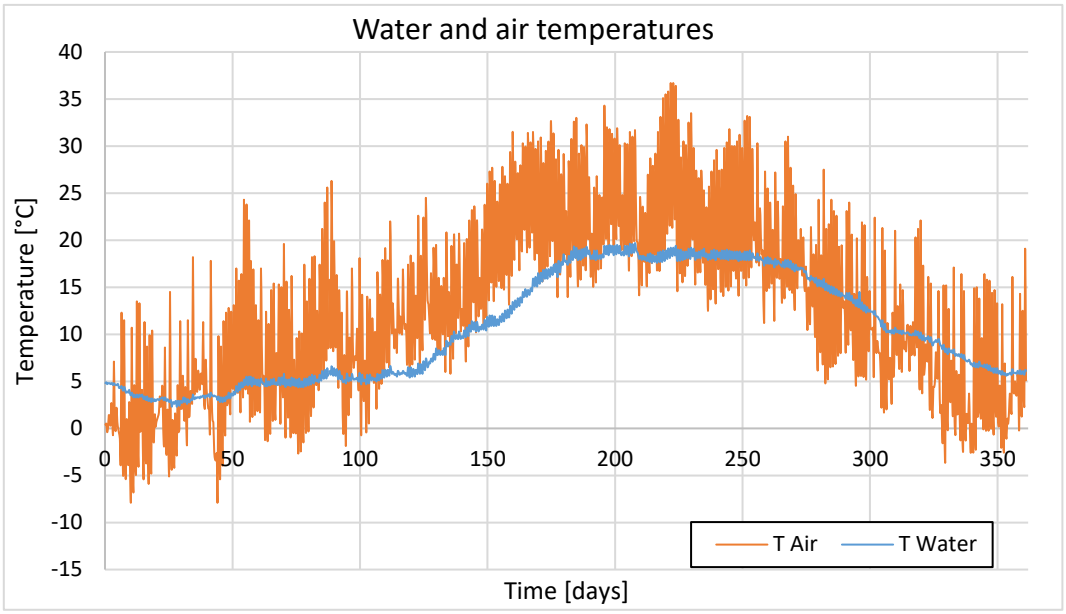

Figure 2.6.3: Water and air temperatures

3. FEM Modelling

3.1. Basic principles in FEM modelling

The Finite Element Model is a specific type of Numerical Approach used to solve multiple PDEs (Partial Differential Equations). This approach is based on the discretization of the original domain into small sub-domains defined as “elements”, replacing the original function with simpler functions. The process allows us to transform the original PDE into a system of algebraic linear or non-linear equations, which can then be solved from a numerical point of view.

Using this method, we have different advantages, one of which is the ability to calibrate the model using measurement data (temperature, water level, etc.) by applying these as boundary conditions, with the final aim of matching the model’s results as closely as possible to the real ones.

The software used to implement this method is Midas FEA NX, a structural analysis software used to study problems of bi- or tri- dimensional concrete structures, damage and cracking of concrete, interaction of soil-structure and many other applications.

3.2. Preliminary Analysis on Simple Geometries

The first step in modelling is to understand how to best reproduce the reality within the model and how the software responds to our inputs. The creation of a simple model, for which the expected behavior under the application of certain loads is known, is fundamental for determining if the conditions applied in the software are correct to achieve the goals. In this chapter, the model of a cube is created with the application of two temperature functions averaged with different time scales to compare the behavior, resolution and sensitivity of the software.

3.2.1. Study of a cube: Modeling and Application of Thermal Loads

In some past studies related to the Ponte Cola dam, it was decided to streamline the model using daily averaged temperature data, thus risking the loss of variability in the process, both on small scales (hourly) and on slightly larger scales (day-night). The measurement data used in this model are summer data contained in the file "*PCola_temp_invaso_2021-2022"*, in order to capture more pronounced displacements. In particular, data recorded each 4 hours, starting from 8 August 2022 at 21:00, are used, covering a total of 116 hours.

The model is a cube with a volume of 125 m^3, positioned in the positive parts of the space respect to the *x*,*y* and *z* directions. Material is isotropic and elastic, with properties listed in Table 3.2.1.1.

Concrete	
Elastic Modulus *[kN/m²]*	$3 \cdot 10^7$
Poisson's Ratio *[-]*	0.2
Unit Weight *[kN/m³]*	25.8
Thermal Coefficient *[1/T]*	$1 \cdot 10^{-5}$
Thermal Conductivity *[W/(m·T)]*	2.309
Specific Heat *[J/(ton · T)]*	1080000

Table 3.2.1.1: Concrete parameters.

Once the material is created and the properties are applied, we proceed to create the mesh using the tool *Mesh – Generate – 3D*. The mesh used in this model is a tetrahedral, differentiated mesh. Previous attempts have shown that, particularly on the faces affected by the application of convection, there is an accumulation of temperatures near the nodes when the mesh is coarse. To achieve the uniformity of temperature on the faces, it was decided to use a mesh size of 0.2 *m* for the upstream and downstream faces, which are involved in convection, while a mesh size of 0.5 *m* was used for the other faces. Figures 3.2.1.1 and 3.2.1.2 respectively show the solid and the mesh.

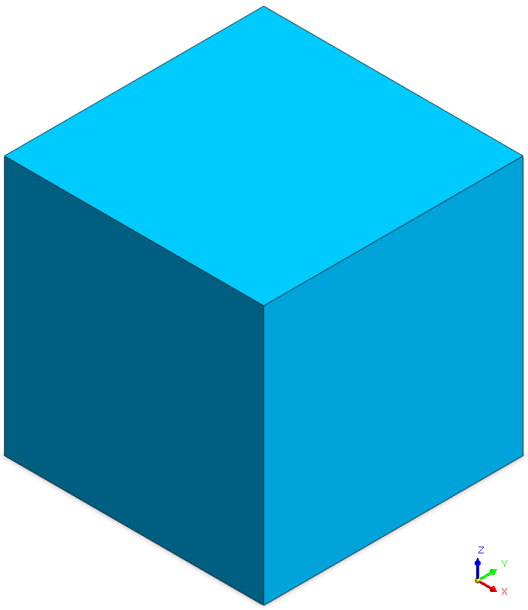

Figure 3.2.1.1: Cube Solid

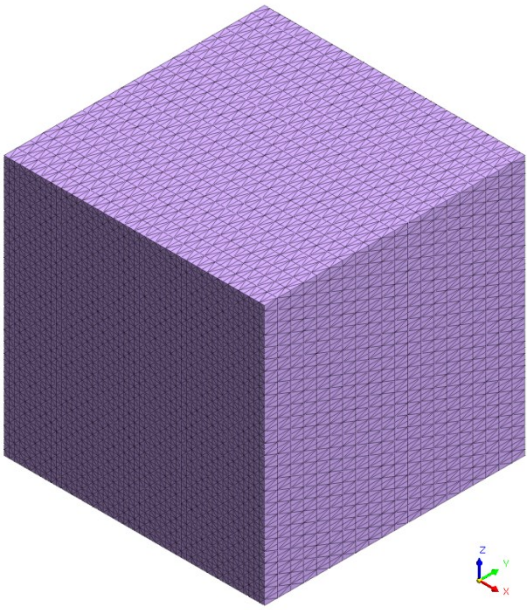

Figure 3.2.1.2: Cube Mesh

The constraints applied involve fixing all translations at the bottom using the *Boundary – Constraint* tool. This boundary condition is implemented through the advanced application, marking as FOS T_x – T_y – T_z and it is applied to all nodes at the bottom of the cube. Another important load to take into account is the self-weight of the structure, that can be simply applied to the model using *Self Weight* tool.

The thermal loads applied to the model are three:

- Prescribed temperature is applied with the *Prescribed temperature* tool to all the nodes of the model and is set to 20.6 *°C*, chosen as the average of selected data;

- Upstream Convection is applied with the *Convection* tool and is related to the interface between water and concrete, while the downstream Convection is related to the interface between concrete and air. The application requires specific properties of the phenomena, such as the film coefficient and the dependence on a time function and is applied to the *3D Element face*.

In Figure 3.2.1.3 and Figure 3.2.1.4 are visible respectively the Prescribed Temperature applied to all the node and the Convection applied to all the upstream 3D element face.

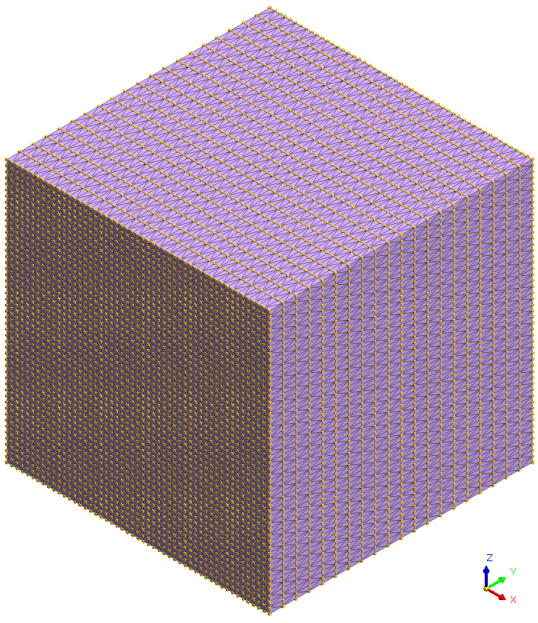

Figure 3.2.1.3: Prescribed temperature applied to all the nodes of the mesh

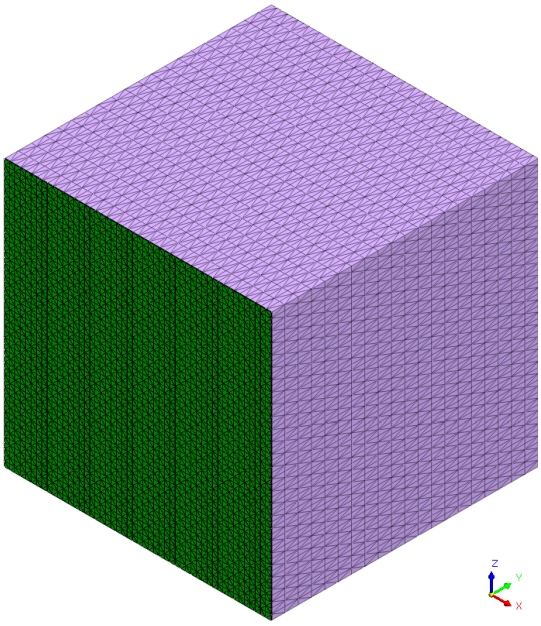

Figure 3.2.1.4: Upstream convection application on the 3D element face

In Figure 3.2.1.5 and Figure 3.2.1.6 are visible the interface of Convection tool of the upstream and downstream face, with relative coefficients.

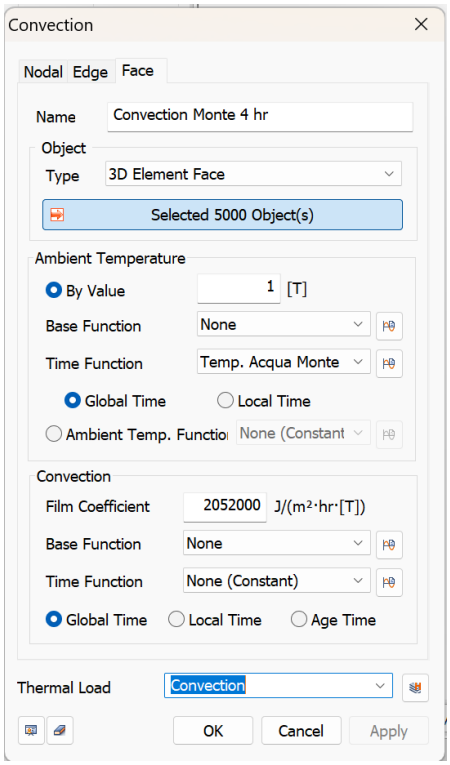

Figure 3.2.1.5: Convection Interface tool, water – concrete

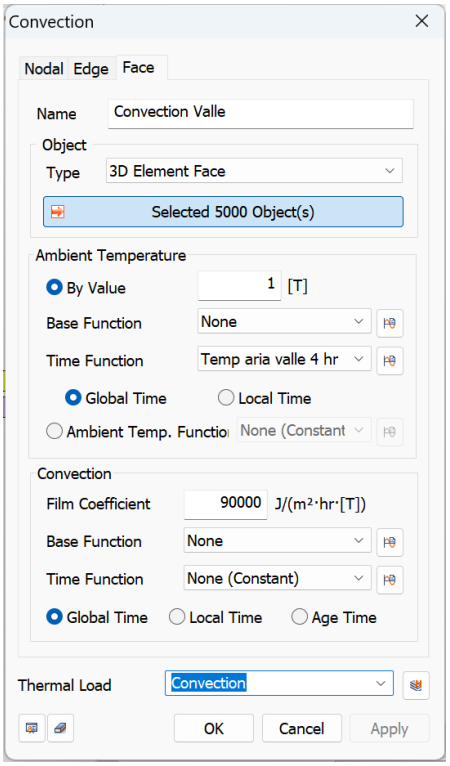

Figure 3.2.1.6: Convection Interface tool, air – concrete

3.2.1.1. Monitoring Temperature Data

In this preliminary analysis, the goals are to understand the functioning of the software and the correct resolution, in terms of time scale, to avoid losing the temporal variability of the heat transfer. To analyze this, monitoring data from 8 August 2022 at 21:00 have been chosen, covering a total of 116 hours. These data have been managed to create three different scenarios:

- Temperature data each 4 hours, as the measurement frequency of the monitoring system;
- Temperature data averaged for day and night hours, in order to have two averaged temperature values per day;
- Temperature data averaged daily, losing the short-term temporal variability of the temperature.

For each scenario, two different time functions are created to be applied to the convection: one for the downstream water temperature and the other for the upstream air temperature. In Figure 3.2.1.1.1, the behaviors of the temperatures of water and air measured through the monitoring system are shown. It is easy to see how the air temperature varies more than the water temperature, and this is due to the different specific heat capacities.

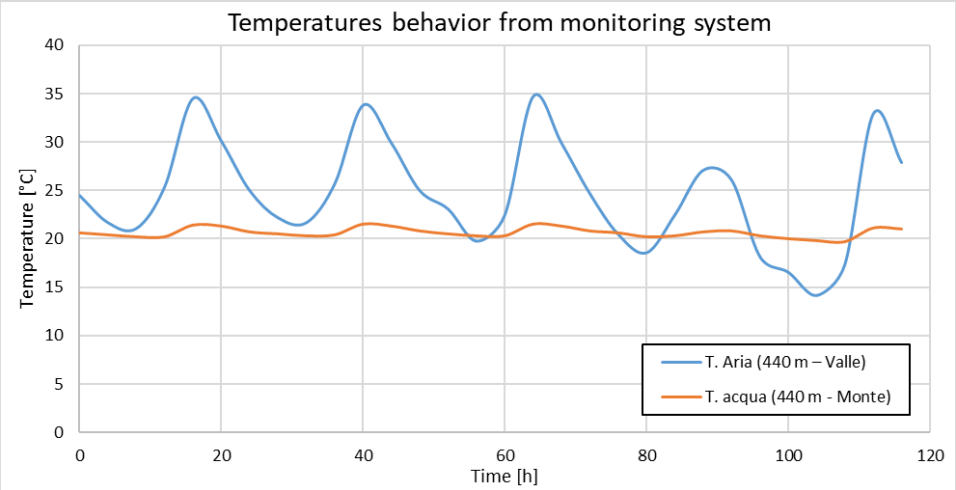

Figure 3.2.1.1.1: Temperature behavior from monitoring system

3.2.1.2. Heat of Hydration – Thermal stress analysis

The types of analysis used in the various studies of this thesis are all heat of hydration analyses. In certain concrete structures with considerable mass, the amount of heat generation due to hydration is important. Non- uniform thermal expansion and contraction due to heat of hydration and cooling of concrete, accompanied by changing constraints, create undesirable stresses that may cause detrimental cracking in the concrete, thereby reducing its strength and durability. This analysis enables us to predict and control temperature and stress distribution within a structure to avoid potential issues. It entails temperature distribution analysis for conduction, convection, heat sources and other types of heat transfer phenomena. In our studies, only convection will be used, defined as a heat transfer whereby heat is transmitted between a fluid and the surface of a solid through the fluid's relative molecular motion. From an engineering perspective, the heat transfer coefficient h_c is defined to represent the heat transfer between a solid and a fluid, where T represents the surface temperature of the solid, and the fluid flowing on the surface retains an average temperature T_∞.

$$q = h_c \cdot (T - T_\infty)$$

The heat transfer coefficient widely varies with the flow type, geometric configuration, the area in contact with the flow, the physical properties of the fluid, the average temperature on the surface in contact with convection, location and many others, and as such it is extremely difficult to formulate. In general, convection problems associated with temperature analysis of mass concrete structures relate to the type of heat transfer occurring between the concrete surface and atmosphere. Accordingly, the following empirical formula is often used, which is a function of an atmospheric wind speed *[m/sec]*.

$$h_c = h_n + h_f = 5.2 + 3.2\text{v}$$

All the analyses performed in the preliminary tests are made of two stages. The first is a steady-state step in which the prescribed temperature of the model is defined; the second is a transient step in which, based on the chosen time function and the defined time step, the evolution of the results over time is given.

3.2.1.3. Analysis Results and Comparison of cases

In order to monitor the progress of the analysis, nodes are identified for extracting temperature and total displacement data: specifically, one node at the upstream edge in the middle of the side ID 1096, the same for the downstream face ID 1166, and one located at the center of the top face with ID 1656.

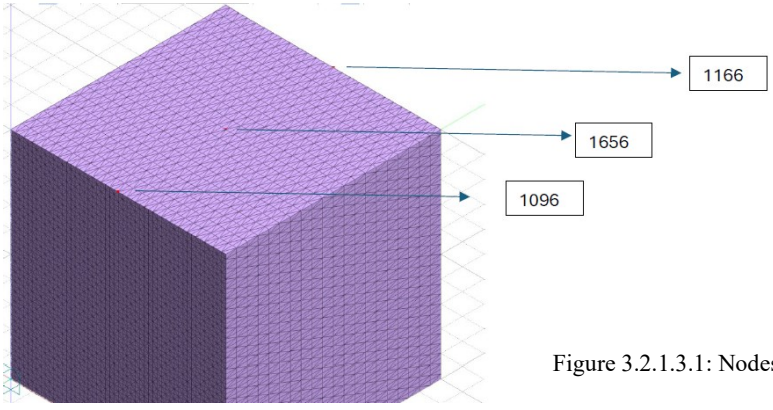

Figure 3.2.1.3.1: Nodes ID and position of analyzed results

In Case 1, in which the time functions of temperature are based on measurements sampled every 4 hours, the temperature curves more or less follow the behavior of the functions. However, as can be seen in the second graph of the node 1656, there is no variation in temperature, due to multiple factors as the thickness of the solid, the analysis time and the thermal properties of the material. The displacement curve exhibits behavior that is most often correlated with temperature; however, it is observed that the displacements do not follow the variations in temperature in terms of amplitude and timing. Displacements increase in correspondence with rising temperatures, although there is sometimes a phase shift of the peaks, which could be due to the material's response to thermal changes.

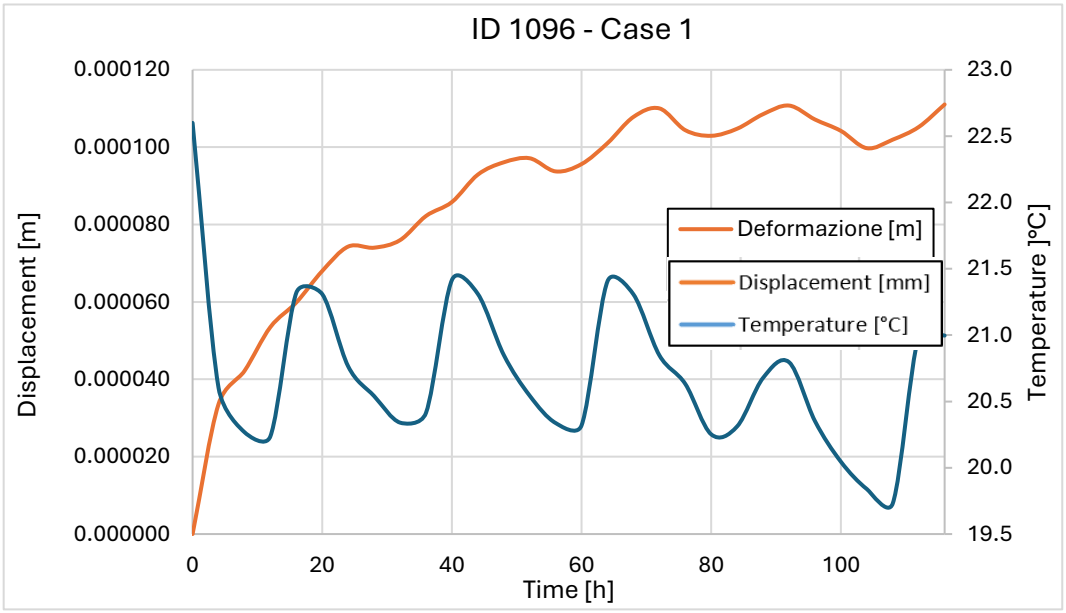

Figure 3.2.1.3.2: Temperature and Displacements of node 1096 – Case 1

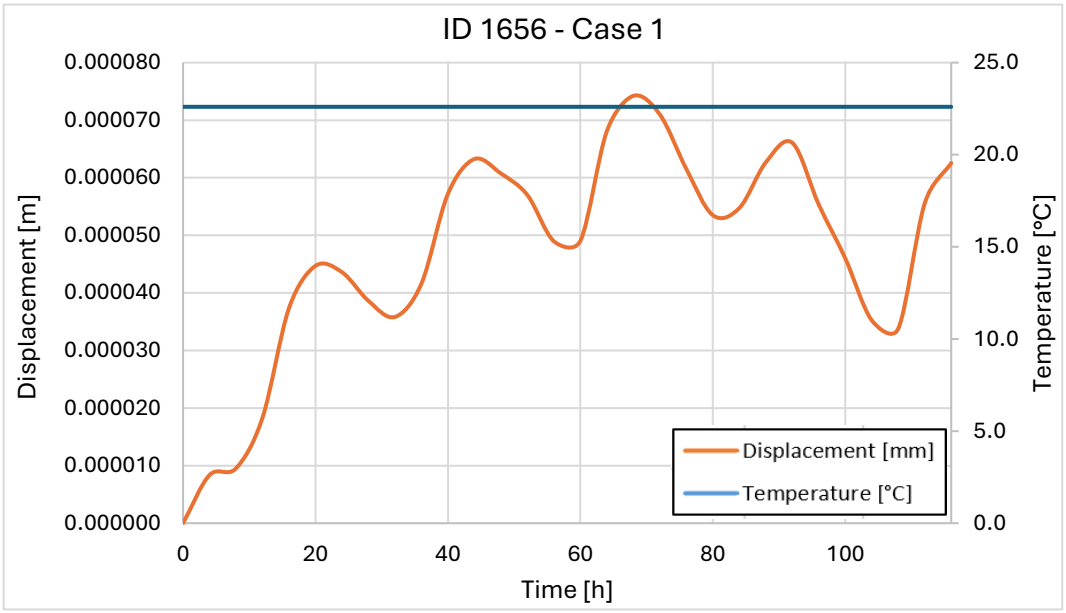

Figure 3.2.1.3.4: Temperature and Displacements of node 1656 – Case 1

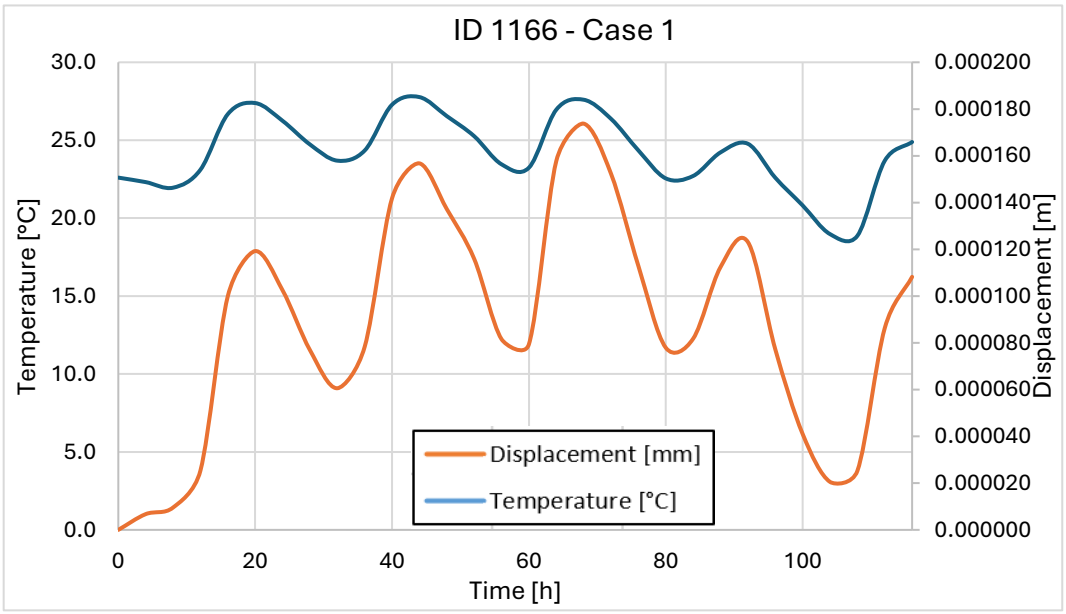

Figure 3.2.1.3.5: Temperature and Displacements of node 1166 – Case 1

In Case 2, instead, the time functions of temperature applied to downstream and upstream faces are averaged in time, making a distinction between day and night temperatures. By doing this, the behavior of temperature is more pronounced and peaked.

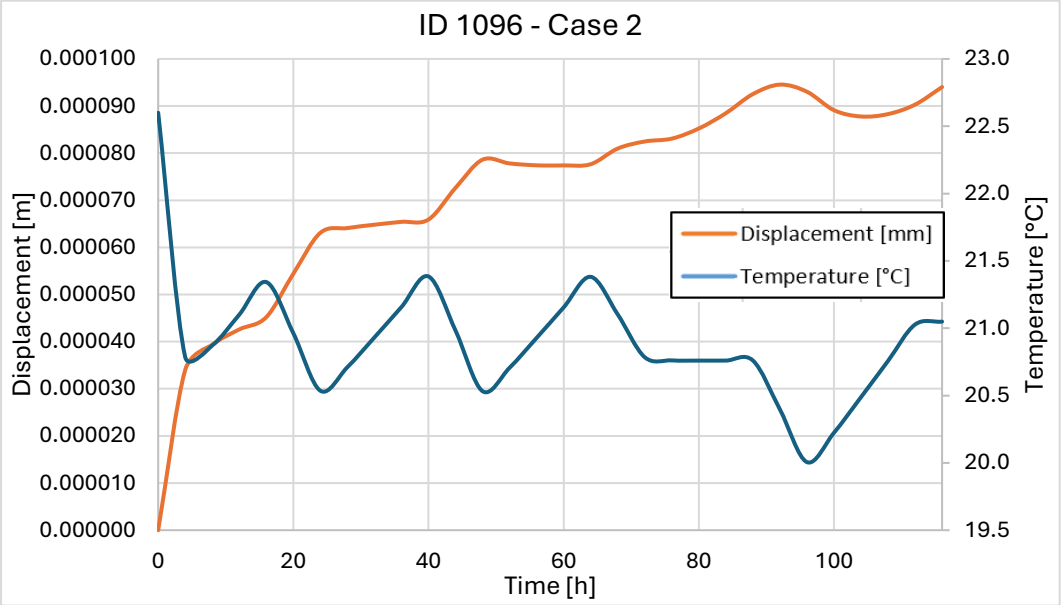

Figure 3.2.1.3.6: Temperature and Displacements of node 1096 – Case 2

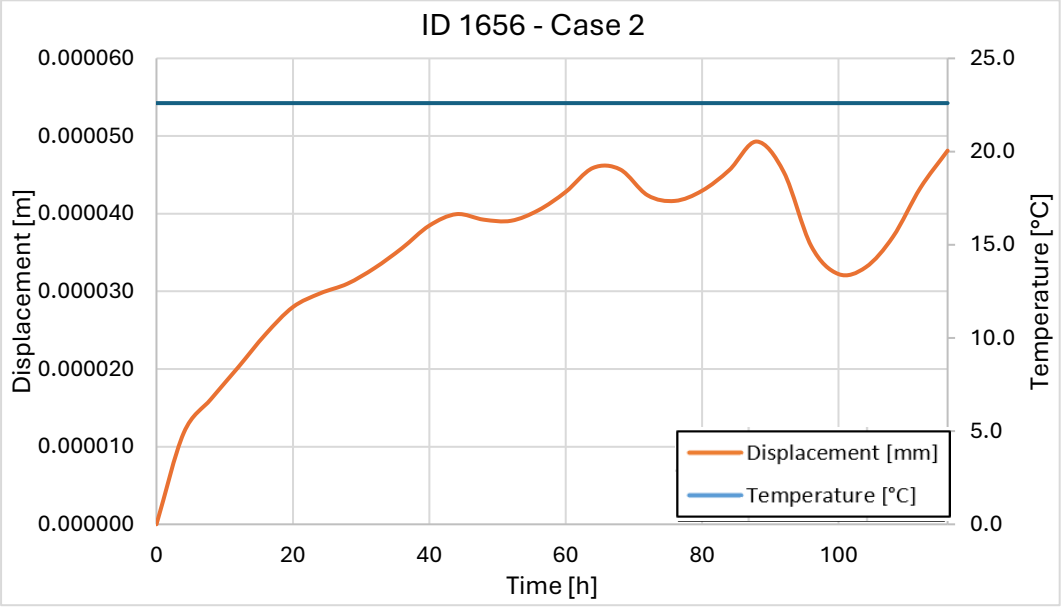

Figure 3.2.1.3.7: Temperature and Displacements of node 1656 – Case 2

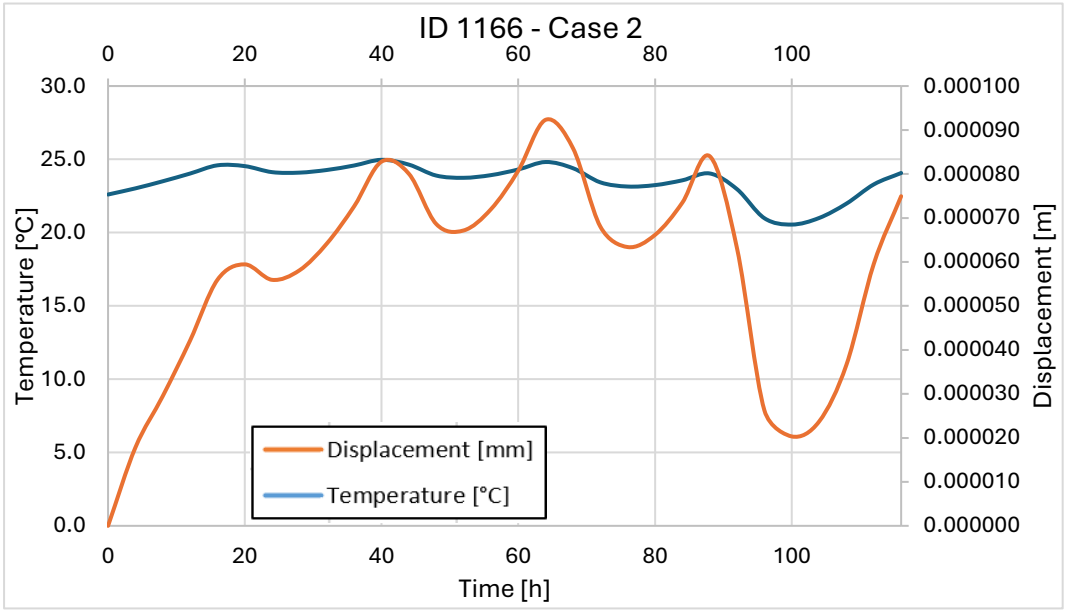

Figure 3.2.1.3.8: Temperature and Displacements of node 1166 – Case 2

In Case 3, the time functions of temperature applied to downstream and upstream faces are averaged at the daily time scale.

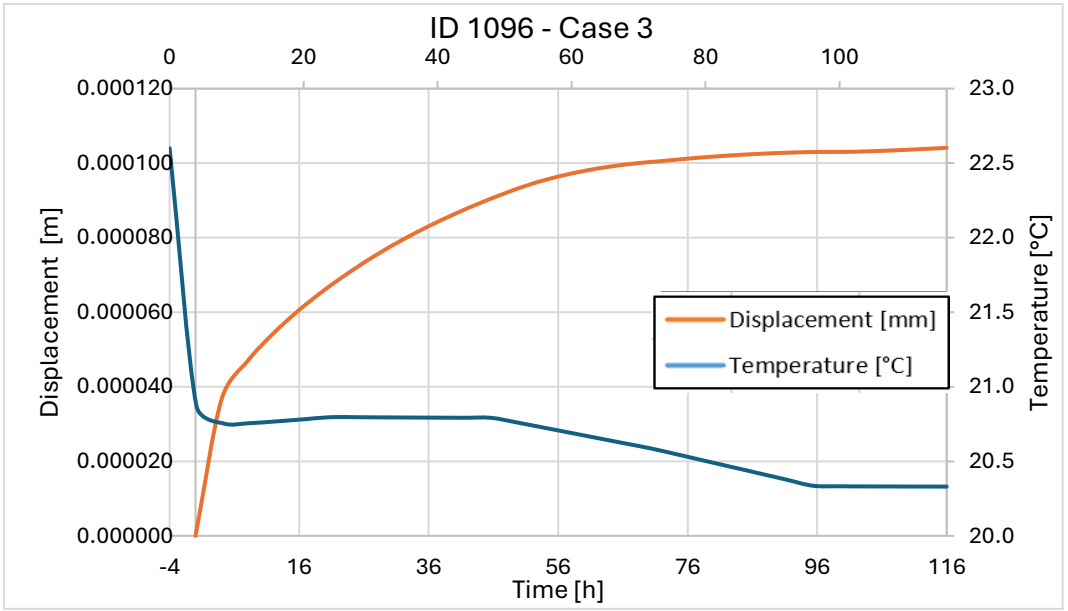

Figure 3.2.1.3.9: Temperature and Displacements of node 1096 – Case 3

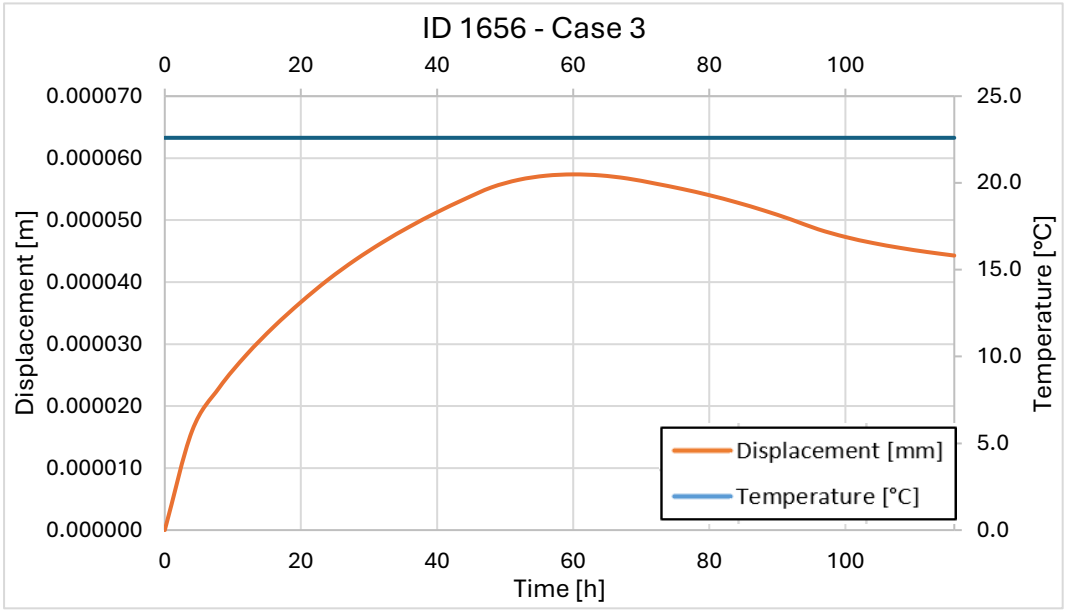

Figure 3.2.1.3.10: Temperature and Displacements of node 1656 – Case 3

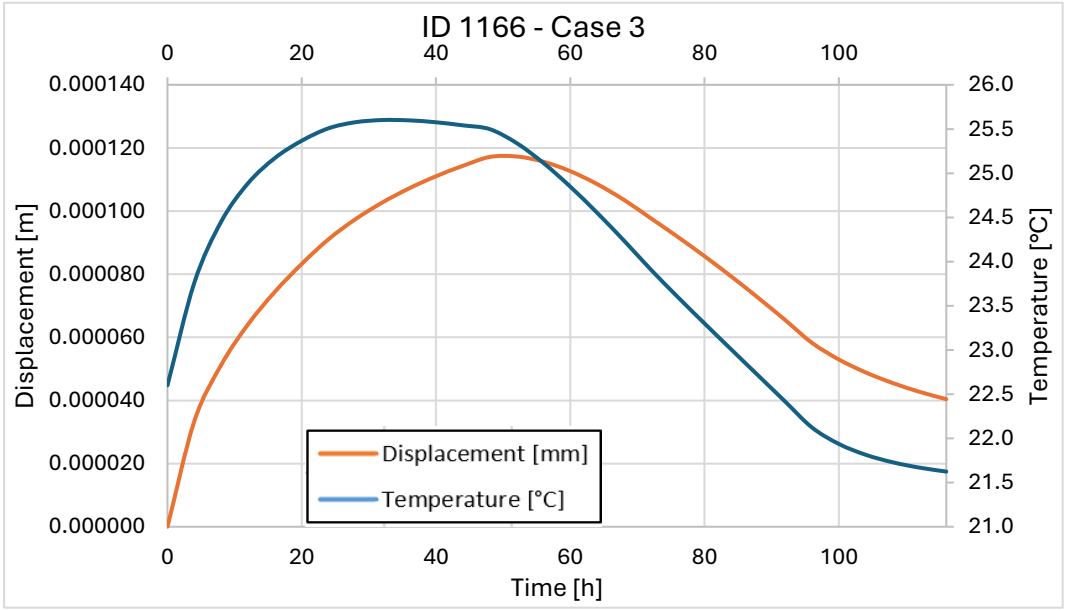

Figure 3.2.1.3.11: Temperature and Displacements of node 1166 – Case 3

By comparing the displacements over time of cases 1, 2 and 3, it can be noted how the daily average flattens the peaks present in the "hourly" data, thus neglecting peaks that are sometimes much bigger if we consider the data available every 4 hours, even if the displacements remain limited and not excessive in size (for this specific domain). In all the three cases, it can be observed how there is an accumulation of displacements, especially for the nodes at the edges of the domain, and an increase in them even when

the temperature does not vary or even decreases. In the following figures, it is possible to observe the differences in displacement of nodes in the three different cases.

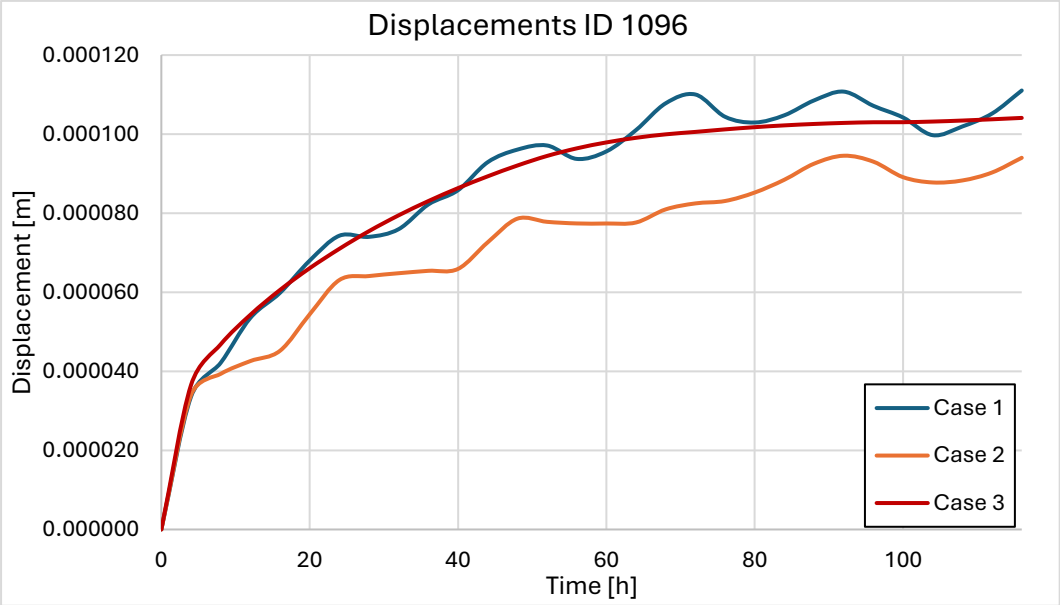

Figure 3.2.1.3.12: Displacements comparison between the 3 Cases, Node 1096

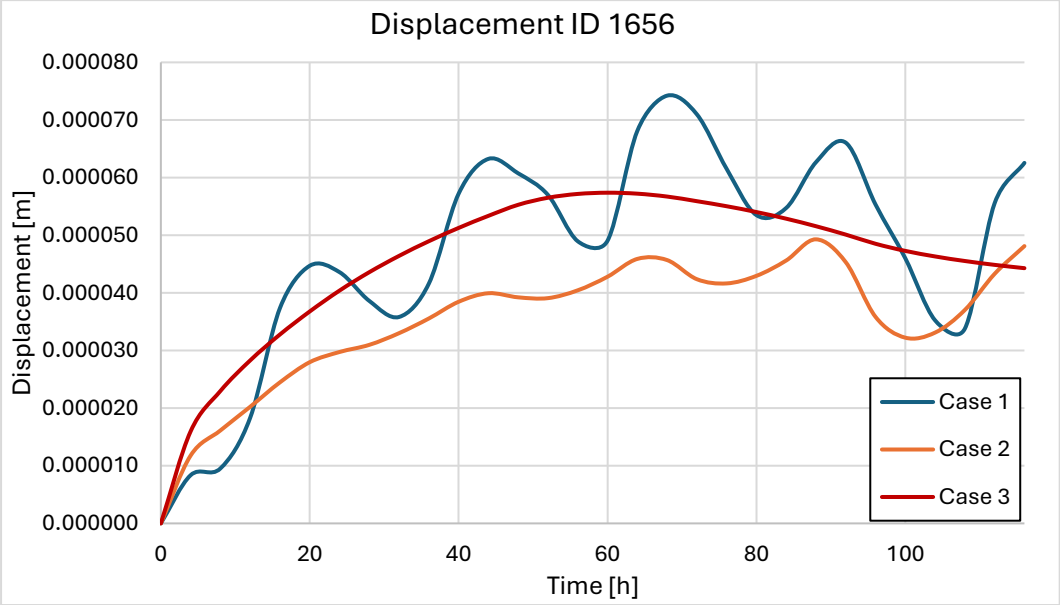

Figure 3.2.1.3.13: Displacements comparison between the 3 Cases, Node 1656

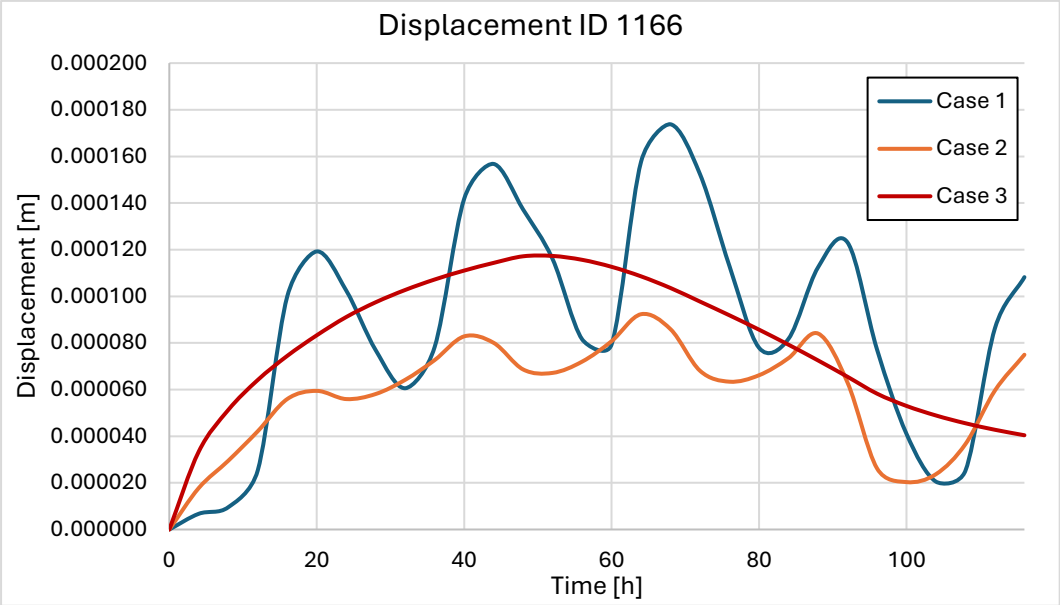

Figure 3.2.1.3.14: Displacements comparison between the 3 Cases, Node 1166

3.3. Analysis on a Parallelepiped

The creation and use of a new model is necessary to verify the correct setting of the thermal loads and the parameters that govern the heat transfer. Furthermore, by looking at the graphs of the temperature trend in the central node of the cube in the previous cases, you can see how, although it is affected by the continuity of displacement, it is not affected at all by the temperature functions applied to the two faces.

In order to verify the influence of the thermal parameters and consequently of a displacement conforming to reality, a parallelepiped similar to a wall is built, narrow and tall, in order to be affected as little as possible by the constraints imposed on the bottom. This model will be used in two different applications: in both, a temperature function composed of a heating phase and a subsequent cooling phase will be used. The first case involves the application of the convection on the lateral, narrow and long face of the parallelepiped and the influence of the thermal parameters will be studied. In the second case, however, convection will be applied to the larger face and the expected displacement will be verified.

3.3.1. Temperature Function

In the thermal analysis of the parallelepiped, a built temperature function is applied, made up of hourly data for a total duration of one day. The function is characterized by a heating phase, from 10 $°C$ to 33 $°C$, and a cooling phase, from 33 $°C$ to 0 $°C$. In Figure 3.3.1.1, the temporal behavior of the temperature function is shown.

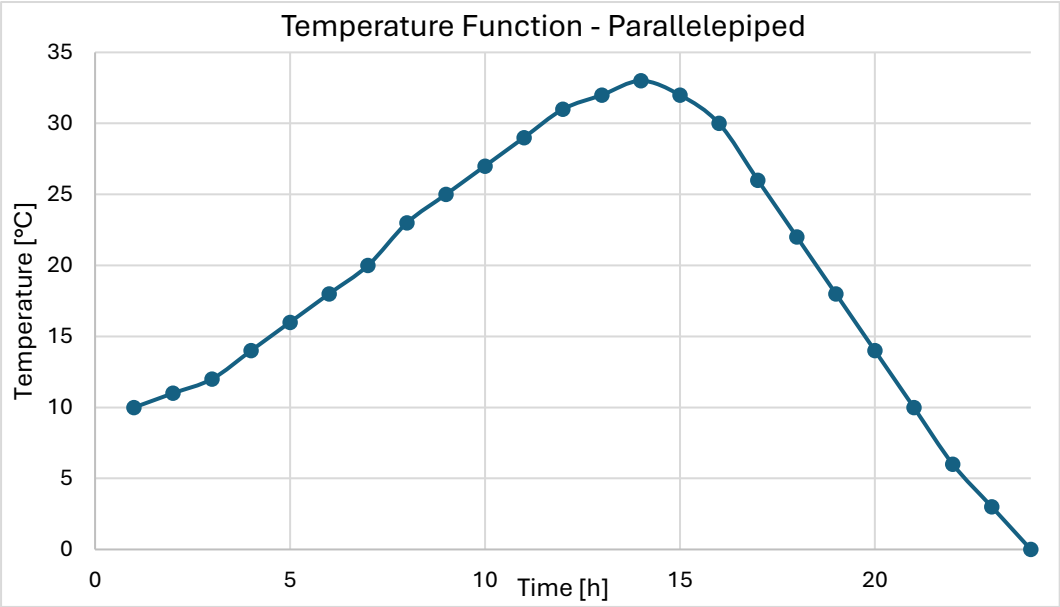

Figure 3.3.1.1: Temperature Function for Parallelepiped cases

3.3.2. Parallelepiped Case 1

In the first case, a parallelepiped $1 \cdot 10 \cdot 20$ m is built in Midas FEA NX. The materials and the mesh properties are the same as those of the concrete used in the previous cases. In the meshing process, as in the previous case, it was decided, after several attempts, to use a more refined mesh on the face affected by convection. Using the *Size Control* tool and selecting the edges of the affected face, a mesh of size 0.1 m is set, while on the other sides, a size of 0.5 m is applied.

In addition to the *Self Weight*, *Constraints* are also applied, neglecting all translations (along x, y and z directions) at the bottom of the solid.

The *Prescribed Temperature* applied to all the nodes of the mesh and used in the steady-state step, is the temperature from the function at day 0 of analysis, equal to 10 $°C$.

The *Convection* is applied to the *3D Element Face* of the smaller lateral face, using the temperature function created earlier as the time function.

In the following figures, the geometry, the mesh and the application of convection are shown.

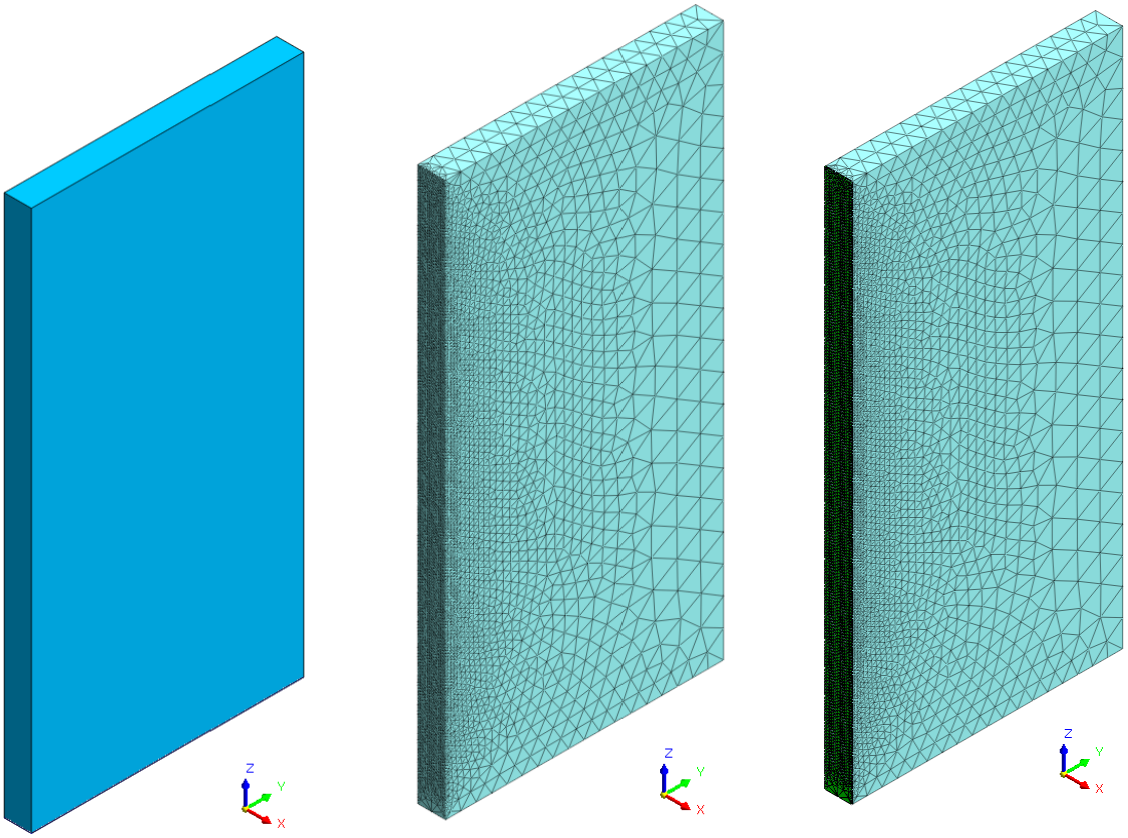

Figure 3.3.2.1: Geometry, mesh and convection application on Parallelepiped Case1

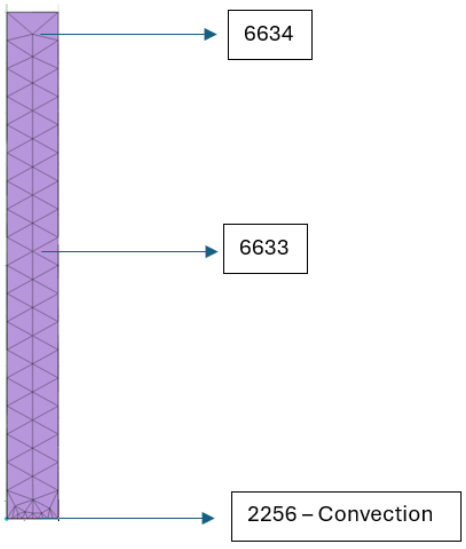

In order to analyze the behavior of the displacements induced by the temperature, the nodes positioned on the top face with IDs 2256, 6633 and 6634 are monitored.

Figure 3.3.2.2: Monitored Nodes positions, Parallelepiped Case 1

The results can be seen in the following Figures, representing the behavior of temperature and displacement in time for each of the three nodes chosen for monitoring.

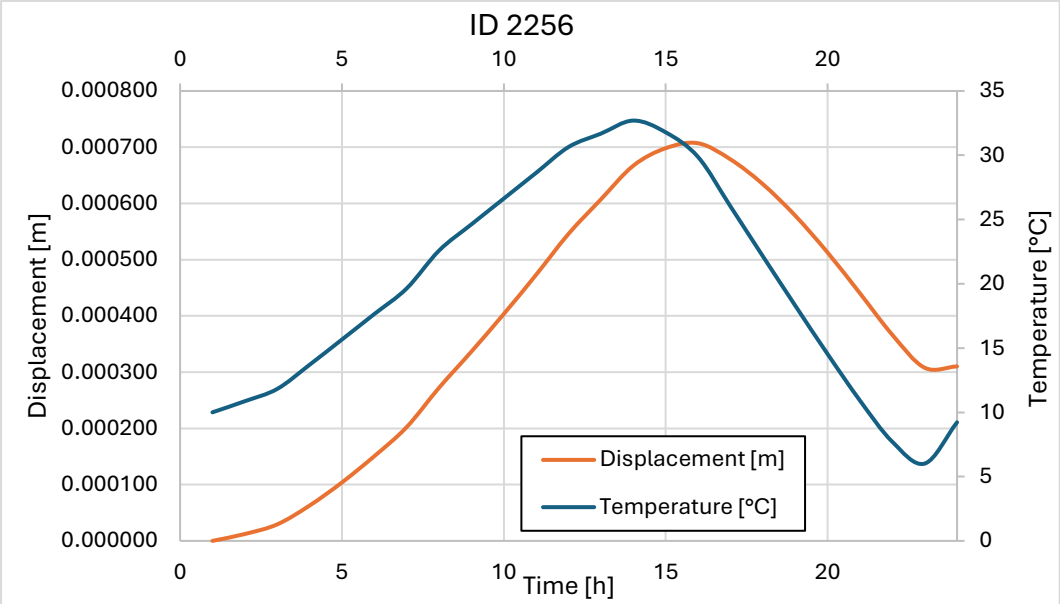

Figure 3.3.2.3: Temperature and displacement behavior, Parallelepiped Case 1, Node 2256

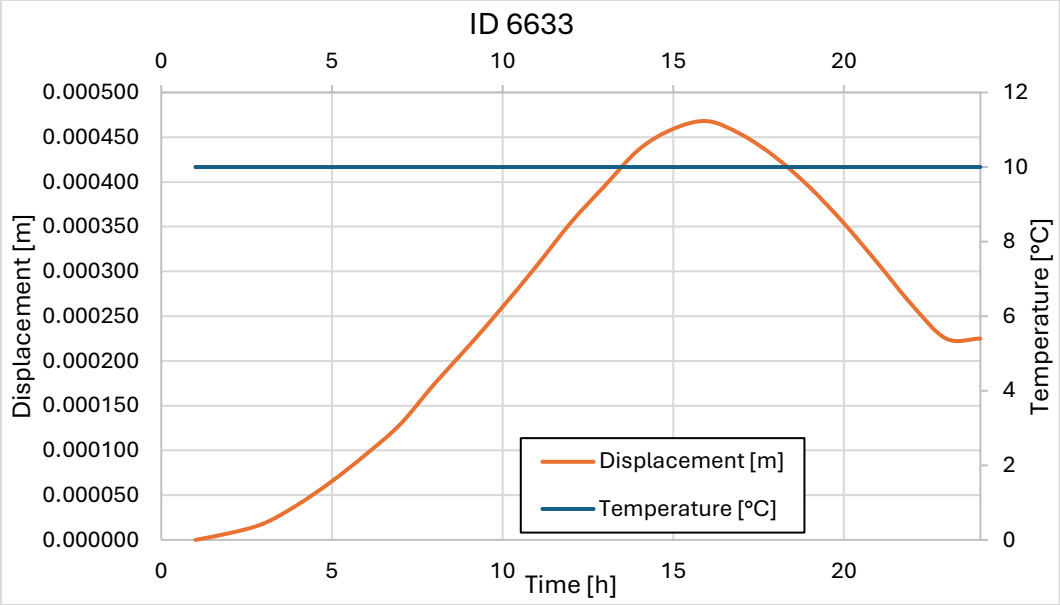

Figure 3.3.2.4: Temperature and displacement behavior, Parallelepiped Case 1, Node 6633

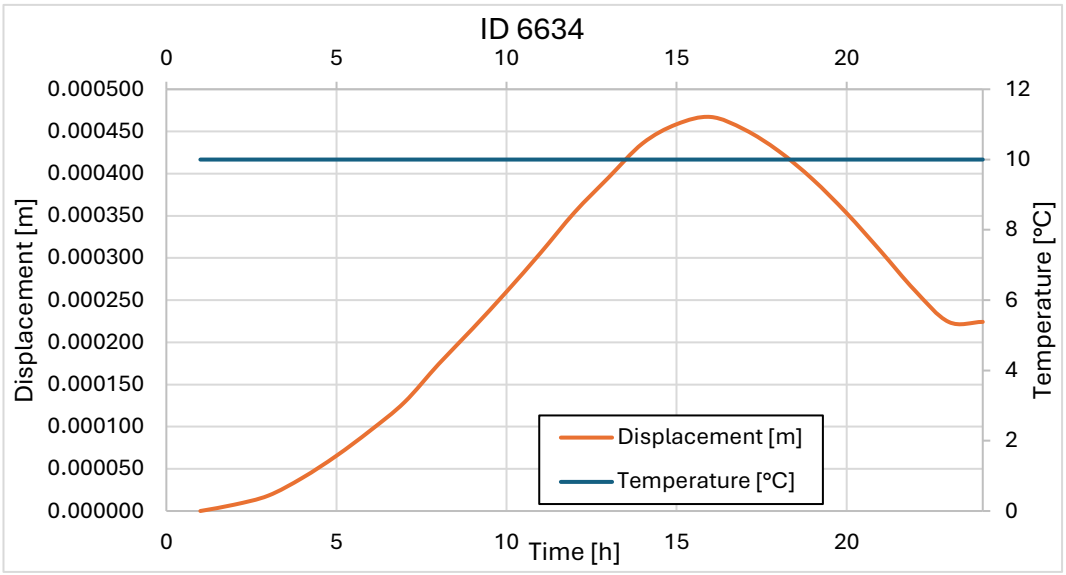

Figure 3.3.2.5: Temperature and displacement behavior, Parallelepiped Case 1, Node 6634

As can be seen from the graphs, the only node experiencing the convection process is the one positioned on the face of application. This node allows us to define a delay between the heating and the displacement processes, which is a function of the specific heat of the concrete. From other graphs, it can be easily observed how other nodes experience displacement in the solid, even though they are not directly affected by temperature variation. The following figures show the deformed condition of the solid from different perspectives.

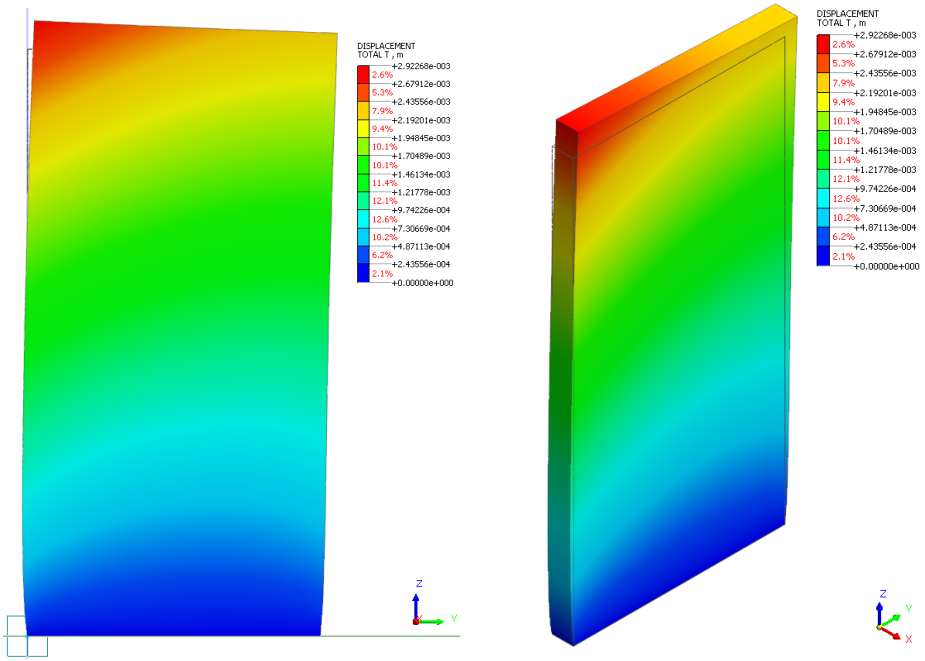

Figure 3.3.2.6: Total maximum displacement of Parallelepiped Case 1 from different perspective

In the following part, it will be shown how the thermal parameters involved in the Heat of Hydration analysis change the heat transfer process in the solid. The thermal conductivity and the specific heat of different materials will be compared with those of concrete, in order to understand how the heat transfer depends on these parameters.

Thermal conductivity is a physical property that measures the capacity of the materials to transfer heat. It defines the quantity of heat that pass through a unitary surface of material per unit of time, in the presence of a temperature gradient. It is defined in *W/(m·K)*.

	Material	Thermal Conductivity *[W/m·K]*	Maximum temperature of the face *[°C]*
Left Figure	Concrete	2.309	25.53
Central Figure	Steel	60	16.17
Right Figure	Aluminum	200	13.82

Table 3.3.2.1: Thermal Conductivity of different materials, and maximum temperature reached by the face

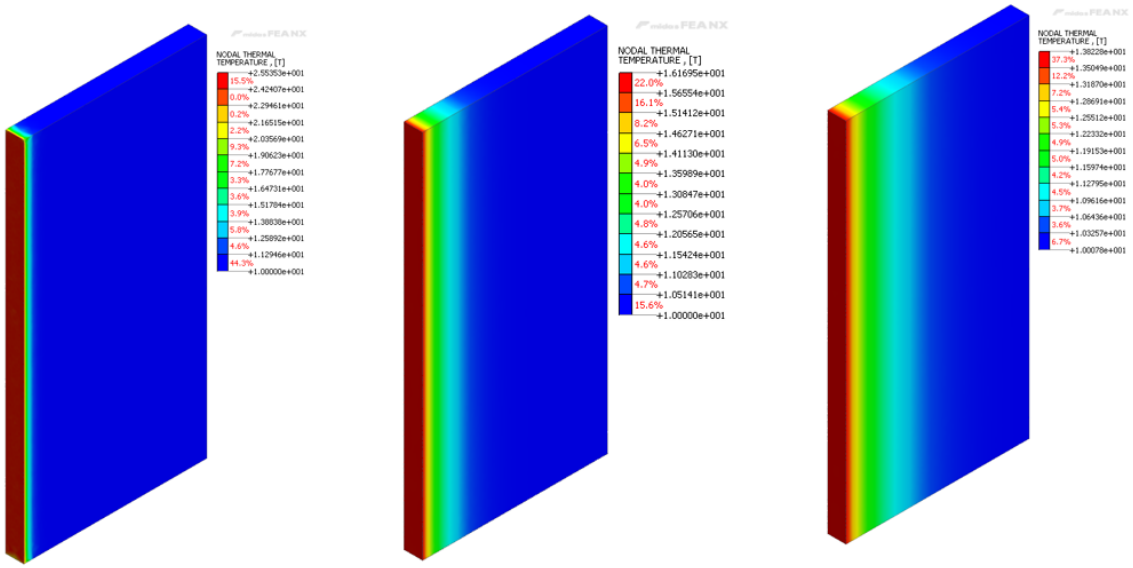

Figure 3.3.2.7: Temperature distribution of material with different Thermal Conductivity, from the left: Concrete, Steel and Aluminum

As can be seen from Figure 3.3.2.6, an increase of thermal conductivity allows for faster heat transfer through the material on short time scales, reducing the temperature gradient and reaching the thermal equilibrium in a shorter time.

The same has been done with the specific heat, defined as the quantity of heat required to increase the temperature of a unit mass of material by one Celsius degree (or Kelvin), and expressed in $J/(kg \cdot K)$. What is expected with an increase in this property is that the material will be able to absorb more heat without increasing its temperature too much. This means that it will need more energy to reach a certain temperature compared to a material with a lower value.

	Material	Specific Heat *(J/ton · K)*	Maximum temperature of the face *[°C]*
Left Figure	Concrete	880 000	25.53
Central Figure	Steel	490 000	27.32
Right Figure	Aluminum	200	32.9

Table 3.3.2.2: Specific Heat of different materials and maximum temperature reached by the face

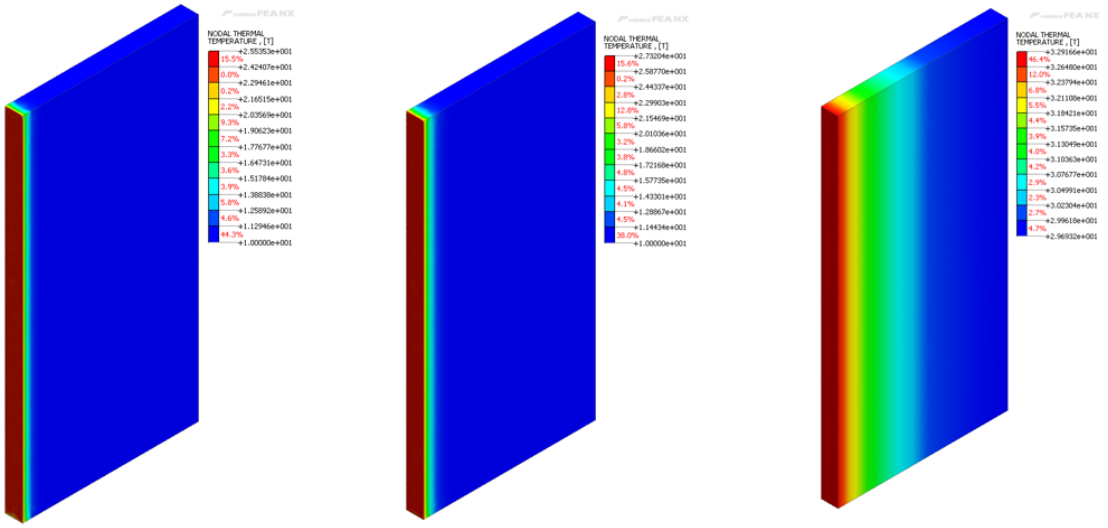

Figure 3.3.2.8: Temperature distribution of material with different Specific Heat, from the left: Concrete, Steel and Aluminum

What is expected and highlighted by the results of the analysis is that, as the specific heat increases, the material requires more energy to heat up. This means that, whit the same amount of applied energy, the temperature variation will be smaller compared to a material with a lower specific heat.

3.3.3. Parallelepiped Case 2

In the second case, a parallelepiped $1 \cdot 10 \cdot 20$ *m* is built in Midas FEA NX. The materials and the mesh properties are the same as those of the concrete used in the previous cases. During the meshing process, as in the previous case, it was decided, after several attempts, to use a more refined mesh on the face affected by convection. Using the *Size Control* tool and selecting the edges of the affected face, a mesh of size 0.1 *m* is set, while a size of 0.4 *m* is set for the opposite face.

In addition to the *Self Weight*, *Constraints* are also applied, which neglect all the translations (along *x*, *y* and *z* directions) at the bottom of the solid.

The *Prescribed Temperature* applied to all the nodes of the mesh and used in the steady-state step, is the initial temperature of the function, which is 10 °*C*. The *Convection* is applied to the *3D Element Face* of the larger lateral face, using the previously created time function. In the following figures, the geometry, mesh and application of the convection are shown.

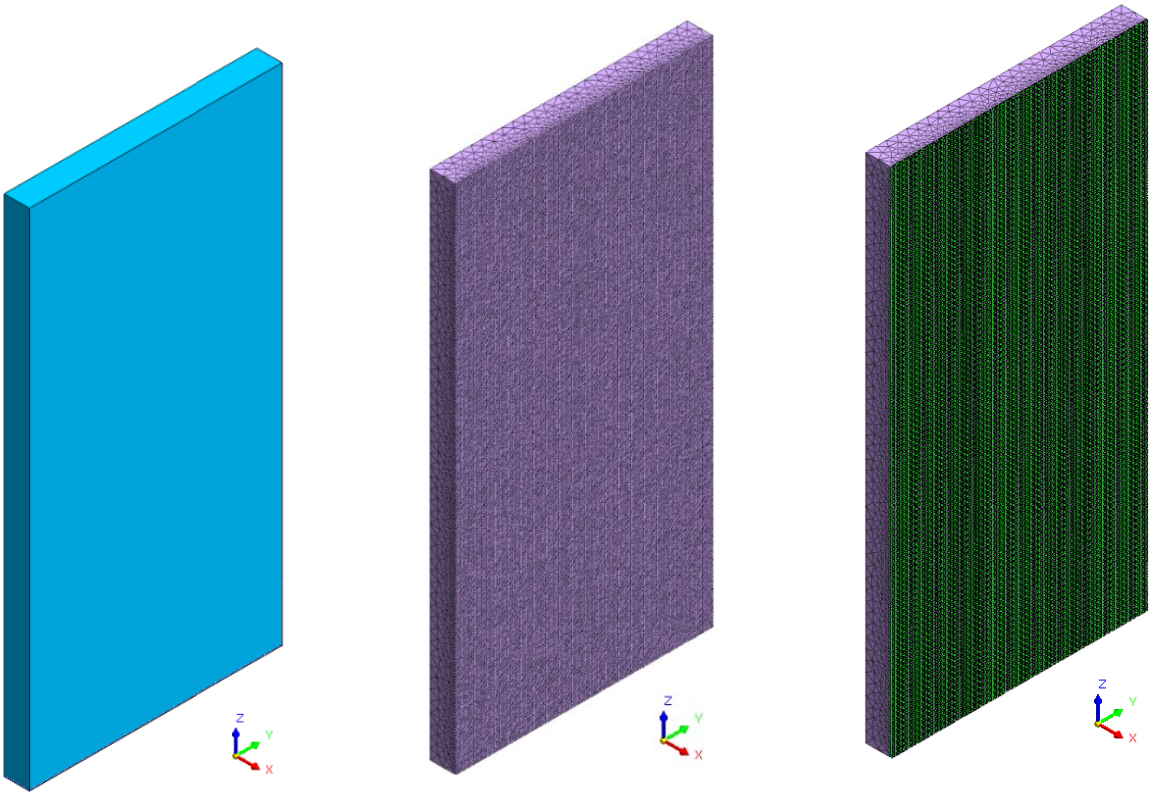

Figure 3.3.3.1: Geometry, mesh and convection application on Parallelepiped Case 2

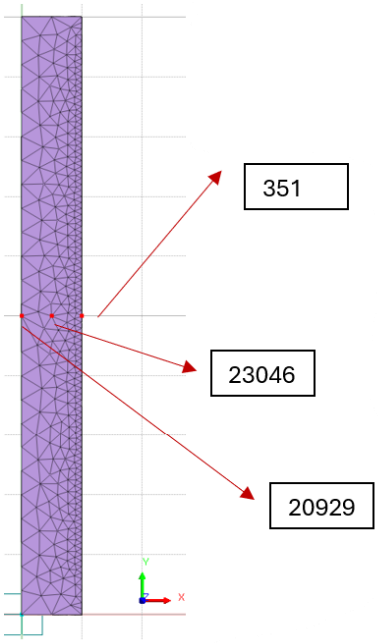

In order to analyze the behavior of the displacement induced by the temperature, the nodes positioned on the top face with IDs 351, 23046 and 20929 are monitored.

Figure 3.3.3.2: Monitored Nodes positions, Parallelepiped Case 2

In this case, we are interested in verifying that the structure behaves as expected, depending on the constraints and loads applied to it. As can be seen in the following Figures, the parallelepiped expands on the face where the convection is applied, while it contracts on the opposite face, creating a bending of the structure towards the unaffected face.

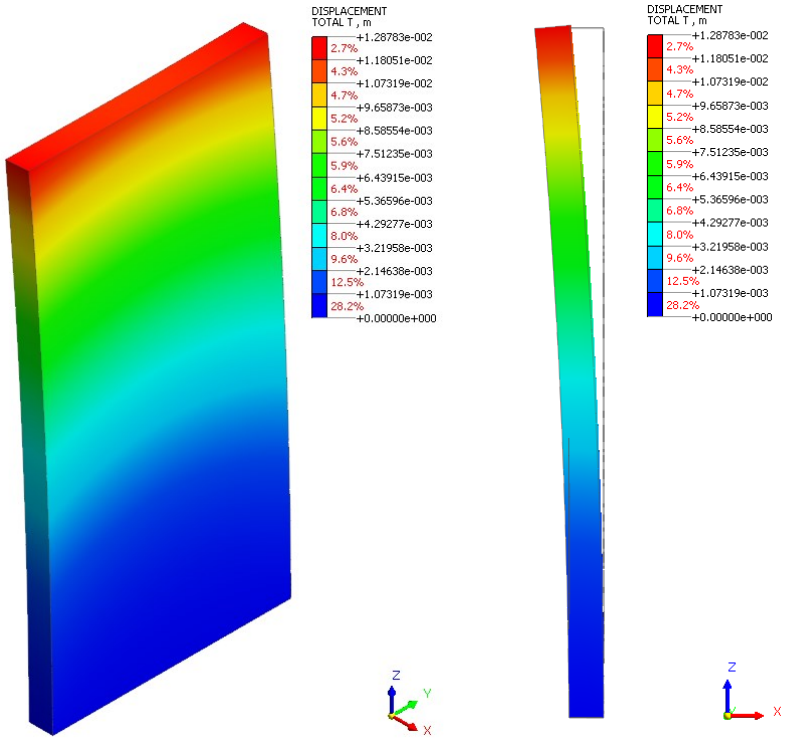

Figure 3.3.3.3: Maximum displacement of the structure, Parallelepiped Case 2

3.4. Preliminary Modeling of a Simplified Dam Structure

After understanding how the Midas software works in applying constraints and loads, the model can be further complicated, getting closer and closer to the final model of the dam. In this subchapter, a simplified model of the dam will be built, with the same dimensions but without the arch, for construction simplicity. The aim is to compare the order of magnitude of the displacements of the model with those of the Ponte Cola dam, in order to make considerations relating to the correct setting of the model.

The geometry of the model starts from the real dimensions of the dam, it was decided to replicate its dimensions without the presence of the arch. A trapezoid with rectangular bases is therefore created with the following characteristics: the bottom rectangular base has dimensions $24 \cdot 50\ m$, the top base has dimensions $3.4 \cdot 282\ m$, and the height is $124\ m$.

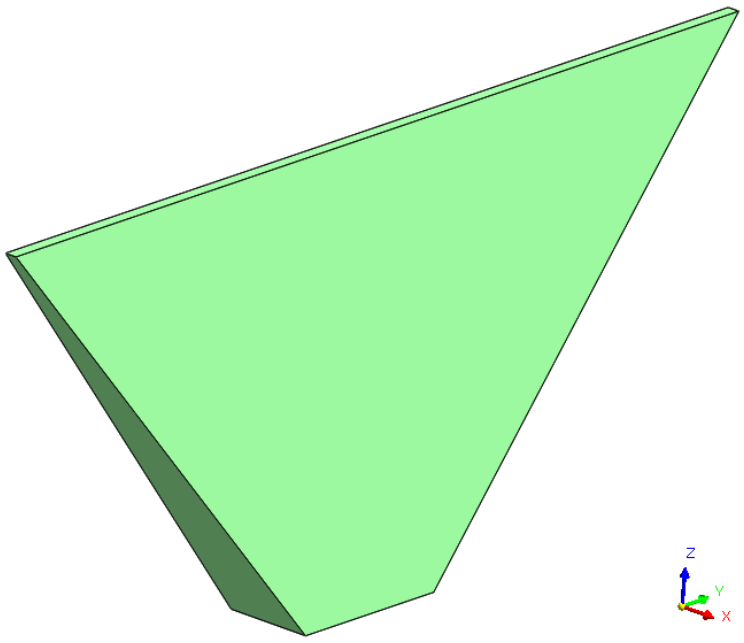

Figure 3.4.1: Simplified geometry of the dam

For the construction of the mesh, it was decided to use the *Size Control* tool, setting a mesh size of 1.6 *m* on the face affected by convection and 3 *m* on the opposite face. This choice was modified several times due to computational demands.

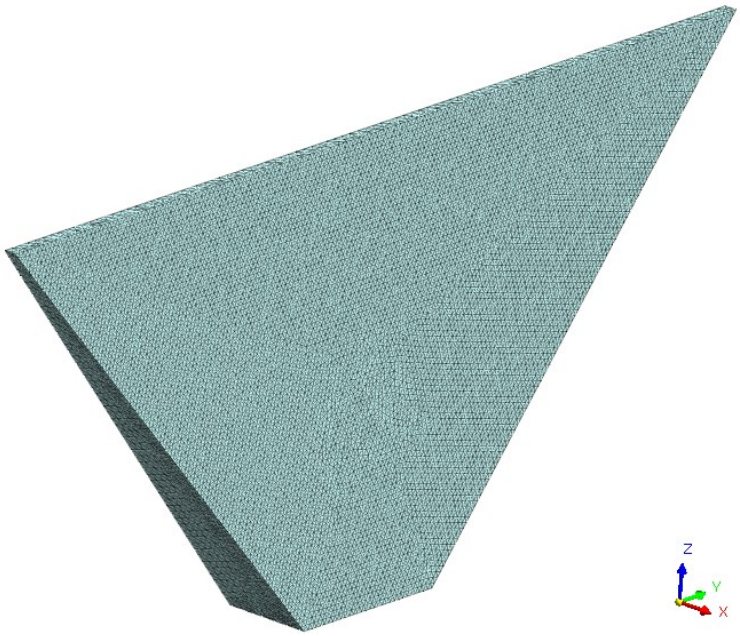

Figure 3.4.2: Mesh of the simplified dam model

In addition to the *Self Weight*, *Constraints* are also applied to prevent all translations (along *x*, *y* and *z* directions) not only on the bottom of the solid but also on the smaller lateral faces of the trapezoid. These constraints allow the top part of the dam to splay out, replicating the behavior observed in the real structure due to the terrain.

As for the *Prescribed Temperature* applied to all the nodes of the mesh and used in the steady-state analysis, the initial temperature of the function of 10 °*C*, is used. The *Convection* is applied to the *3D Element Face* of the larger lateral face, using the previously created time function.

Due to the large number of elements and nodes in the model, 177571 and 1014692 respectively, the time required for the Heat of Hydration analysis to produce results was very long, approximately 6 hours, also considering the size of the output file generated.

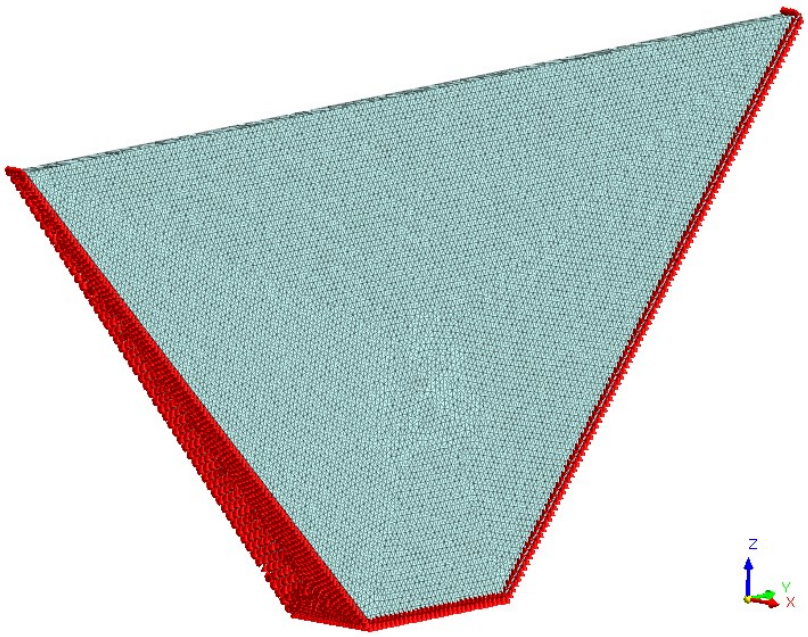

Figure 3.4.3: No translation constraints applied to the bottom and lateral face of the trapezoid

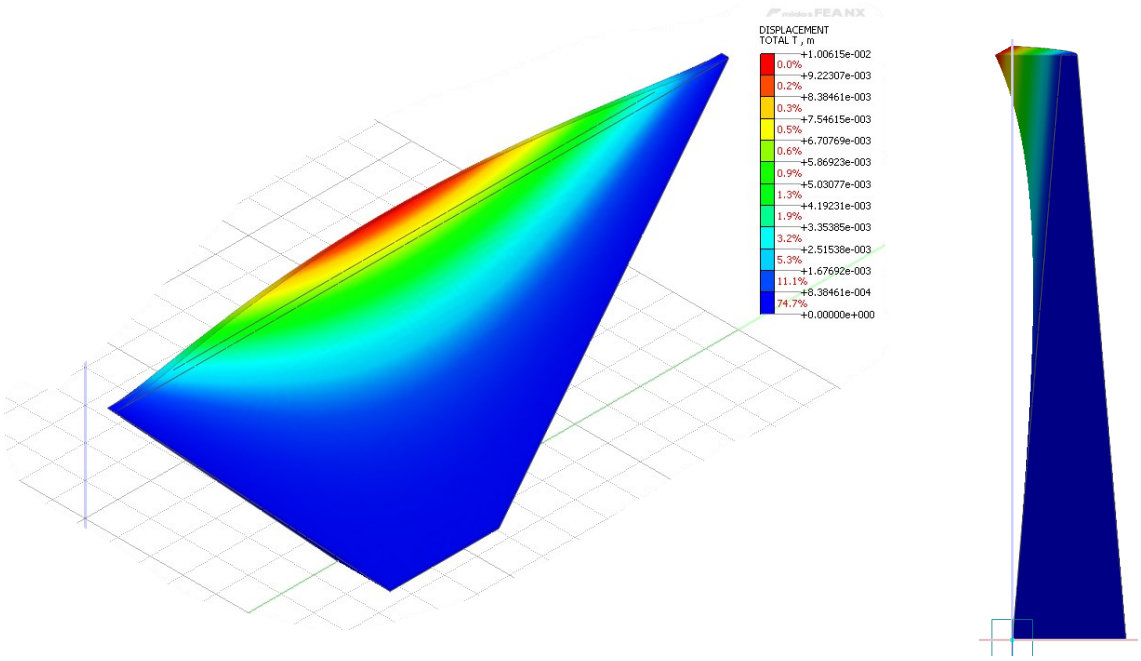

Figure 3.4.4: Deformed shape in the x-direction of the simplified dam model

In particular, the translations along the *x*-axis (with negative sign because in the opposite direction to *x*) of the central node of the crown, node 529767, show a maximum translation of 1 *cm*, consistent in terms of order of magnitude with results from previous studies and from monitoring data of the dam.

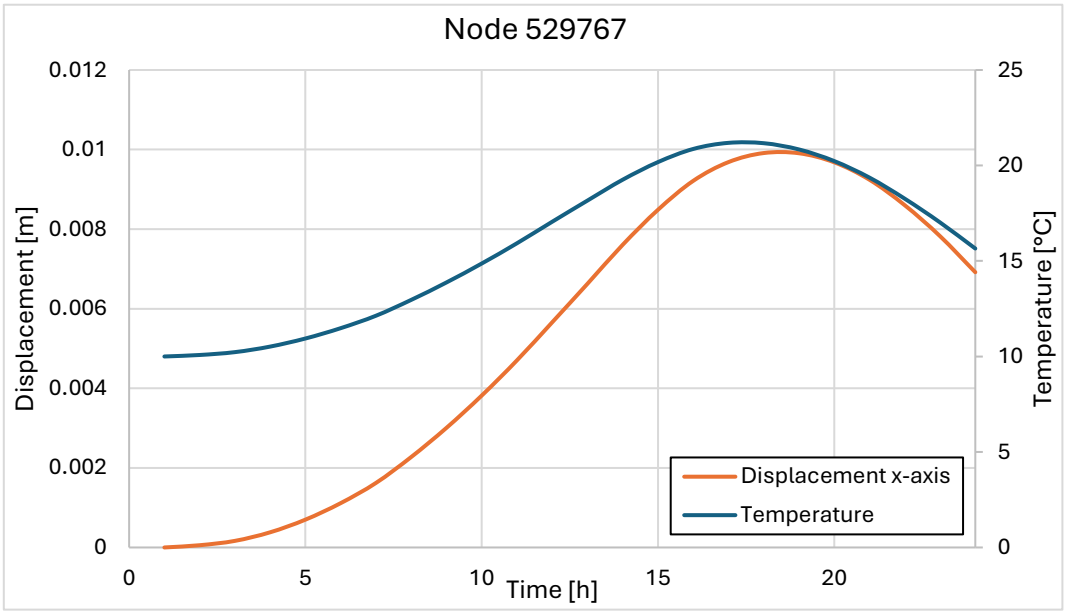

Figure 3.4.5: Temperature and Displacement behavior Node 529767

As can be seen from the graph, the displacement trend follows the temperature trend, although the latter behaves as the applied function, with heating and cooling phase, but never reaches the same values. This is primarily due to the film coefficient, a parameter that describes the efficiency of the heat transfer by convection between the surface of the solid and the surrounding fluid. If this coefficient is limited or low, the surface of the solid does not immediately reach the temperature of the fluid or the imposed function.

To compare the model's displacement with the real one, the temporal triangulation data of the topographic targets present on the dam crown are used. The monitoring data are contained in the file "*Stazionetot_coronamento2021.xsls*", and in particular, we focus on segment 11 since it is positioned in the central part of the crown, the area most likely to be affected by the displacements. From the Excel analysis of the topographic data, it can be seen that the following displacements occurred, considering a time period of one year:

	Maximum Abs. Displacement in y *[mm]*	Time Period
Upstream	17.802	16 Aug. 2021 – 18 Aug. 2021
Downstream	15.976	10 Jan. 2022 – 12 Jan 2022

Table 3.4.1: Displacement of topographic target of the Ponte Cola Dam

As can be seen, by comparing the model results with the monitoring data, the displacements are of the same order of magnitude, confirming the correct application and operation of the software for the resolution of this type of analysis. An important factor to consider is that the displacements along the *x*-axis in the model are not directly comparable to those of the real dam in terms of axis direction. The dam in fact is actually rotated with respect to the reference system used in the model. This aspect will be addressed later, once the dam-terrain model has been constructed.

4. Modelling of Ponte Cola dam and surrounding environment

In this chapter, the results from the preliminary analysis previously presented will be used, the process of generation of the soil starting from a Digital Terrain Model (DTM) will be described. This will be followed by the construction of the dam solid based on curves derived from the original documentation. A fundamental step is the georeferentiation of the dam model with the real-word location and respect to the contour lines extracted from the DTM. Different software such as QGIS, AutoCAD 3D and Midas FEA NX, are used for this purpose. To complete the model, the thermal and mechanical calibrations need to be performed in order to produce a model comparable with reality.

4.1. Soil model construction

The construction of the soil model starts with downloading the raster file containing the Digital Terrain Model (DTM) from the web portal of the Lombardy region, which has a resolution of 5 $m \cdot 5$ m. The software QGIS was used to manage this file, allowing for the overlay of a preloaded *Google Hybrid* layer to better understand the correct positioning of the dam in relation to the entire Lombardy region. In Figure 4.1.1, the overlap between the two layers is shown, along with the DTM layer modified using the *Hillshade* tool to better understand the terrain's conformation.

Figure 4.1.1: Hillshade DTM tool and Google Hybrid layer in QGIS.

To crop the raster file to the area of interest, the layer must be selected and applied on it the command *Crop raster from Extension*, by specifying the input layer and drawing on the map, it is possible to crop the desired area.

The use of QGIS is crucial for extracting the contour lines, which provide information about the elevation of the area. To extract them, the tool *Raster – Extract – Contour lines* is used, paying attention to mark the option *Produce 3D Vector*. In Figure 4.1.2, are shown the contour lines in presence of the dam and with the level of the water in the reservoir, while in Figure 4.1.3, the modified contour lines without the dam and the water level are shown.

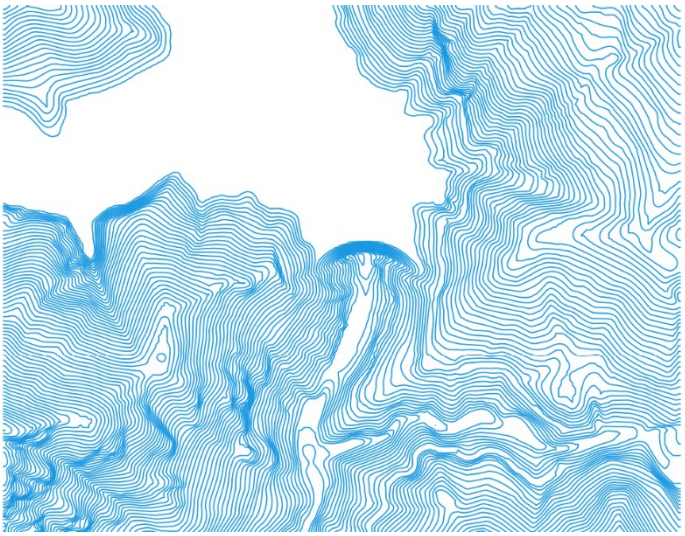

Figure 4.1.2: Original contour lines with dam and water in the reservoir

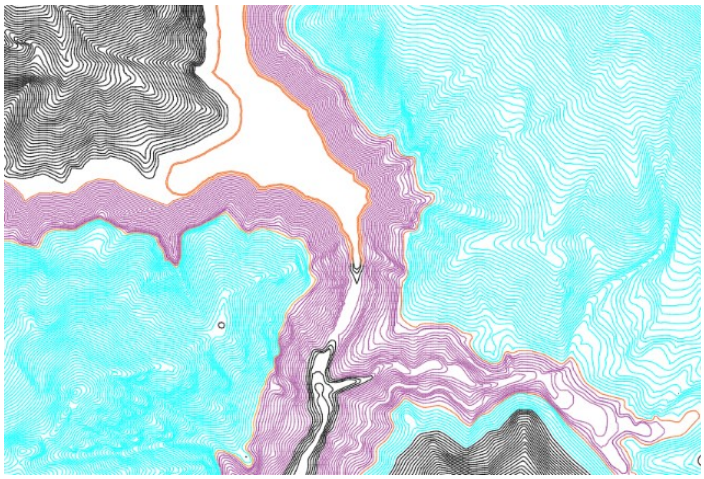

Figure 4.1.3: Modified contour lines without dam and water in the reservoir

4.1.1. Georeferentiation of dam curves and soil

Once the contour lines are extracted and modified, the curves of the dam are imported into QGIS for georeferencing. To do it, is fundamental the presence of the *Google Hybrid* layer in order to move directly the curves in the corresponding position of the dam from satellite. The *Georeferencer* tool is used to perform this step and results can be seen in Figure 4.1.1.1 .

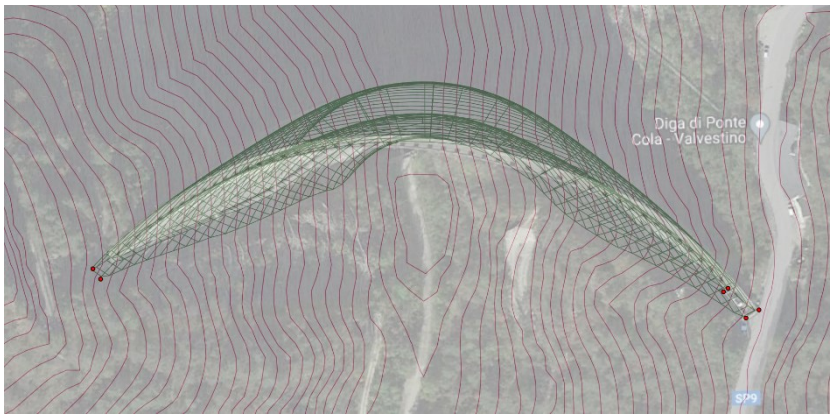

Figure 4.1.1.1: Dam georeferenced respect to the contour lines

The contour lines and the curves of the dam are now properly georeferenced in the coordinate system *EPSG: 32632 – WGS84 / UTM zone 32 N*. However, this reference system is not suitable for creating the model, due to the fact that the extension of the area is too big to be managed in Midas. In fact, using these coordinates, the *Terrain Geometry Maker* tool crashes, giving an error related to terrain reconstruction. To solve this problem, the curves of the dam and the contour lines need to be imported separately, from QGIS to AutoCAD, through the *.dxf* extension of the files.

Working in the dam curves file in AutoCAD, also the contour lines are imported, and both are moved along XY directions till the origin of the reference system.

The next step is to import the files of the dam and the soil, separately into Midas, where the *Terrain Geometry Maker* tool will be applied to create a *.tms* file and generate the solid of the dam to finally join them.

4.1.2. Terrain Geometry Maker

The software Midas FEA NX allows users to directly import *.dxf* files with specific contour lines using the *Terrain Geometry Maker* tool. The tool requires a *.dxf* file for import. Once imported, the working area of the tool must be explicitly defined by specifying the size of the area, the corners of the domain and the number of sampling points in *x* and *y* directions, exporting at the end a *.tms* file.

The tool allows to import this file, creating a surface that will be used to generate the solid of the terrain. Once imported the dam in Midas, it is possible to determine the right position of the terrain and the dam in order to cut part of the terrain to reduce as much as possible the domain of analysis.

The first step to creating the terrain solid is to make the rectangular base of a parallelepiped with the same dimensions of the chosen domain. As shown in Figure 4.1.2.1, the *Extrude* tool can be used to extrude the base in the *z*-direction, paying attention to make the parallelepiped higher than the maximum elevation of the terrain, in order to intersect all points.

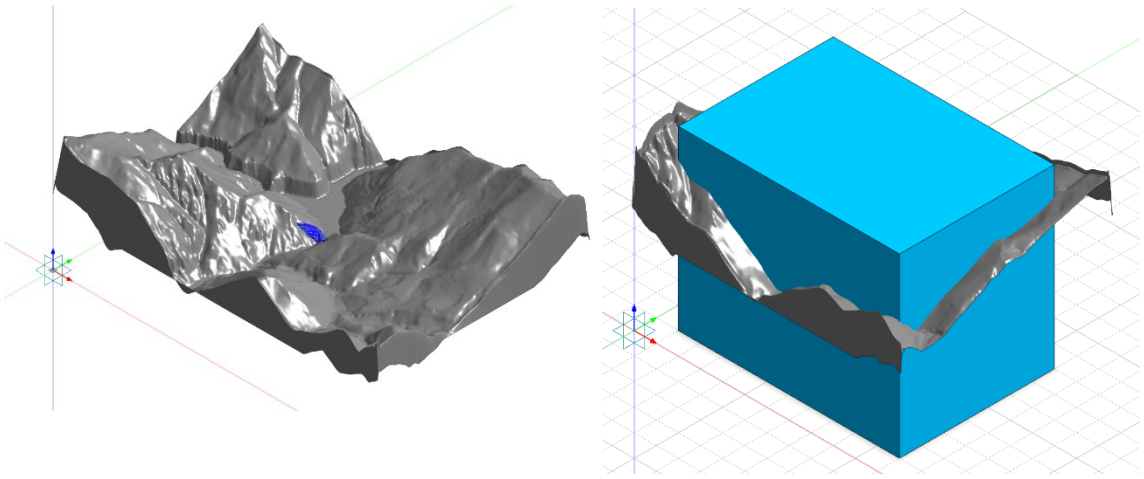

Figure 4.1.2.1: Terrain surface and extruded parallelepiped in Midas

The second step is to divide the parallelepiped using the *Divide – Solid* tool, splitting it into two parts: the top part, which can be deleted and the bottom part characterized by the terrain's conformation. Figure 4.1.2.2 shows the bottom part of processed parallelepiped and the dam curves.

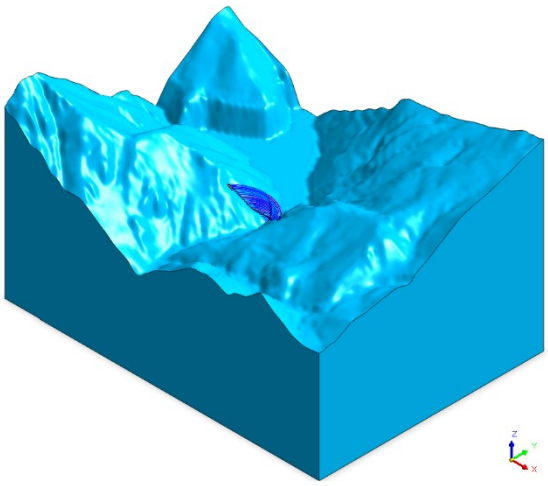

Figure 4.1.2.2: Terrain solid and dam curves

4.2. Dam Model Construction

The reconstruction of the dam solid is crucial for the next analysis. Starting from the *.dxf* file, georeferenced with respect to the terrain, it is possible to import it directly in Midas, ensuring that the curves are imported as arches and not as polylines. As shown in Figure 4.2.1, the first step involves creating shared surfaces between the different blocks of the dam and the creation of those surfaces that will form the more geometrically complex solids.

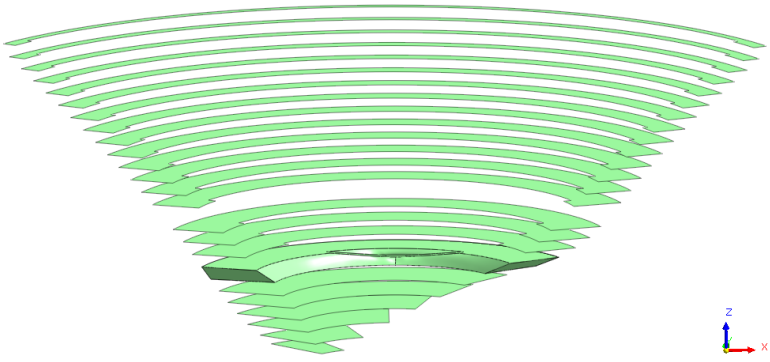

Figure 4.2.1: Shared surfaces of the dam blocks

The second step consists in the application of the *Protrude – Loft* tool, which creates a shell or solid by connecting the selected sections in order of selection based on their shapes. For the geometrically more complex parts of the dam, it was decided to create the solid by creating all the faces with the *Make Face* tool and joining them to form a solid using the *Sew* tool. It is crucial to check the connections between different solids during these steps, applying alternately *Autoconnection – Imprint* and *Check Duplicates* tools. Figures 4.2.2 e 4.2.3 illustrate these steps, including the decision to *Fuse* together different blocks of the dam in order to have the correct connection between all the dam solids.

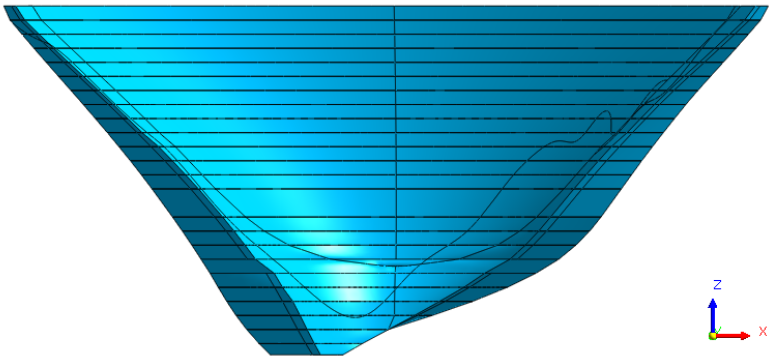

Figure 4.2.2: Dam solid

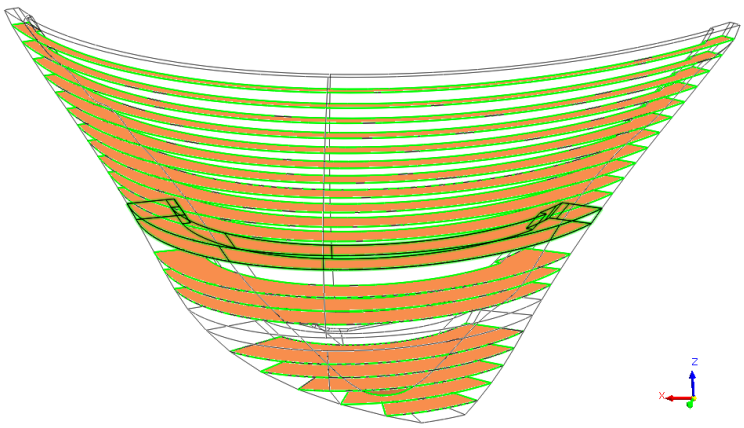

Figure 4.2.3: Connected surfaces with Check Duplicates tool

4.3. Dam - Terrain Connection

The connection between the dam and terrain is directly made in Midas by using the *Boolean – Embed* tool, which removes the portion of the dam that intersects with the terrain, embedding it into the terrain model. The next step is the connection of the dam with the modified terrain model, to do it is possible to apply as before the *Autoconnection – Imprint* tool and the *Check Duplicates* tool in order to verify the contact surfaces, as shown in Figure 4.3.1 .

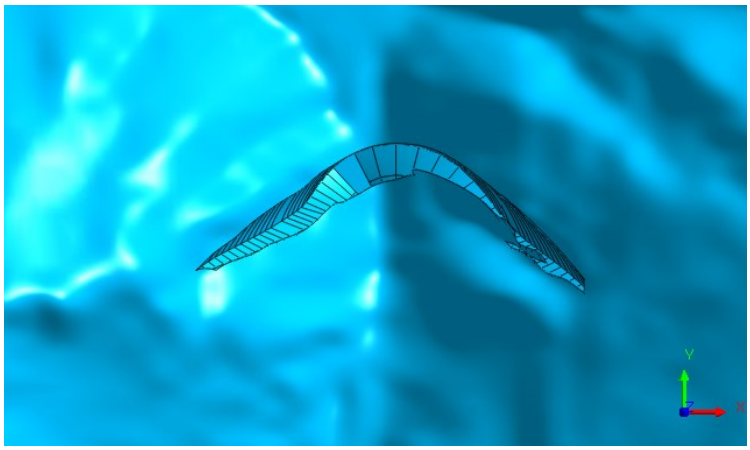

Figure 4.3.1: Part of the terrain removed with the embed tool

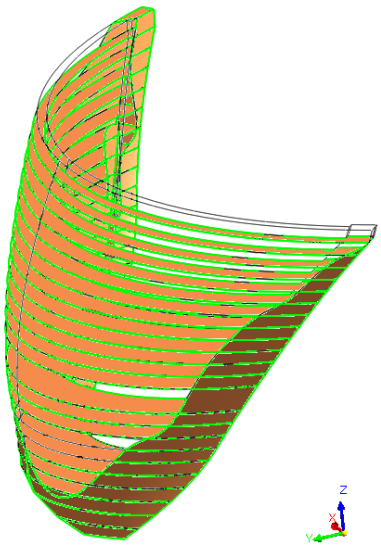

Figure 4.3.2: Connected surfaces between dam and terrain

4.4. Material properties and Mesh creation

Once the solids of the terrain and the dam are created, it is possible to assign the material properties that compose the system. In particular, only two materials are used: reinforced concrete and rock. This choice is due to the fact that the available data about the stratigraphy are not representative of the environment surrounding the dam. Some of the material properties derive from the official documents of the dam, while the thermal parameters are initially taken in accordance with A. A. Abdulzareg (2014). These properties are shown in Tables 4.4.1 and 4.4.2.

Concrete	
Elastic Modulus *[kN/m^2]*	$3 \cdot 10^7$
Poisson's Ratio *[-]*	0.2
Unit Weight *[kN/m^3]*	25.8
Thermal Coefficient *[1/T]*	$1 \cdot 10^{-5}$
Conductivity *[W/(m · (T)]*	2.309
Specific Heat *[J/(ton · [T])]*	1080000

Table 4.4.1: Concrete properties

Terrain	
Elastic Modulus *[kN/m^2]*	$4.4 \cdot 10^7$
Poisson's Ratio *[-]*	0.3
Unit Weight *[kN/m^3]*	27.6
Thermal Coefficient *[1/T]*	$1.4 \cdot 10^{-6}$
Conductivity *[W/(m · (T)]*	1.62
Specific Heat *[J/(ton · [T])]*	800000
Cohesion *[kN/m^2]*	600
Friction Angle *[°]*	40

Table 4.4.2: Terrain properties

Once the materials have been created, they can be assigned to the properties, which are necessary to differentiate the dam mesh from that of the ground. The mesh of the dam solids is much more detailed, being both the thermal sensors and the topographic targets

on it, therefore choosing an average mesh size of 2.5 *m*. As for the terrain mesh, it was created coarser since it has a limited thermal and mechanical influence on the dam, therefore is used an average mesh size of 70 *m*. The two meshes are shown in Figure 4.4.1.

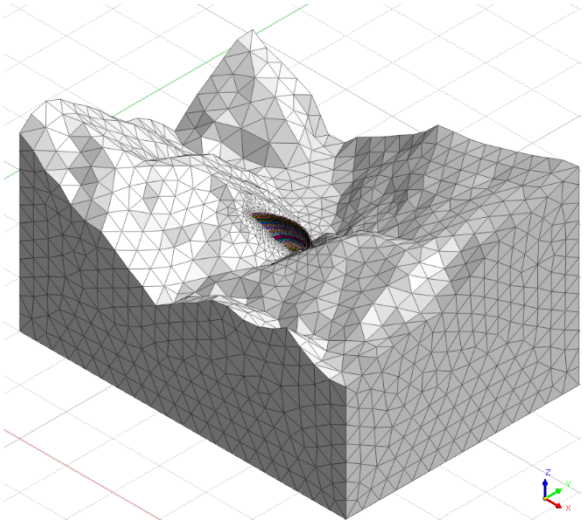

Figure 4.4.1: Dam and terrain meshes

In this step it is essential to identify and, if necessary, to modify the nodes of the model that correspond to the sensors in reality, of which we have the monitoring data in terms of temperature and displacement.

The nodes related to the thermal sensors are six in total, two groups of three nodes, positioned on the surface in contact with water, air and one in the middle of the concrete at the elevations of 440 *m a.s.l.* and 490 *m a.s.l.*. The positions of them are shown in Figure 4.4.2 and Figure 4.4.3, in Table 4.4.3. and Table 4.4.4 .

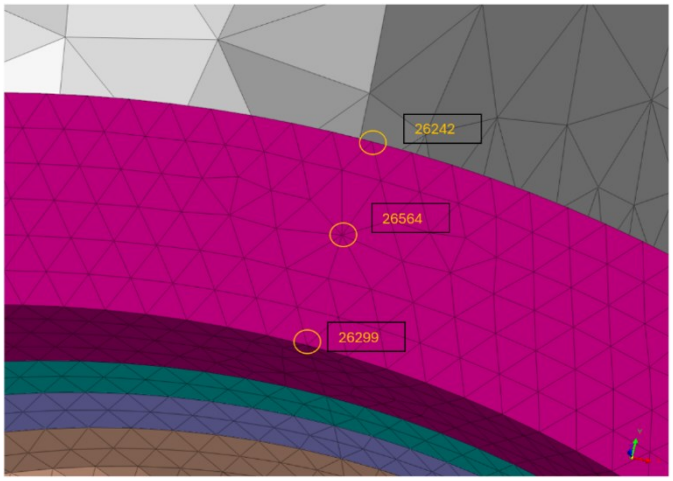

Figure 4.4.2: Nodes position at 440 m

Node ID		x	y	z
1	26299	1300.65	903.103	440
2	26564	1301.06	910.202	440
3	26242	1301.42	916.234	440

Table 4.4.3: Nodes coordinates at 440 m

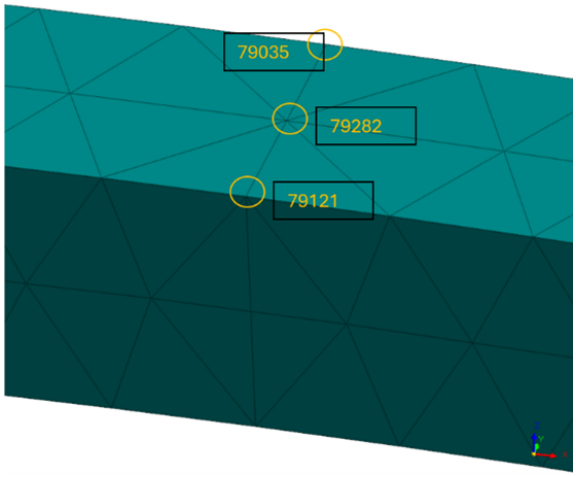

Figure 4.4.3: Nodes position at 490 m

Node ID		x	y	z
3	79121	1300.17	894.796	490
4	79282	1300.35	897.74	490
5	79035	1300.51	900.708	490

Table 4.4.4: Nodes coordinates at 490 m

4.5. Boundary conditions

The boundary conditions are fundamental in a Finite Element model, they define how the model interacts with the surrounding environment or with other parts of the system. Their presence is fundamental in order to ensure that FEM results are realistic and correct with respect to the physical context of the problem.

All translation in x, y and z directions of the bottom of the domain are neglected by imposing a hinge constraint, as can be seen from the Figure 4.5.1..

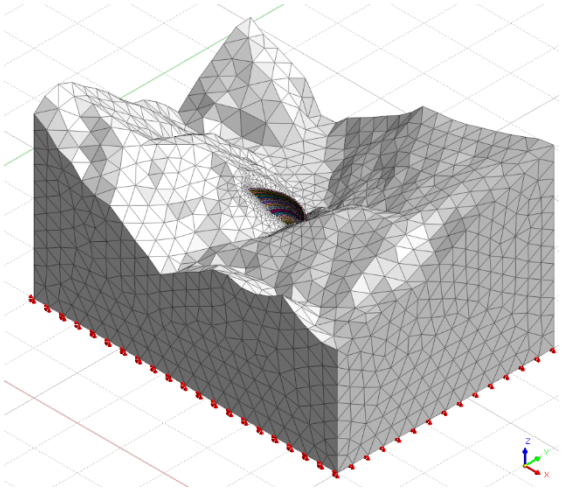

Figure 4.5.1: No translations of the bottom

$$Tx = Ty = Tz = 0$$

The translations along the *y* direction are neglected in the downstream and upstream face using a roller constraint, as it is shown in Figure 4.5.2 .

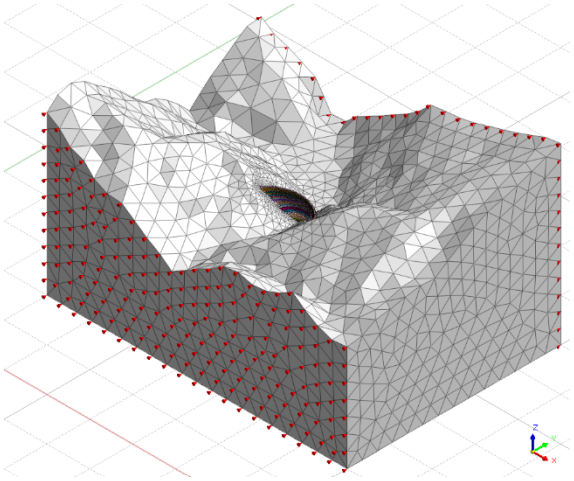

$$Ty = 0$$

Figure 4.5.2: No translations in y direction

The same kind of constraint is applied along the x direction, on the lateral faces of the terrain solid, as it is shown in Figure 4.5.3 .

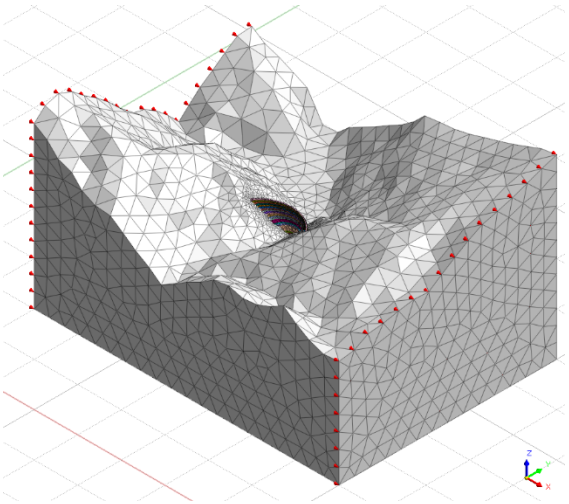

$$Tx = 0$$

Figure 4.5.3: No translations in x direction

4.6. Thermal Calibration of the Model

Thermal calibration of the model allows to improve the accuracy of simulations so that the thermal results obtained by the model are as similar as possible to those monitored in reality. This is possible by experimenting with different values of thermal parameters, starting from the values found in literature and varying the value at each test, until the optimal match is found. The parameters that influence this type of calibration are thermal conductivity and the specific heat of materials.

To proceed with thermal calibration, it is necessary to choose a monitoring period to extract the initial temperatures of the model and subsequently compare the results of the thermal calibration. The chosen analysis period goes from 01/03/2021 to 29/04/2021, processing the temperature data in order to obtain daily averages to streamline the computational burden of the model. Below in Figure 4.6.1, it is possible to observe the trend of the temperatures monitored in this period in the sensors immersed in the concrete at an elevation of 440 *m a.s.l.* and 490 *m a.s.l.*.

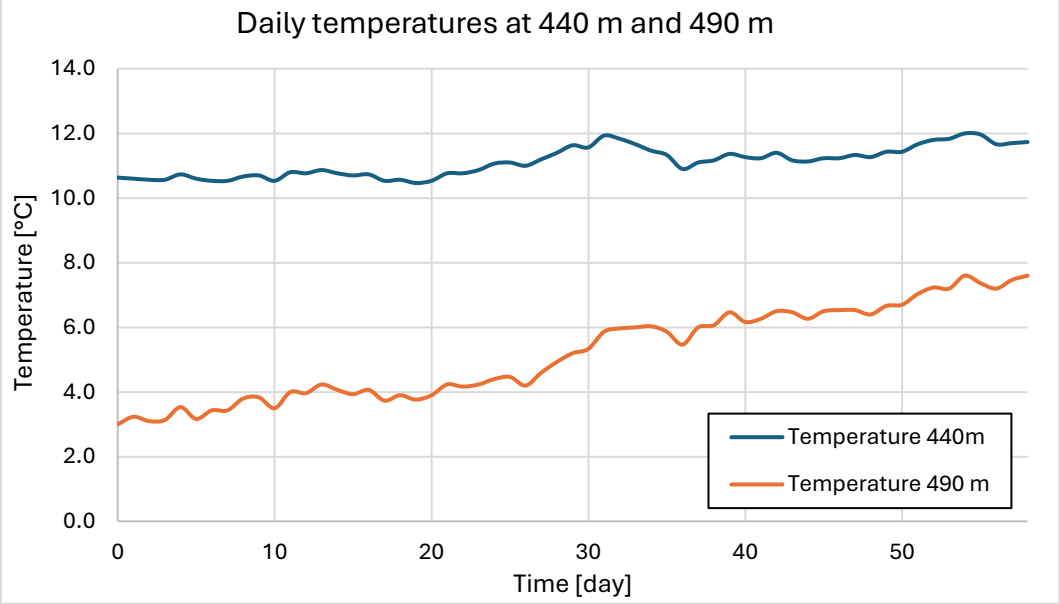

Figure 4.6.1: Daily temperatures

For the sake of brevity and to avoid repeating numerous graphs, only the most relevant tests for calibration purposes will be reported, however the complete results are available upon request.

4.6.1. Prescribed temperature application

To proceed with the thermal calibration, it is necessary to apply all the thermal loads to the model. One of the fundamental things for the study in steady-state condition and preliminary for a transient analysis is the application of the prescribed temperatures to the model, values known in specific nodes of the model, deriving from monitoring, which allow to start from conditions as similar as possible to the reality.

The setup to perform the thermal calibration is made of three steps, a steady-state analysis and two transient analyses. In the steady-state analysis the prescribed temperature applied to the terrain and dam body are considered. To satisfy the heat continuity between the dam and the terrain, the temperature of the nodes of the dam below 440 *m a.s.l.* and all the nodes of the terrain are assumed to be at the initial temperature of 10.63 *°C*, equal to the temperature of the concrete at 440 *m a.s.l.* on the day zero of the analysis, as shown in Figure 4.6.1.1 .
Then we proceed with the application of the prescribed temperature on the nodes of the dam at an elevation higher than 440 *m a.s.l.*, applying an initial temperature of 3 *°C*, which corresponds to the temperature of the concrete at 490 *m a.s.l.* on the day zero of the analysis. In Figure 4.6.1.2 the nodes affected by this temperature are shown.

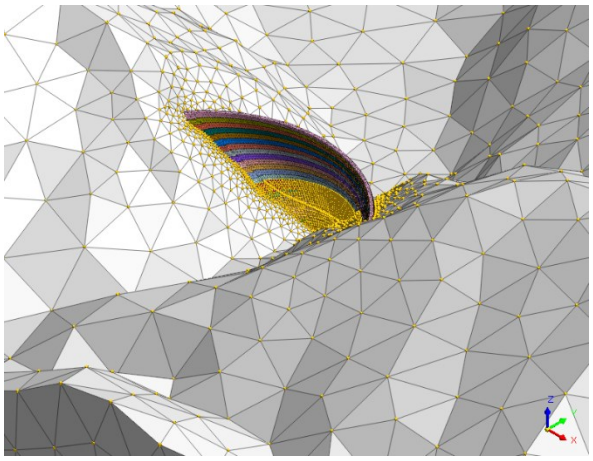

Figure 4.6.1.1: Prescribed Temperature of 10.63 °C

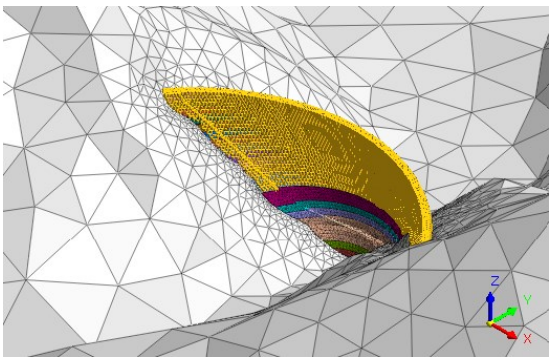

Figure 4.6.1.2: Prescribed Temperature of 3 °C

4.6.2. Convection application on the faces

To simulate the heat transfer between the body surface and the surrounding fluid, such as water or air in our case, the *Convection* tool is used to apply the heat flux across mesh faces. The 440 *m a.s.l.* height allows us to distinguish the parts of the model that are always in contact with the water, from those that are occasionally or never in contact with the water located at higher heights. This is not only valid for the dam but also for the surrounding terrain, to consider this therefore, before applying the real water table level, a rectangular surface of the same dimensions as the model is built and brought to a height of 440 *m a.s.l.* in order to understand the faces affected or not, by the water table level. In Figure 4.6.2.1 is shown the surface representing the level of 440 *m a.s.l.*.

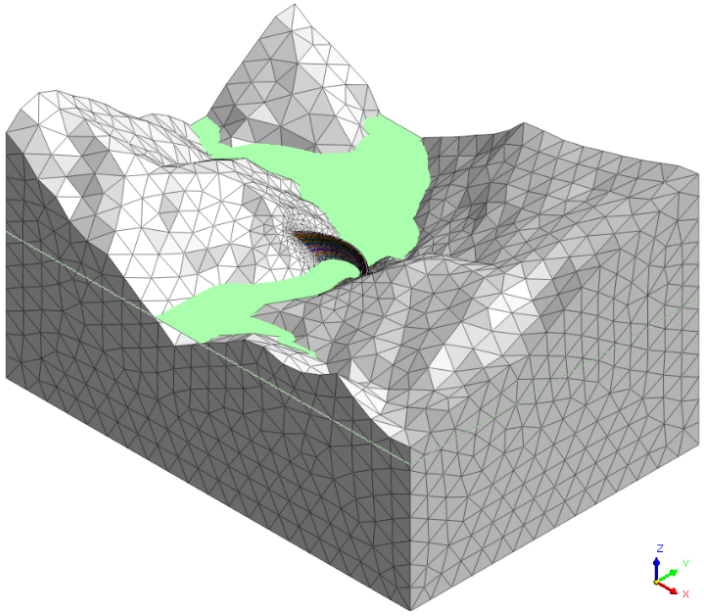

Figure 4.6.2.1: Surface simulating the level of 440 m

The first transient analysis is required to allow the nodes in contact with the water and air to reach the realistic value before applying the temperature function along two months of analysis. This step is necessary because, particularly at 440 *m a.s.l.* where the dam is thicker, it requires more time to be influenced by external temperatures and reach equilibrium.

In the model, two different convection conditions are applied, both based on temporal but constant temperature functions, applying an unchanged temperature for a period of 7 days.

The first convection is applied to all the *3D Element Faces* of the model in contact with the water, applying a constant temperature of 4.90 *°C*, equal to the temperature measured by the sensor in the water placed at 440 *m a.s.l.* on day zero of the analysis.

The second convection is applied to all the *3D Element Faces* that are in contact with the air, applying a constant temperature of 9 *°C*, which is equal to the average temperature measured by the sensors available on the face of the dam exposed to the air on day zero of the analysis. Figures 4.6.2.1 and 4.6.2.3 show the temperature behavior in the nodes used for calibration. It is possible to observe how the application of this transient step allows to reach the temperature of the imposed function and to get closer to the values of internal nodes on the day zero of the analysis.

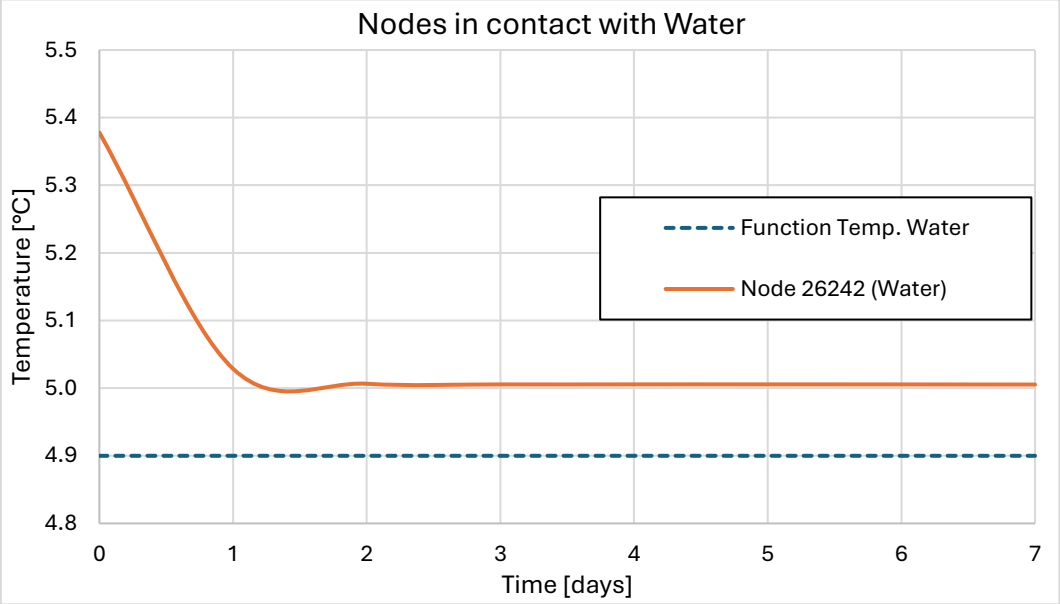

Figure 4.6.2.2: Temperatures behavior after first water convection

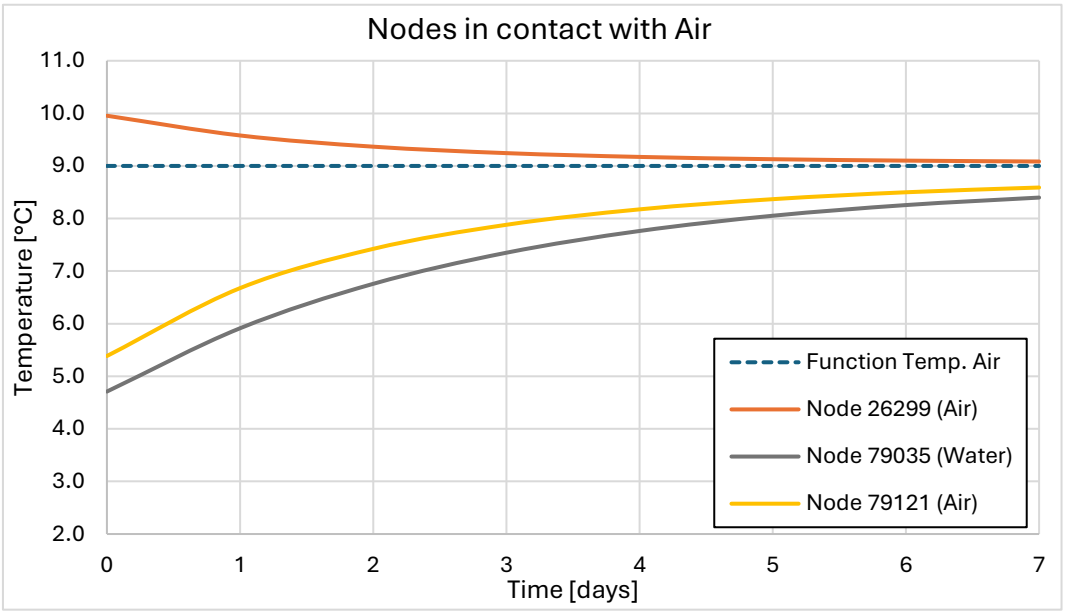

Figure 4.6.2.3: Temperatures behavior after first air convection

The last transient analysis is carried out by applying the water and air temperature values averaged daily from 01/03/2021 to 29/04/2021 through the convection applied in the same faces of the previous analysis. The faces subjected to convection can be seen in Figure 4.6.2.4 and Figure 4.6.2.5 .

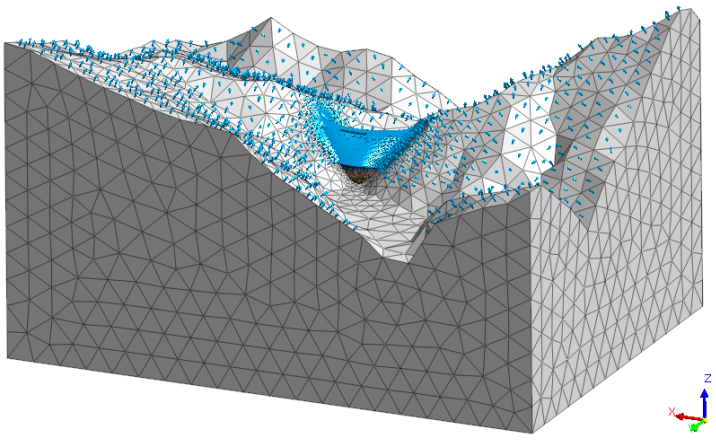

Figure 4.6.2.4: Convection applied to the faces in contact with air

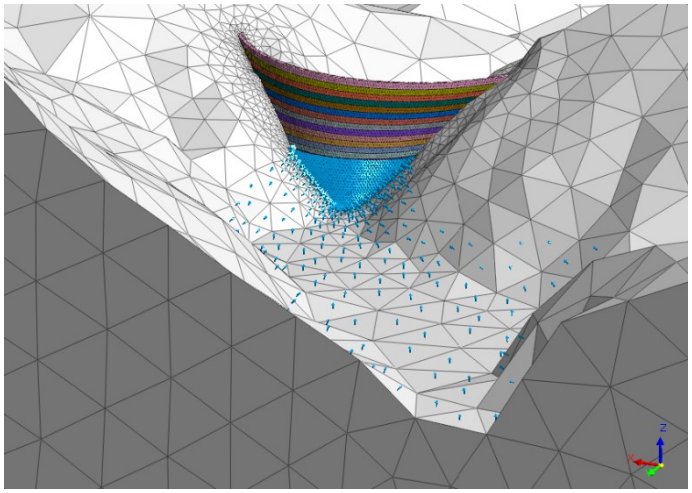

Figure 4.6.2.5: Convection applied to the faces in contact with water

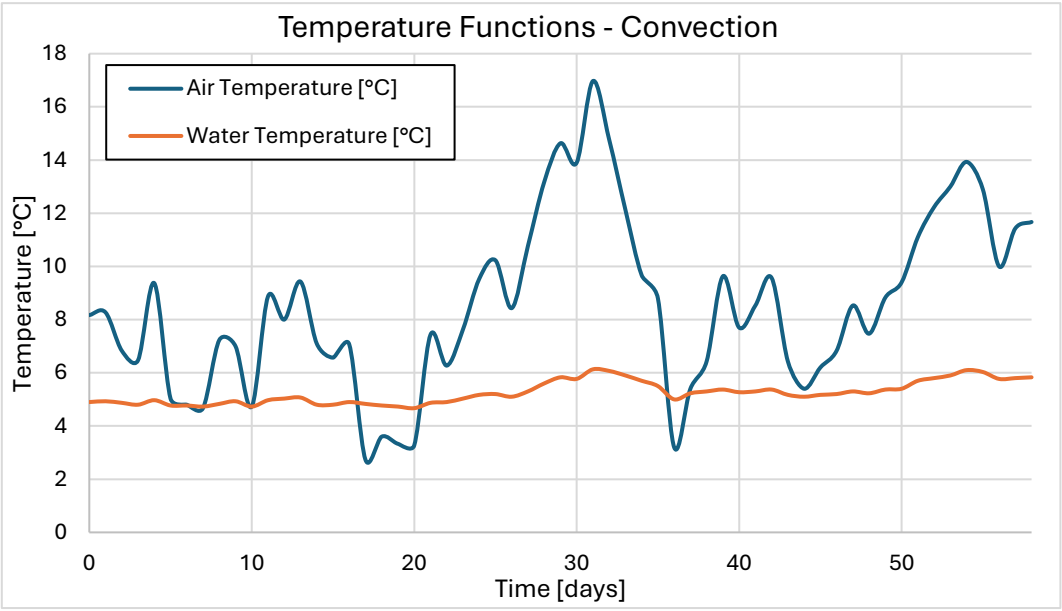

Figure 4.6.2.6: Temperature functions applied with Convection tool

During the application of the *Convection* Midas requests for a *Film Coefficient*, also called heat transfer coefficient, which represents the proportionality constant between the heat flux and the thermodynamic driving force for the flow of heat. A higher value of it permits the heat to move faster between the surface and the surrounding fluid, allowing the solid heating or cooling in a faster way. The values depend on the type of material and of the fluid, for convection between concrete (or terrain) and air is assumed equal to 25 $W/m^2 \cdot K$, while the one used for the convection between concrete (or terrain) and water is higher and equal to 570 $W/m^2 \cdot K$.

4.6.3. Calibration Results

In total, eight calibration tests were performed on the concrete, the first five by varying the thermal conductivity, while the last three using the calibrated conductivity value and varying the specific heat. The parameters used in each test are summarized in Table 4.6.3.1 below:

Test	Conductivity *W/(m · (T)*	Specific Heat *J/(ton · [T])*
1	2.309	$1.08 \cdot 10^6$
2	23.09	$1.08 \cdot 10^6$
3	0.2	$1.08 \cdot 10^6$
4	1.8	$1.08 \cdot 10^6$
5	1.6	$1.08 \cdot 10^6$
6	1.6	$1.08 \cdot 10^7$
7	1.6	$1.08 \cdot 10^5$
8	1.6	$9 \cdot 10^5$

Table 4.6.3.1: Thermal calibration parameters

To evaluate the accuracy of the model with respect to the monitored data, the RMSE has been calculated in MATLAB for each test. The RMSE (Root Mean Square Error) is a measure of the prediction errors, how far the predicted values are from the actual values. The lower the RMSE, the better the model's accuracy and it means the model results are closer to the real values.

$$\mathrm{RMSE} = \sqrt{\frac{1}{n}\sum_{i=1}^{n}(y_i - Y_i)^2}$$

In the equation the y_i are the concrete monitored data and the Y_i are the results of the model. In the next Table 4.6.3.2 are shown the RMSE of the nodes at 440 *m a.s.l.* and 490 *m a.s.l.* for each test.

Test	RMSE 440 *m* [°C]	RMSE 490 *m* [°C]
1	1.4808	0.7304
2	3.2402	3.5485
3	0.7495	2.1711
4	1.3313	0.4992
5	1.2680	0.4905
6	0.7326	2.3925
7	2.9065	3.7389
8	1.3672	0.5599

Table 4.6.3.2: RMSE results for nodes at 440 m and 490 m, in °C

In the first test, using the literature parameters, the temperatures behavior at the central node in the concrete was found to be consistent with those recorded by the sensors, although the node located at 440 *m a.s.l.* exhibited a certain difficulty in following the trend, as it was positioned in a thick section of the dam body and therefore much less sensitive to temperature variations than the node placed at 490 *m a.s.l.*. The graphs of the first test are shown in the Figure 4.6.3.1 and Figure 4.6.3.2 .

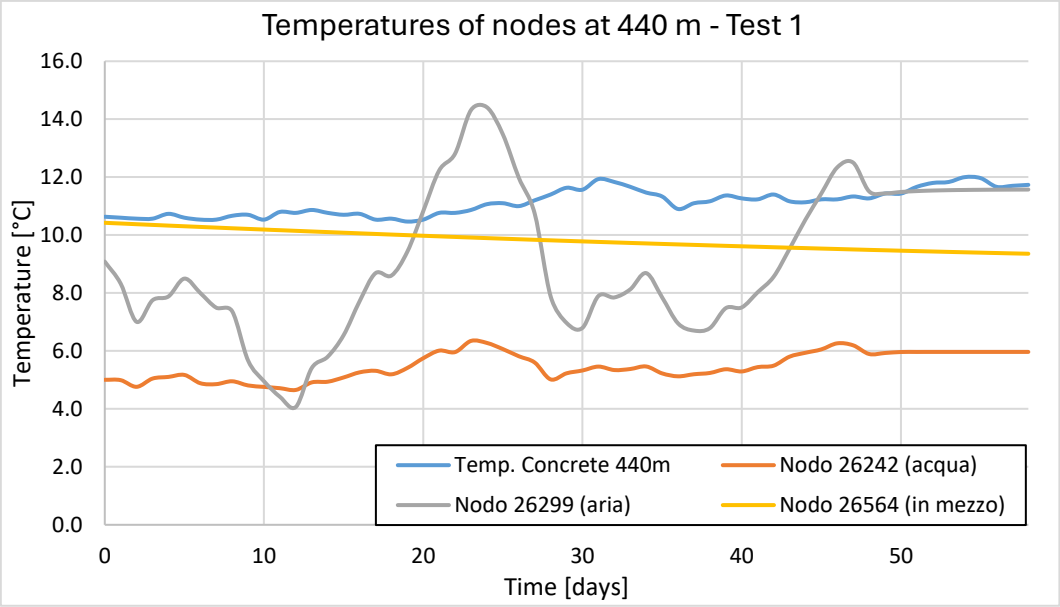

Figure 4.6.3.1: Temperature behavior at 440 m – Test 1

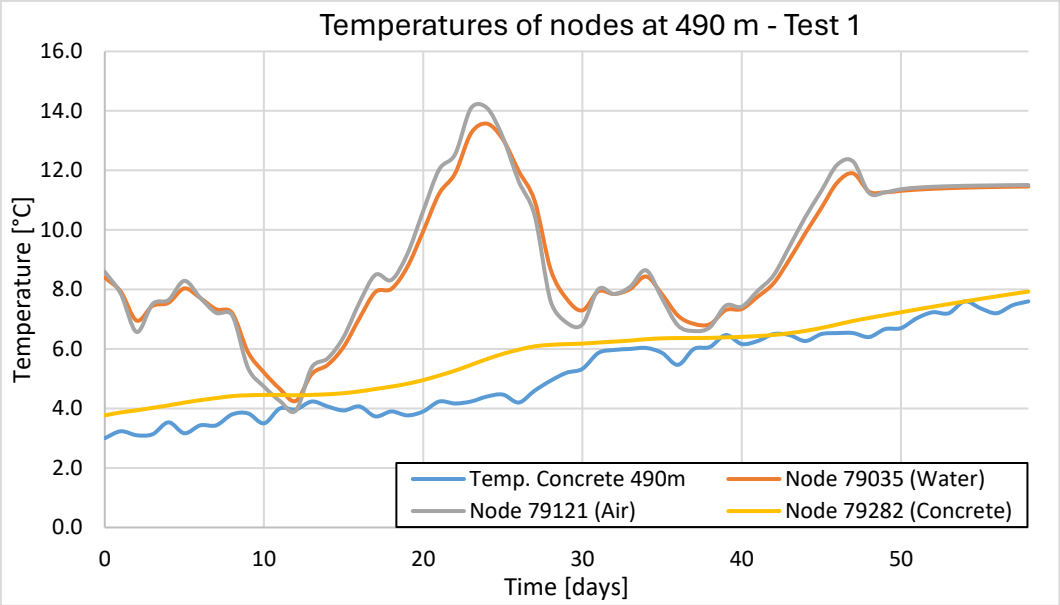

Figure 4.6.3.2: Temperature behavior at 490 m – Test 1

In test 2, the conductivity was increased by an order of magnitude to observe its influence on a complex model such as that of the dam-soil. The increase shows a greater sensitivity to temperature variations of the nodes positioned at the center of the dam. However, identifying large differences between the monitored and modeled data, as is shown in Figures 4.6.3.3 and 4.6.3.4 .

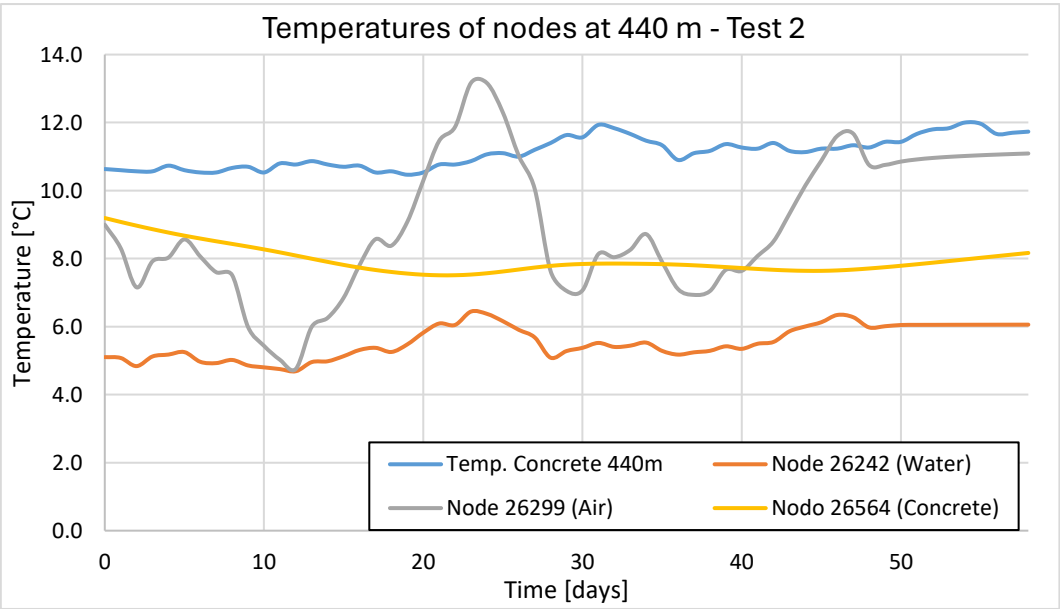

Figure 4.6.3.3: Temperature behavior at 440 m – Test 2

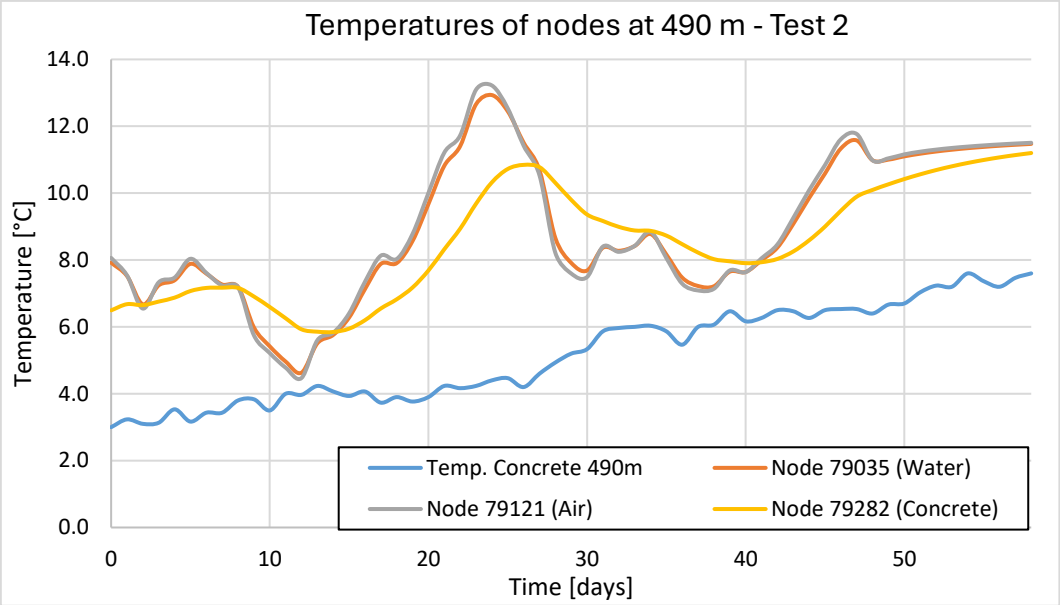

Figure 4.6.3.4: Temperature behavior at 490 m – Test 2

The test number 5 is the one that gave the best results in terms of RMSE, the behavior of the central node follows more ore less the behavior of the thermal sensor in the concrete at 440 *m a.s.l.*, the difference between the two series of data is very small, in the order of about 2 *°C*. The overlapping of the series of data at 490 *m a.s.l.* is improved respect to the previous tests, reaching the lowest value of RMSE of this calibration. The results of this test are shown in Figure 4.6.3.5 and 4.6.3.6 .

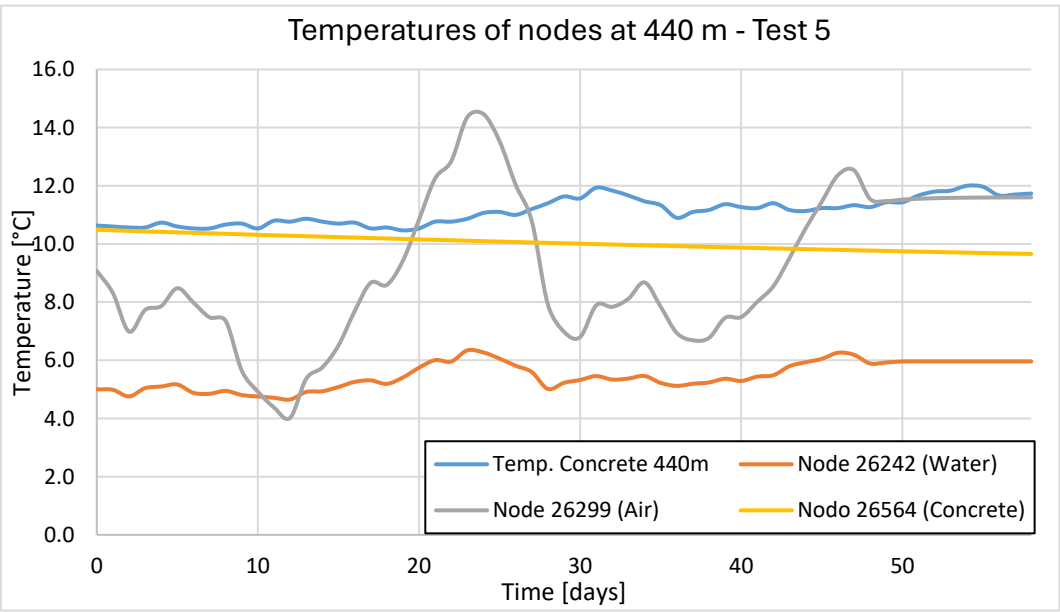

Figure 4.6.3.5: Temperature behavior at 440 m – Test 5

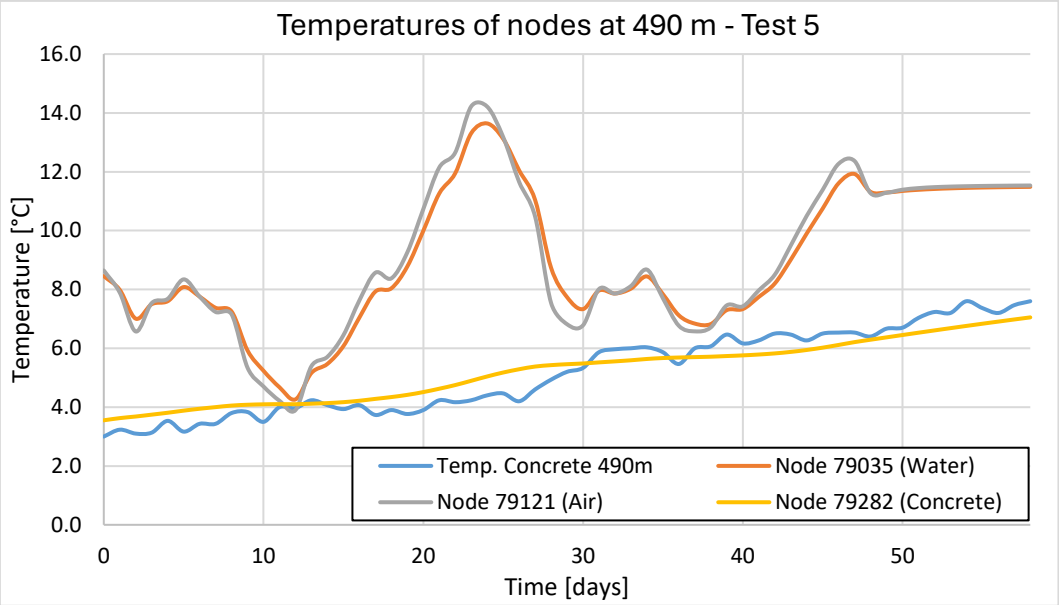

Figure 4.6.3.6: Temperature behavior at 490 m – Test 5

Once the conductivity value that best simulates the temperature trend in both sensors has been found, the specific heat is now calibrated. It is decided to show the Test 7, set with a very low specific heat value. In particular, the temperature trends in Figure 4.6.3.7 and 4.6.3.8 are observed, which show a marked difference between the monitored data and the model results in both the sensors.

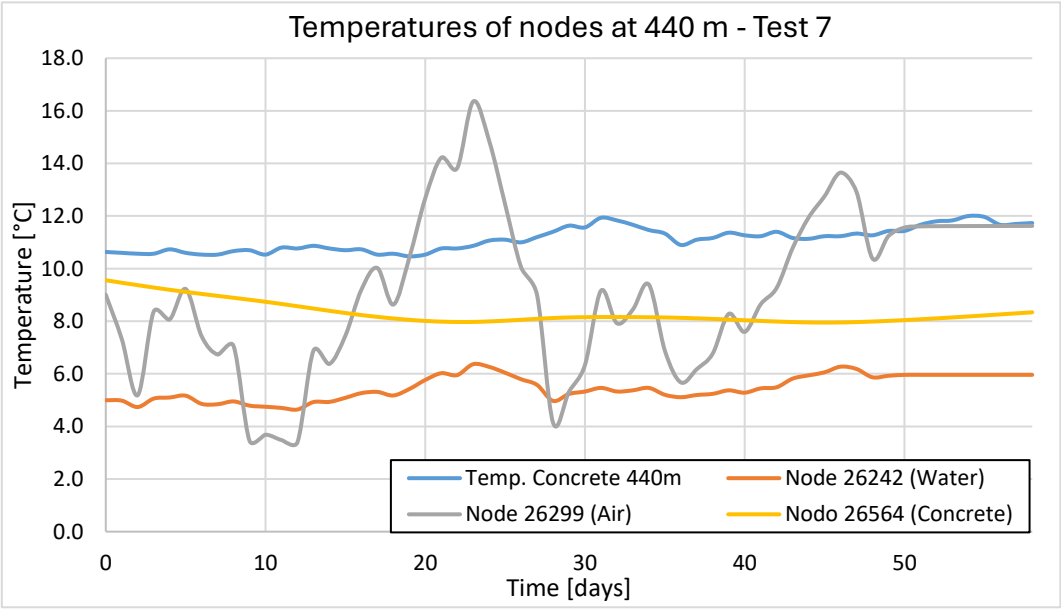

Figure 4.6.3.7: Temperature behavior at 440 m – Test 7

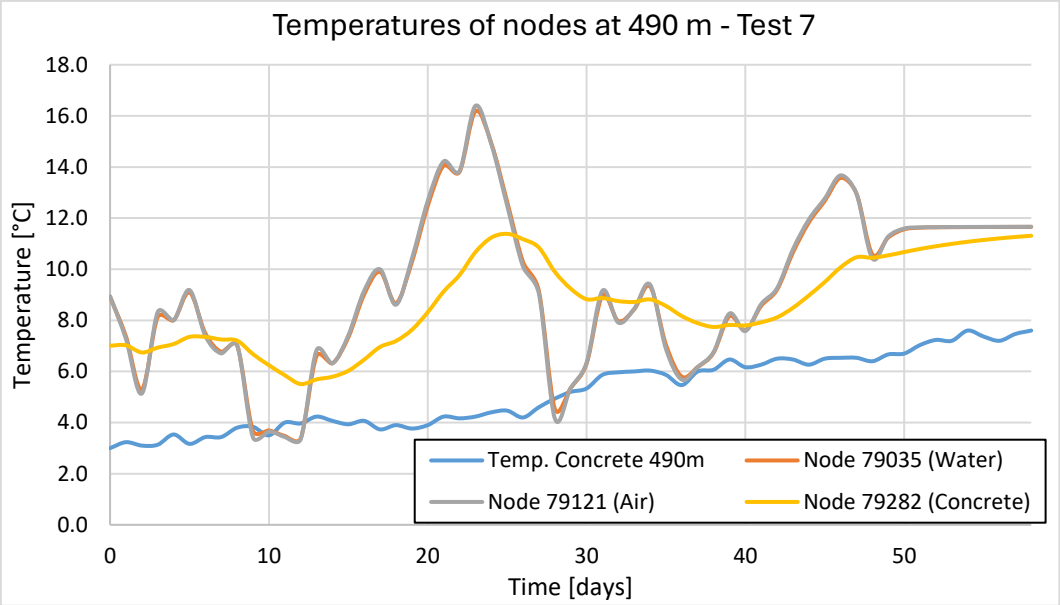

Figure 4.6.3.8: Temperature behavior at 490 m – Test 7

After comparing the most significant results, the model can be defined as thermally calibrated with the parameters used in Test 5, considering the low RMSE values for both the elevations and evaluating the behaviors of the modelled temperatures compared to those monitored by the sensors.

The following Figures show the temperature trends inside the dam and on the upstream face in contact with the water. Figures 4.6.3.9 and 4.6.3.10 show the day zero of the analysis, the effect of the application of the transient stage set applied for 8 days can be seen, which gradually brings the concrete to temperature.

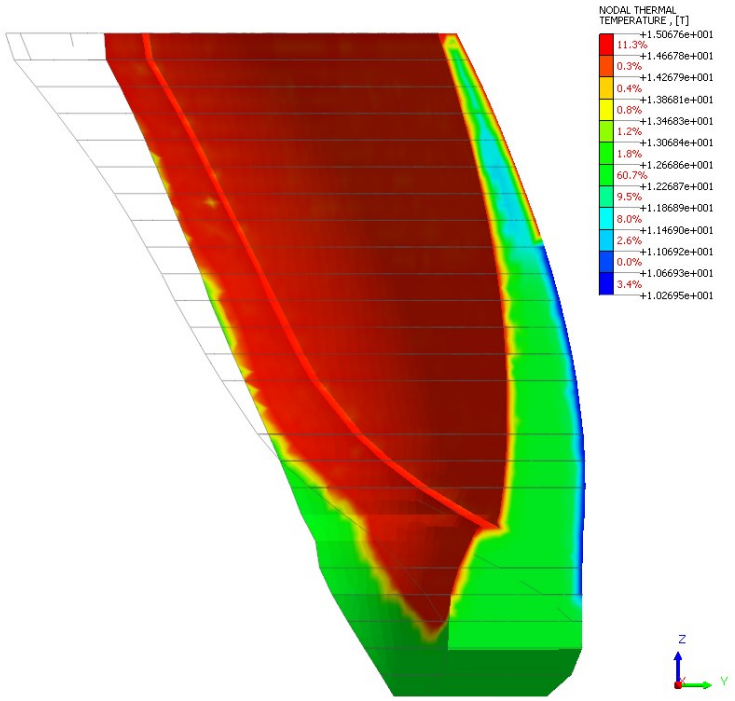

Figure 4.6.3.9: Temperature trend inside the dam – Day 0

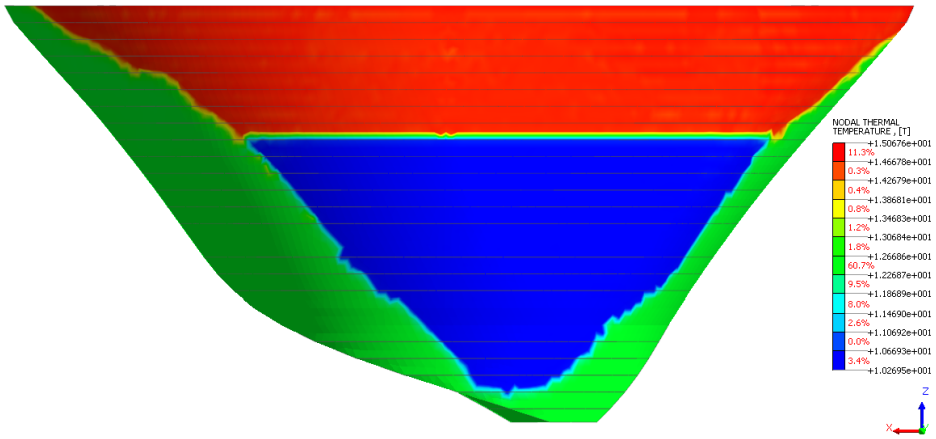

Figure 4.6.3.10: Temperature trend in the upstream face – Day 0

Considering the growth trends of both air and water temperatures, an increase in the internal temperature of the concrete is expected, highlighting however the dependence of the heat transfer on the thickness of the material. In fact, it can be noted how after 30 and 60 days, as the thickness of the dam body increases, the external influence of the temperature functions is increasingly less felt.

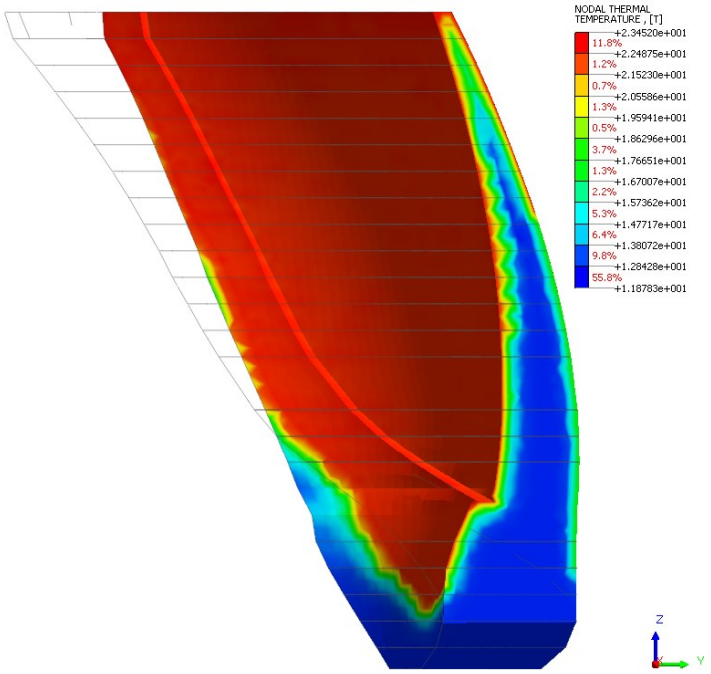

Figure 4.6.3.11: Temperature trend inside the dam – Day 30

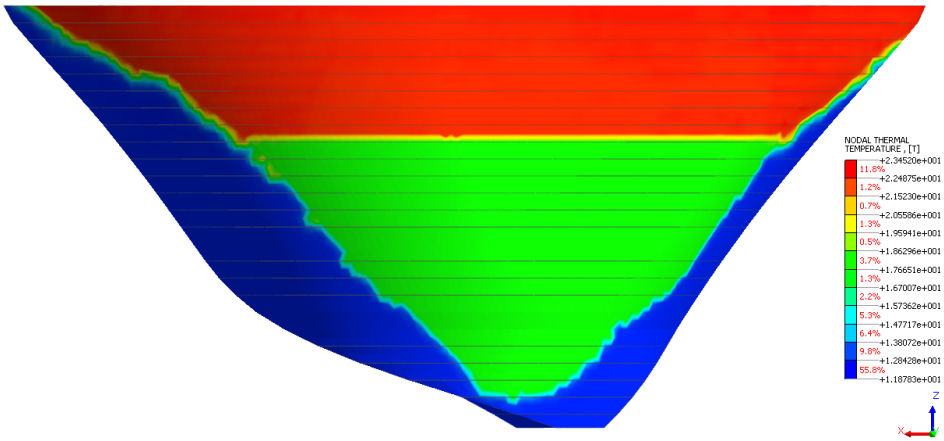

Figure 4.6.3.12: Temperature trend in the upstream face – Day 30

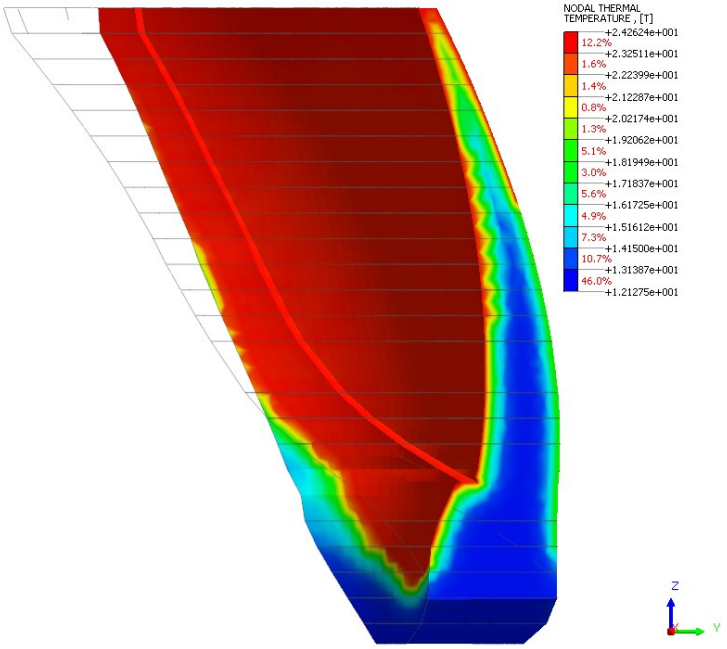

Figure 4.6.3.13: Temperature trend inside the dam – Day 60

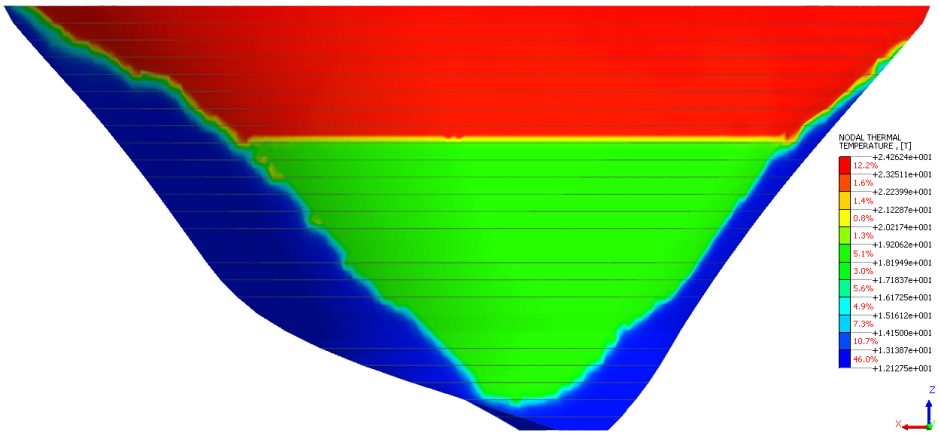

Figure 4.6.3.14: Temperature trend in the upstream face – Day 60

4.7. Mechanical Calibration

A mechanical calibration of the FEM model is necessary to ensure that the model simulates as best as possible the behavior of the real structure. This step allows us to adapt the displacement results of the model to the real ones, by modifying in each test a parameter responsible for the material response. In this calibration, the thermal expansion coefficient is varied, which has a direct impact on the displacements of the structure. The application of temperatures is identical to that of thermal calibration, obviously modifying the values with those of the chosen analysis period.

Prescribed Temperature Concrete at 440 m a.s.l.	Prescribed Temperature Concrete at 490 m a.s.l.	Convection constant temperature – Air	Convection constant temperature – Water
12.40 °C	11.27 °C	14.51 °C	10.27 °C

Table 4.7.1: Prescribed and convection temperatures applied in mechanical calibration

In this phase, six different models are studied, starting with values of the coefficient taken from literature, and changing time by time the values in order to improve the performance of the model respect to the monitored data.

The coefficient values tested in this step are summarized in the table below:

Thermal Expansion Coefficient *[1/T]*	Literature Test	Test 1	Test 2	Test 3	Test 4	Test 5
Concrete	$1 \cdot 10^{-5}$	$6.5 \cdot 10^{-6}$	$7 \cdot 10^{-6}$	$9 \cdot 10^{-6}$	$8 \cdot 10^{-6}$	$6 \cdot 10^{-6}$
Soil	$1.4 \cdot 10^{-6}$	$1 \cdot 10^{-6}$	$1.2 \cdot 10^{-6}$	$2 \cdot 10^{-6}$	$2.2 \cdot 10^{-6}$	$1.2 \cdot 10^{-6}$

Table 4.7.2: Thermal Expansion Coefficients used in the mechanical calibration

4.7.1. Rotation of reference systems

Mechanical calibration requires the comparison between monitored data of the topographic targets and the nodes results of the model. The two series are related to two different reference systems, the topographic targets are referred to the total station positioned in the keeper's house, while the nodes follow the reference system of Midas. The coordinates of the topographic targets are calculated as the yearly average and they are used to identify the position of the nodes in Midas model, later the appropriate nodes have been moved in order to be positioned as in the reality. To do it has been calculated the mutual distances between different targets and used CAD files containing the distances of targets from the keeper's house. In Figure 4.7.1.1. are shown the targets in the model at the elevations of 440 *m a.s.l.* and 505 *m a.s.l.*.

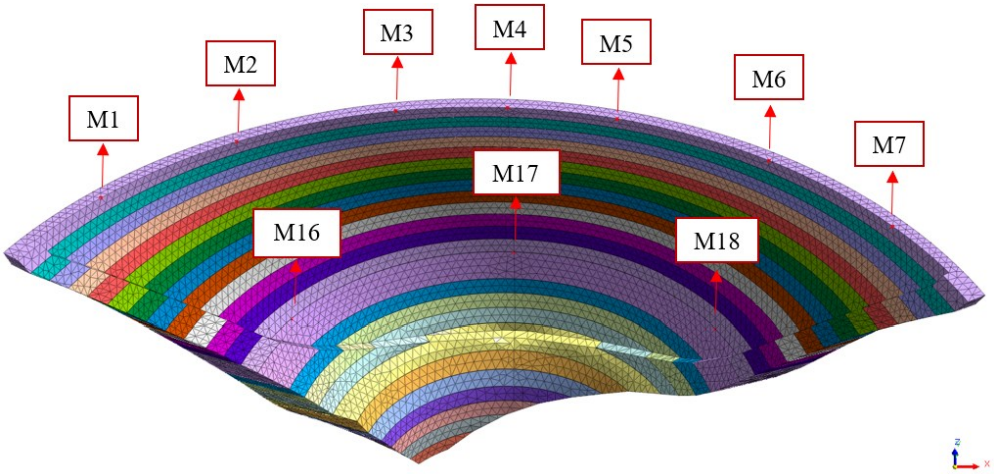

Figure 4.7.1.1: Positions of nodes representing target of the dam

One of the first problems is the positioning of the targets with respect to the model nodes. In Figure 4.7.1.2 is shown the different orientation of the targets respect to the model nodes and vice versa.

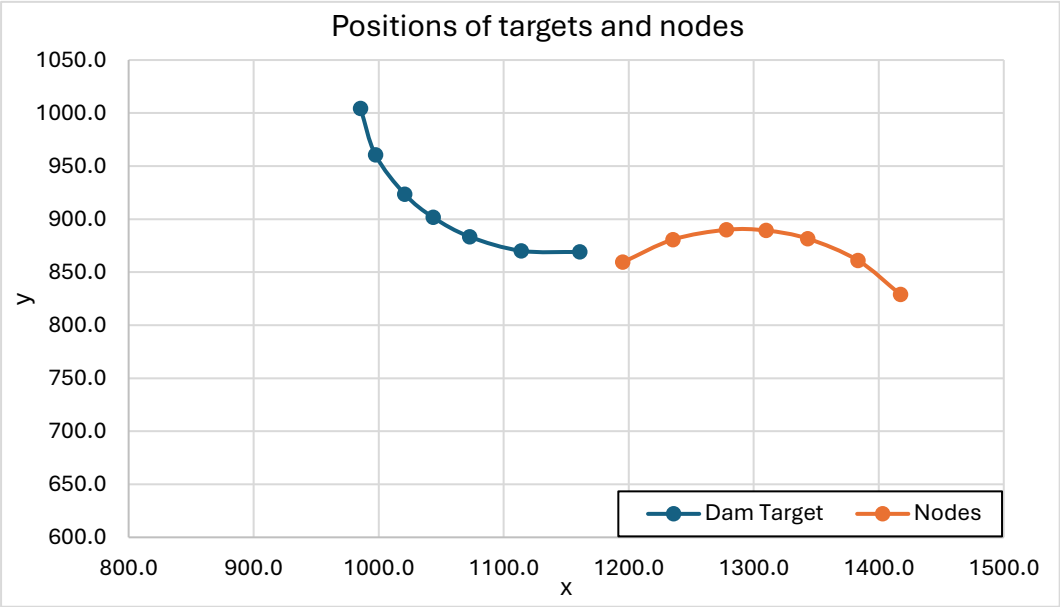

Figure 4.7.1.2: Positions of topographic targets and model nodes

To align the data series to a third reference system, a rotation of coordinates is applied to each series, so they are all aligned to the common reference system. This reference system is oriented to have the *x*-axis pointing conventionally to the right of the dam, the *y*-axis in the upstream direction and the *z*-axis in the vertical direction.

The rotation angles are different for the two data series, in order to calculate them a MATLAB script has been implemented to determine the rotation angles with respect to the horizontal direction. The script takes into account the line segment connecting targets M1 and M7, positioned at the extremities of the dam crest.

The results of the MATLAB script therefore indicate a necessary rotation of 7.81° anticlockwise of the nodes displacements from Midas and of 37.66 ° anticlockwise of topographic targets measurements, considering also that the right and left directions are opposite between the model and the monitored data.

In the analysis of the results of the mechanical calibration, the rotation matrix plays a fundamental role, which allows to rotate a vector or a set of points in a space while maintaining their length and relative shape unchanged. In particular, a rotation matrix with the appropriate angles was applied to all the displacements resulting from Midas and to those monitored. The following formula represents the rotation matrix, where the angle

theta represents the desired rotation angle, while *x* and *y* are the coordinates of the points to which the rotation will be applied.

$$R = \begin{bmatrix} cos\theta & -sin\theta \\ sin\theta & cos\theta \end{bmatrix}$$

4.7.2. Displacements of topographic targets

Once the displacements are rotated, it is necessary to identify the undeformed condition of the dam. This is challenging due to the huge availability of data and the unknown initial configuration of the dam at the time the targets were installed. The central targets M3, M4 and M5 were chosen to study the undeformed condition because they are more subjected to displacements, being further from the terrain constraints, even if also the other targets were used to optimize the model calibration.

The choice of analysis period is based on the evaluation of the time averages, in particular the configuration of 05/27/2021 at 5:00 was chosen as the undeformed condition, assuming this as day 0 of the analysis. The data considered for the mechanical calibration, including thermal loads, were averaged daily for the duration of two months until 07/26/2021 at 5:00 in order to streamline the computation burden.
Figure 4.7.2.1 and Figure 4.7.2.2 show the displacements of the targets at 505 *m a.s.l.* and 440 *m a.s.l.* along the *x* direction; as can be seen, there is a symmetry in the displacements to the right and to the left, while the central target such as the M4 have zero mean displacement being in correspondence of a symmetry axis.

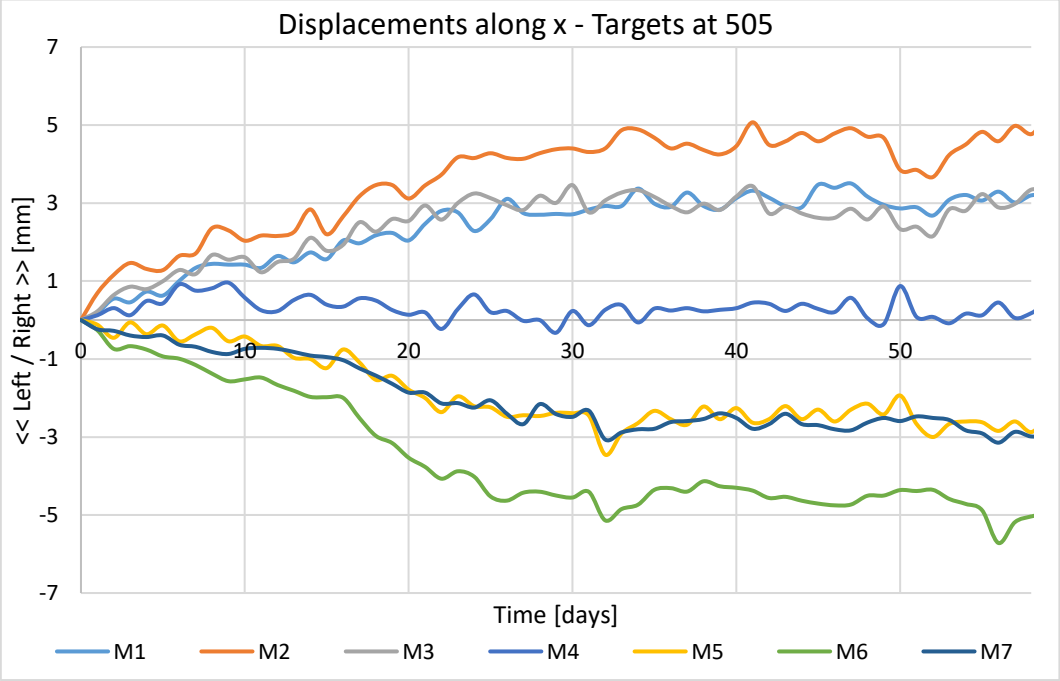

Figure 4.7.2.1: Displacements of targets along x direction at 505 m a.sl.

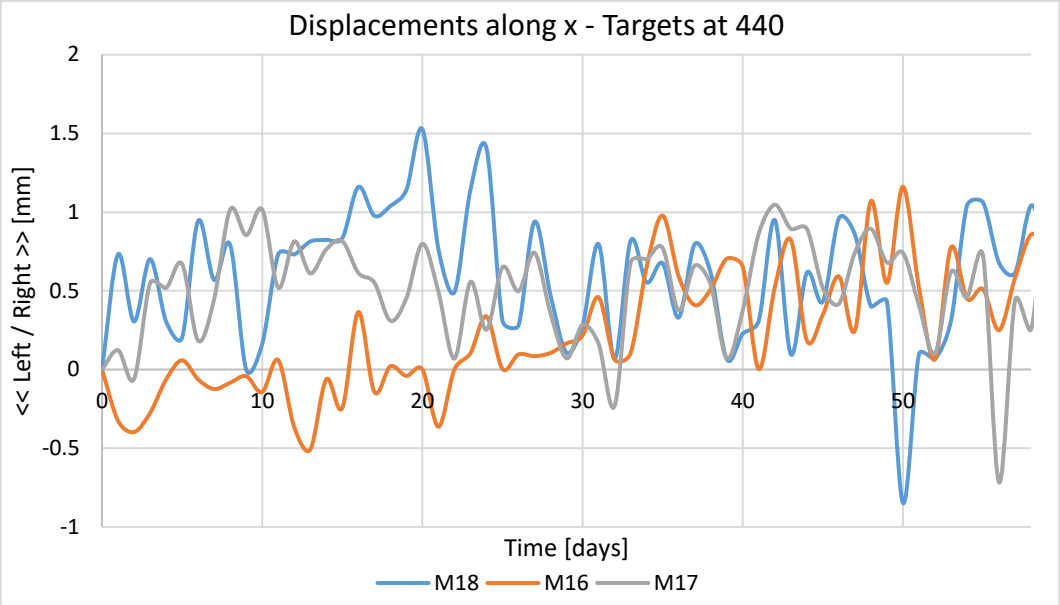

Figure 4.7.2.2: Displacements of targets along x direction at 440 m a.sl.

Figure 4.7.2.3 and Figure 4.7.2.4 show the displacements of targets at 505 *m a.s.l.* and 440 *m a.s.l.* along the *y* direction, as can be seen the targets closer to the terrain are those less deformed, while the central targets such as M3, M4 and M5 are those with the more pronounced displacements.

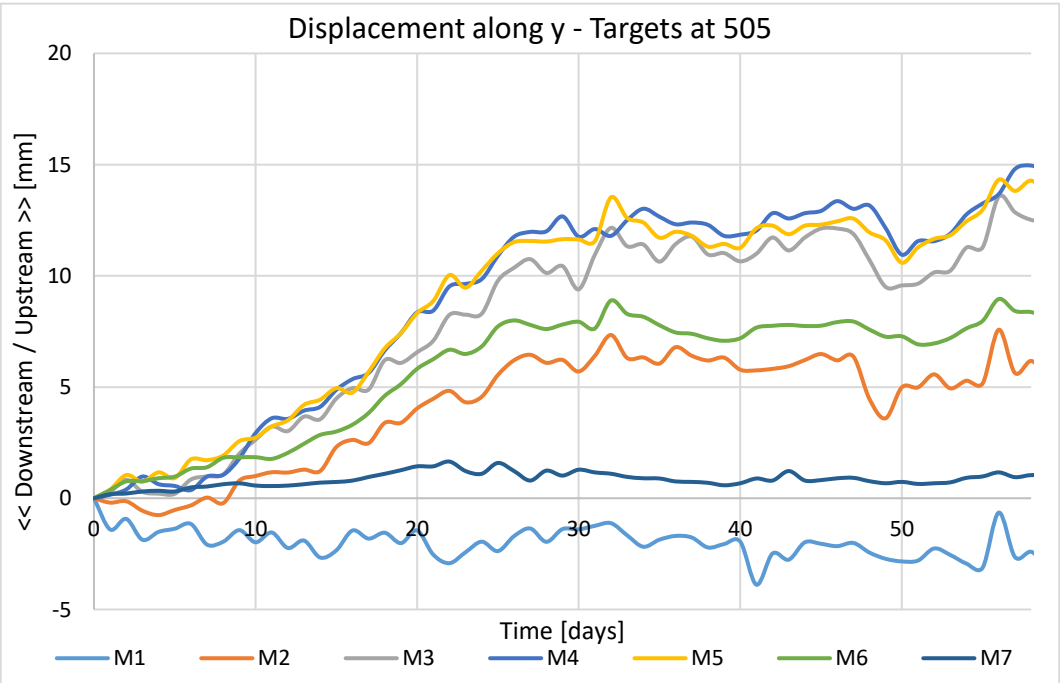

Figure 4.7.2.3: Displacements of targets along y direction at 505 m a.s.l.

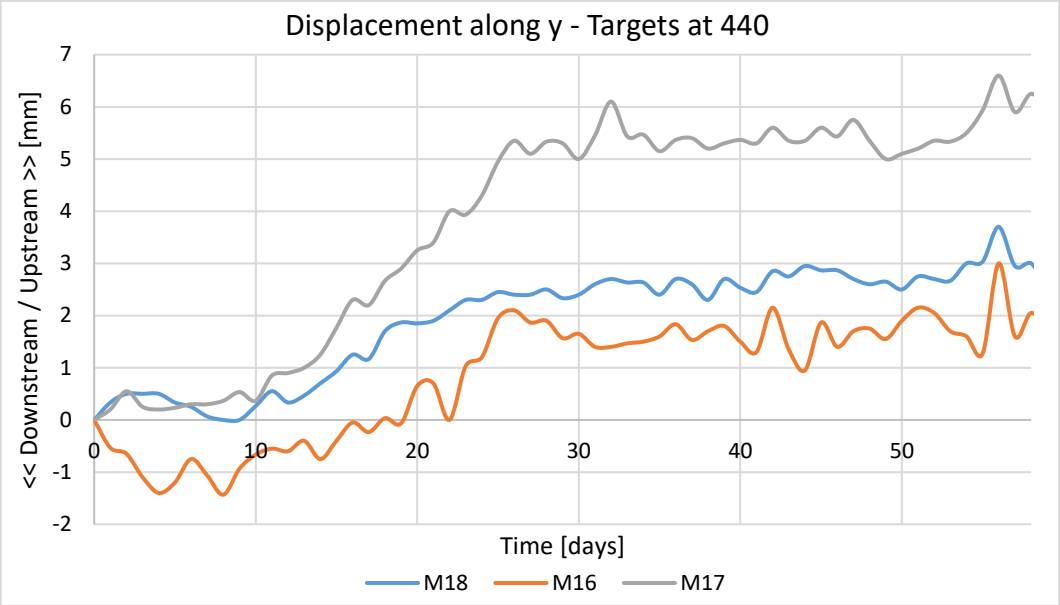

Figure 4.7.2.4: Displacements of targets along y direction at 440 m a.s.l.

4.7.3. Water Level Modelling

The water level implemented in the mechanical calibration of the model is based on the average level in the two months of analysis and equal to approximately 464 *m a.s.l.*. The construction of the water table in Midas is initially based on the assignment of the elevation to a surface, the first step consists of creating a rectangular surface with the same dimensions as the domain at an altitude of 464 *m a.s.l.* and through the *Divide – Surface* tool, obtain the surface representing the water table level, delimited by the upstream terrain and the dam body. Once this is done, a *Surface Function* is created through the *Water Table* tool by selecting the faces of interest, in particular the water table is assigned equal to the extension and positioning of the surface obtained previously.

The second step consists in the application of the hydrostatic pressure exerted by the water as function of the water level in the basin, to do this the *Water Pressure* tool is applied to all the *3D Element Faces*, differentiating those of the soil and those of the dam. This allows us to define all the faces that are potentially affected by hydrostatic pressure as a function of the previously imposed water table. In Figure 4.7.3.1 is shown the application of this last tool.

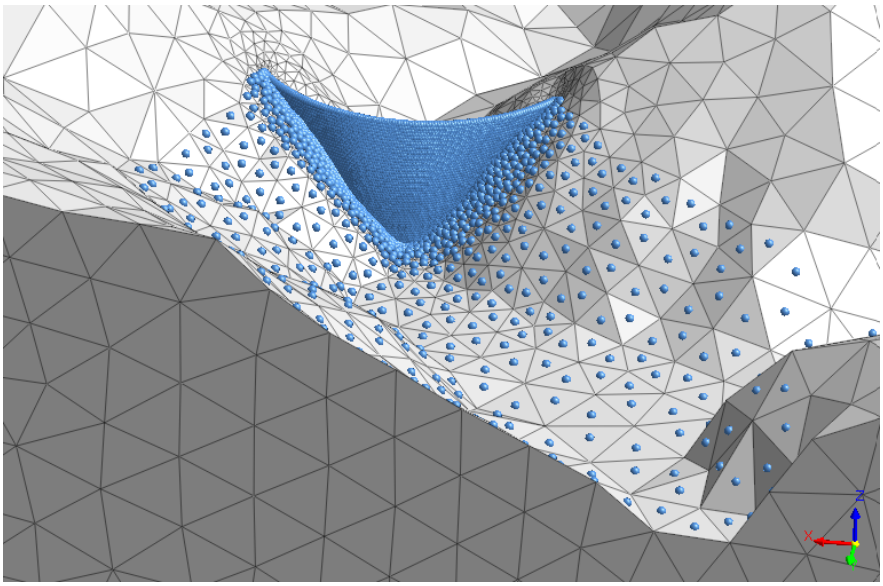

Figure 4.7.3.1: Water pressure tool application

The creation of the surface function is fundamental in the definition of the stage sets of the analysis and has to be imposed where the water level is required. The variation in water level causes a change in the nodes and faces affected by initial temperature and convection, which must be changed manually depending on the water table level considered.

4.7.4. Mechanical Calibration Tests

Before explaining the most significant calibration cases, it is important to clarify that: in almost all the cases analyzed, the trends of the displacements along *y* of the central targets are similar but obviously different in order of magnitude.

The targets M1 and M7 placed at the ends of the dam crown and closer to the terrain show in some cases displacements along *y* different from those monitored. Some differences may also be present in the displacements along *x*, although most show a similar trend.

In all the analyzed tests, the displacements in *x* direction at the elevation of 440 *m a.s.l.* of the nodes corresponding to M16, M17 and M18 have shown displacements comparable to the monitored one, even if of one order of magnitude lower, resulting more constrained than the targets of the dam. The results are considered acceptable, considering that the primary critical issues are mainly localized in the crown of the dam, where the thickness is reduced.

To make the results easier to read, only the most significant considerations and graphs are shown, but all results remain available.

The Literature Test is based on values of the thermal expansion coefficients of the concrete and of the soil of the same order of magnitude of those of literature ("Thermal and structural analysis of RCC double-curvature arch dam" – *Journal of civil engineering and management,* 2014, vol.3, pag. 440, Tab. 2).

$$\alpha_{concrete} = 1 \cdot 10^{-5} \frac{1}{T} \qquad \alpha_{soil} = 1.4 \cdot 10^{-6} \frac{1}{T}$$

The displacements both in *x* direction and in *y* direction are bigger than those monitored. Comparing the results of this test with those of the following tests, it is possible to affirm that the responsible of the differences is mainly the concrete coefficient, in fact is very high respect to the ones used in other tests and permit the development of too big

displacements. The values of the parameters do not satisfy the mechanical calibration, but are useful as a starting point for the following tests.

Test 1 is set to reduce the sensitivity of concrete to the temperature, reducing the coefficient of thermal expansion of about one order of magnitude. Physically, this means that nodes positioned in correspondence of central targets have lower displacements compared to those of the Literature test. Results shows displacements of nodes corresponding to targets M1, M2, M6 and M7 in the *x* direction, consistent as behavior with those monitored by the total station, specifying that due to the non-perfect alignment of *y* axis between the two reference systems (model and total station), the displacements along the *x*-axis could be slightly different from those monitored, mostly for the central targets.

$$\alpha_{concrete} = 6.5 \cdot 10^{-6} \frac{1}{T} \qquad \alpha_{soil} = 1 \cdot 10^{-6} \frac{1}{T}$$

In general, in the *y* direction all the monitored nodes show the same behavior of the monitored displacements showing some little difference in the order of 3-4 *mm*.

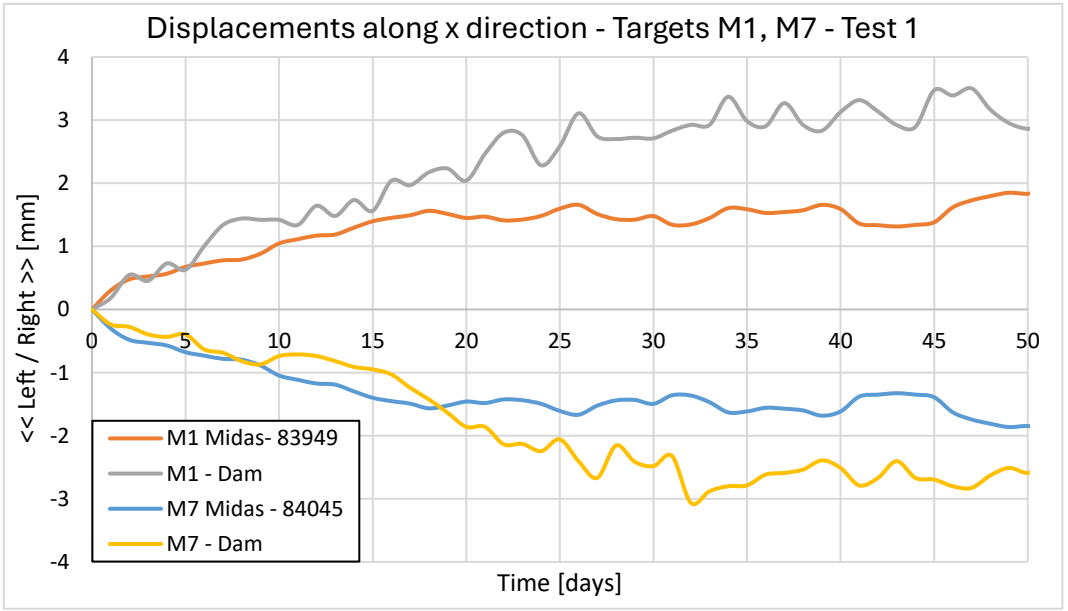

Figure 4.7.4.1: Displacements comparison of M1 and M7 along x – Test 1

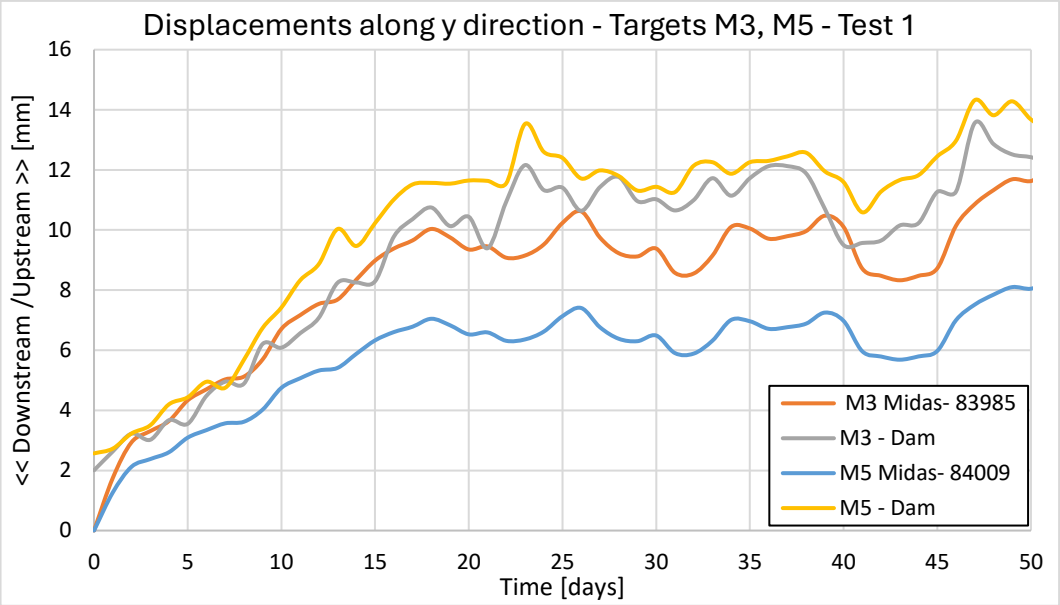

Figure 4.7.4.2: Displacements comparison of M3 and M5 along y – Test 1

Test 1 is fundamental to understand how modify in the best way the next tests, which will not be characterized by significant variations of thermal expansion coefficients, but by small adjustments until reaching the optimal result.

In Test 2 is set a small increase of thermal expansion coefficients, both of the concrete and of the soil. These variations, however, don't cause the development of significant displacements compared to the previous test.

Test 3 shows the development of too accentuated displacements in the nodes corresponding to the central targets, less constrained being far from the terrain. The results are probably due to a too high concrete thermal expansion coefficient.

Test 4 is characterized by a couple of thermal expansion coefficients that gives the best results, the displacements in the *y* direction of nodes corresponding to the central monitored targets are very similar to the ones monitored. There are differences mainly in the nodes corresponding to the M1 and M7 targets that, being positioned closer to the terrain, are more affected by the constraint's conditions, which limits their displacements even when the thermal expansion coefficient of the soil varies.

The displacements of nodes positioned at the elevation of 440 *m a.s.l.* are lower than those monitored, this is probably due to a more influencing constraint related to the thickness of the dam at that elevation. In particular, the nodes corresponding to the M16 and M18 targets, positioned at the extremities of the dam, are closer to the terrain and they feel more the constraint of it. The node relative to the M17 target instead, being positioned in the center of the dam develops bigger displacements, but still 2-3 *mm* lower than those monitored.

$$\alpha_{concrete} = 8 \cdot 10^{-6} \frac{1}{T} \qquad \alpha_{soil} = 2.2 \cdot 10^{-6} \frac{1}{T}$$

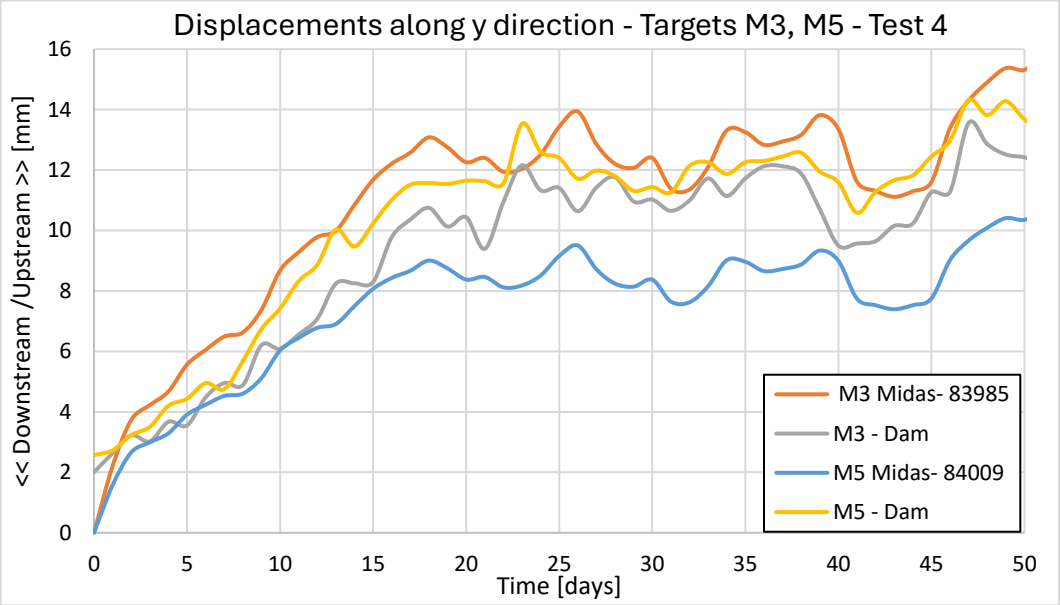

Figure 4.7.4.3: Displacements comparison of M3 and M5 along y – Test 4

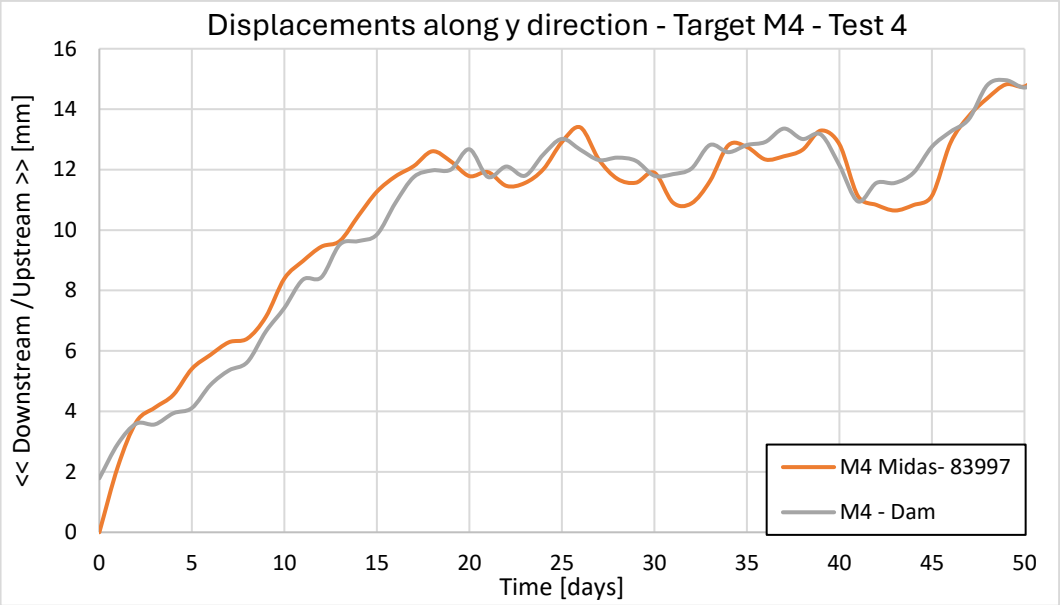

Figure 4.7.4.4: Displacements comparison of M4 along y – Test 4

In the end, Test 5 is set reducing only the thermal expansion coefficient of the concrete, getting as expected, lower displacements of nodes corresponding both to the central and lateral targets.

The comparison between the results of different cases allows us to understand the behavior of the development of displacements and the thermal expansion coefficient dependance.

In order to evaluate the best couple of values that allows to better fit the modeled data to the monitored data, the RMSE of displacements along the *y* direction has been calculated for all the analyzed targets of each tests, as shown in Table 4.7.4.1 .

RMSE *[mm]*	M1	M2	M3	M4	M5	M6	M7	M16	M17	M18	Mean RMSE
Test 1	4.1950	1.1721	1.4291	2.7407	4.7766	4.3593	0.3292	1.1165	2.7716	2.3217	2.5212
Test 2	4.3984	1.6047	1.0260	2.0429	4.2721	4.1675	0.3319	1.0746	2.5923	2.3154	2.3826
Test 3	5.2464	3.6996	3.0507	1.3589	2.2755	3.4684	0.4462	0.9107	1.8793	2.2963	2.4632
Test 4	5.0264	2.9497	1.9783	0.7525	3.0885	3.7930	0.4192	0.9216	2.1202	2.2901	2.3340
Test 5	4.1225	0.9523	1.8130	3.2285	5.1658	4.5280	0.3363	1.1117	2.8727	2.3146	2.6445

Table 4.7.4.1: RMSE comparison of targets along the y direction in mm

The data highlighted in Table 4.7.4.1 represent the optimal RMSE values for each target. Although the Test 4 is not the one with the lower RMSE combination with respect to the other tests, it is the one that maintains an equilibrate performance for all the topographic targets, avoiding the development of excessive RMSE values. In Test 4, the values relative to M5 and M6 are lower than the values of Test 3 and 5, characterized by higher values. The choice of Test 4 is further justified by the position of the target M4 in the center of the dam crown, that results fundamental to study the displacements in the most critical point of the structure, as it is identified as the point with the maximum displacements in *y* direction also by the monitored data. It shows a minimum RMSE for M4 target with respect to other tests, highlighting that while the optimal RMSE combination is not relevant to the Test 4, it does allow for optimal reproduction of the maximum displacements without overly influencing the accuracy of the results of the other targets. This last consideration is reinforced by the calculation of the mean RMSE for each test, which results in a minimum for Test 4.

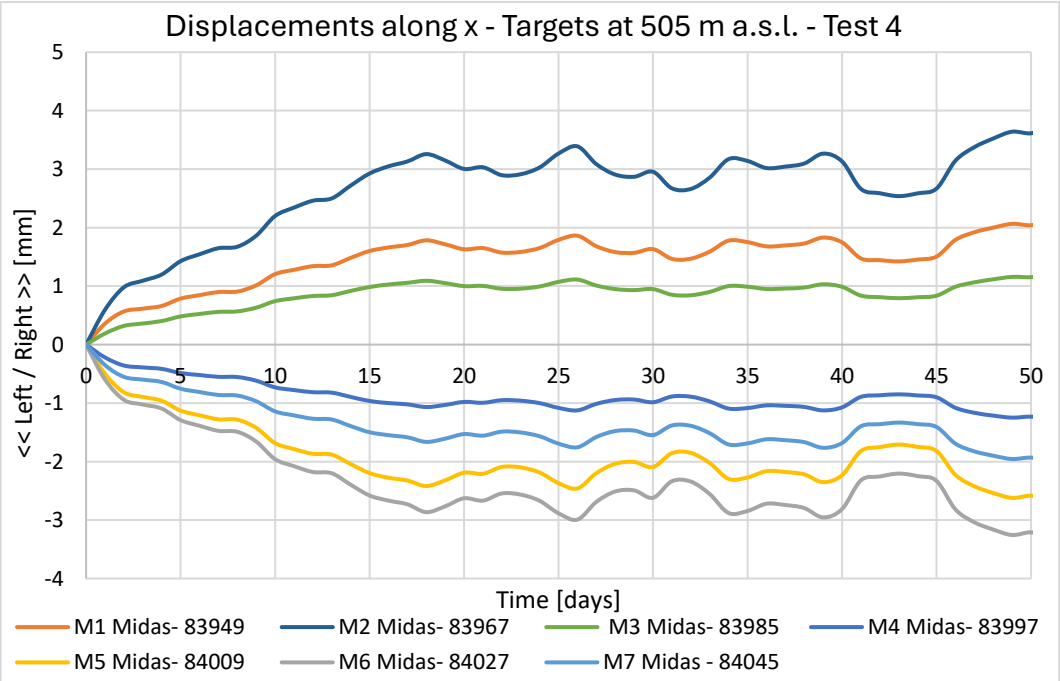

Figure 4.7.4.5: Displacements along x – Targets at 505 m a.s.l. – Test 4

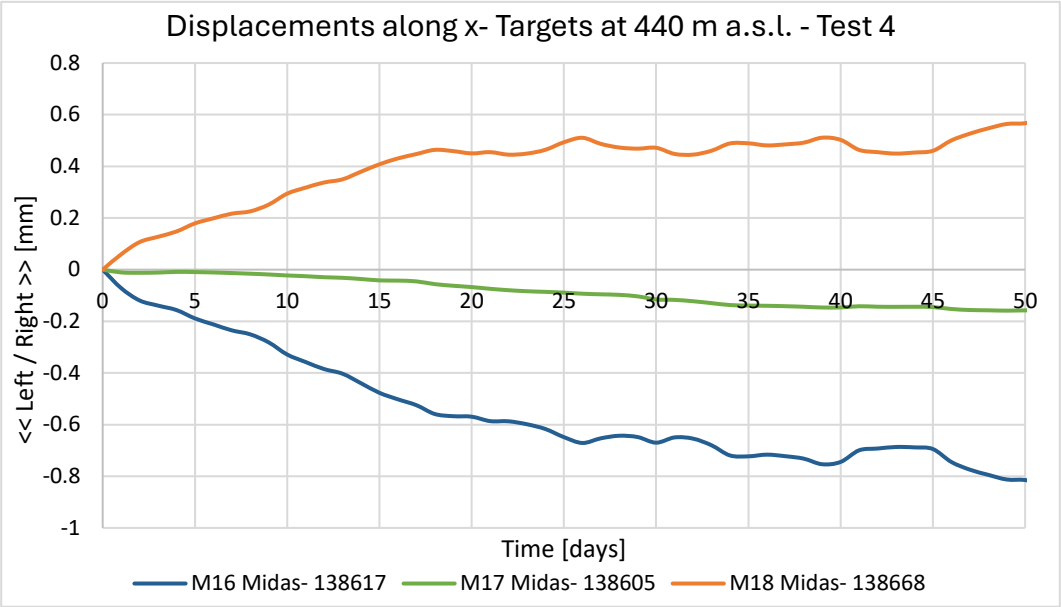

Figure 4.7.4.6: Displacements along x – Targets at 440 m a.s.l. – Test 4

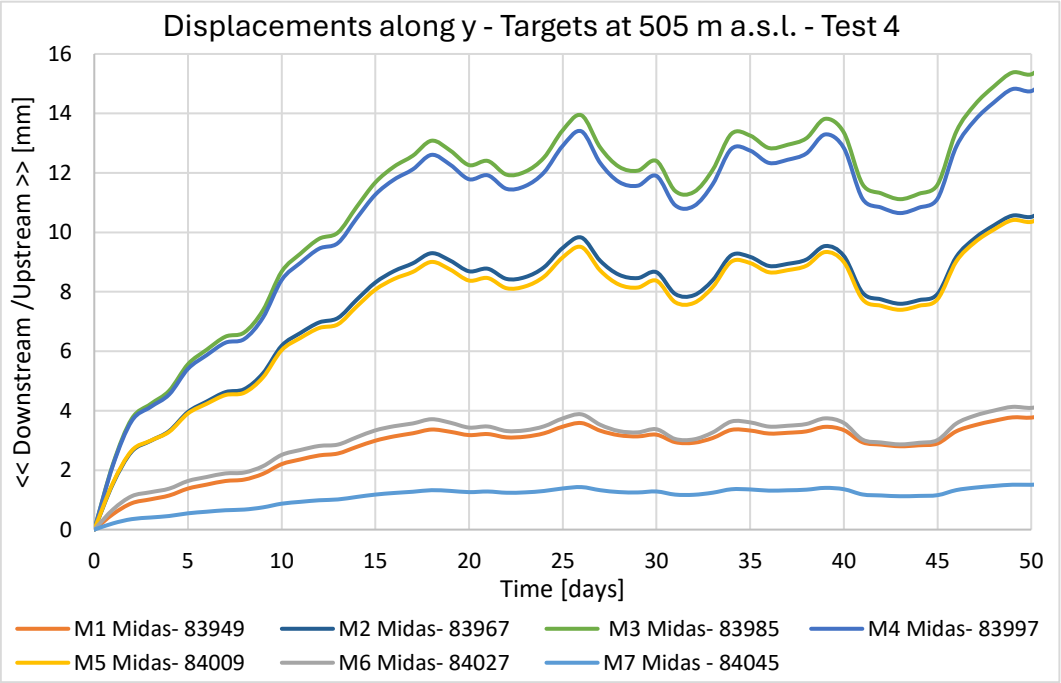

Figure 4.7.4.7: Displacements along y – Targets at 505 m a.s.l. – Test 4

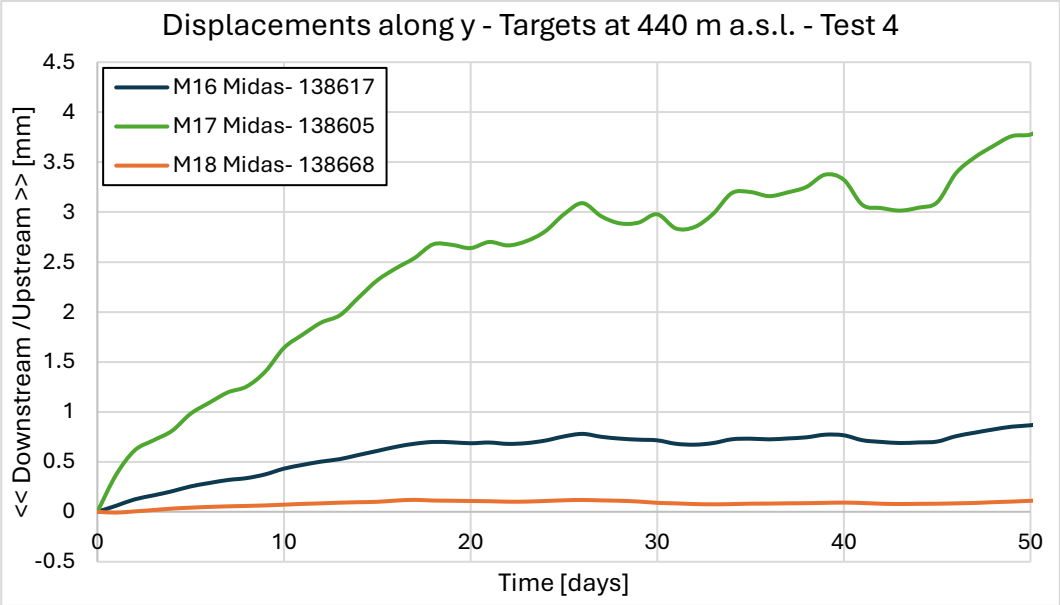

Figure 4.7.4.8: Displacements along y – Targets at 440 m a.s.l. – Test 4

In Table 4.7.4.2 the significant results of the model calibrated in the period of analysis of mechanical calibration are summarized.

Maximum Temperature *[°C]*	25.95	Node 148905
Minimum Temperature *[°C]*	10.70	Node 160106
Maximum Displacement – y *[mm]*	16.18	Node 84128

Table 4.7.4.2: Maximum temperature and displacement values in Test 4

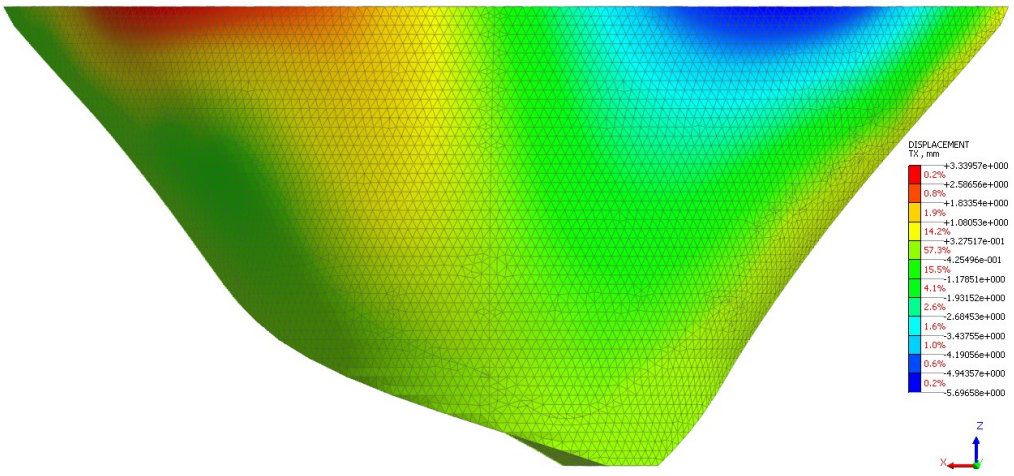

Figure 4.7.4.9: Maximum displacements along x – Upstream face – Test 4

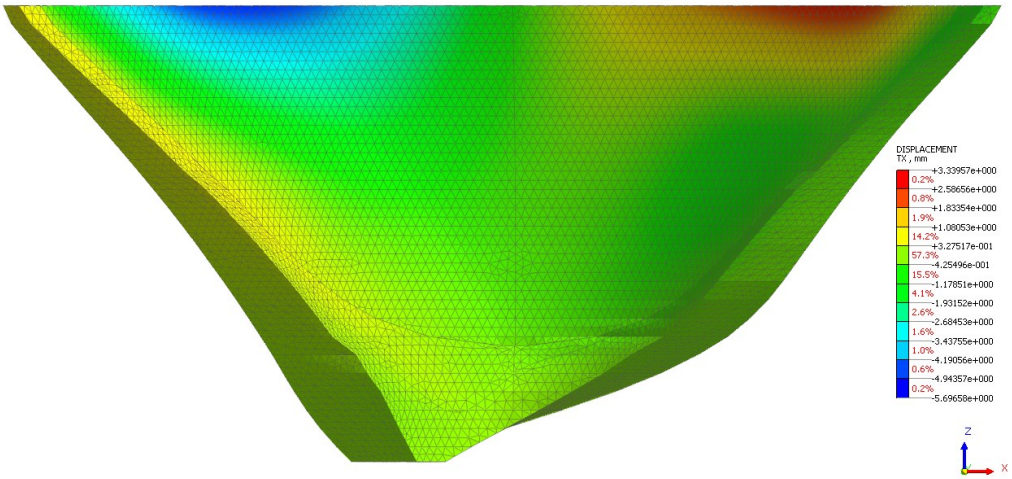

Figure 4.7.4.10: Maximum displacements along x – Downstream face – Test 4

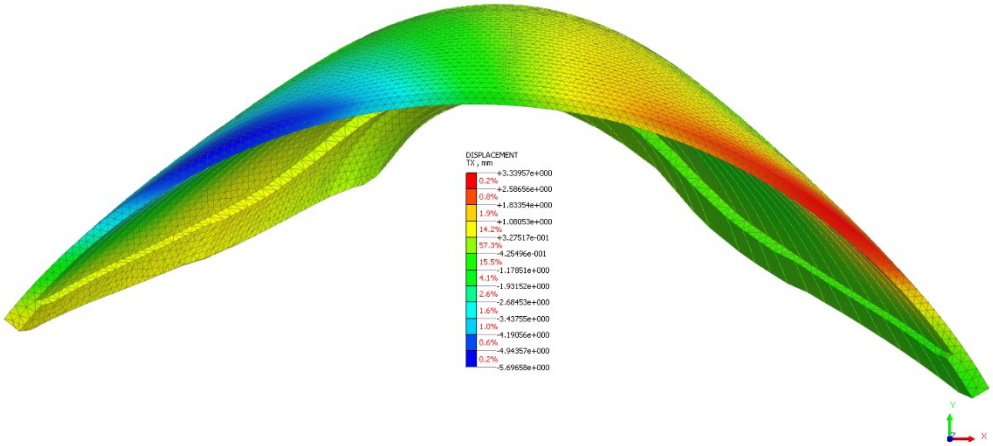

Figure 4.7.4.11: Maximum displacements along x – Top view – Test 4

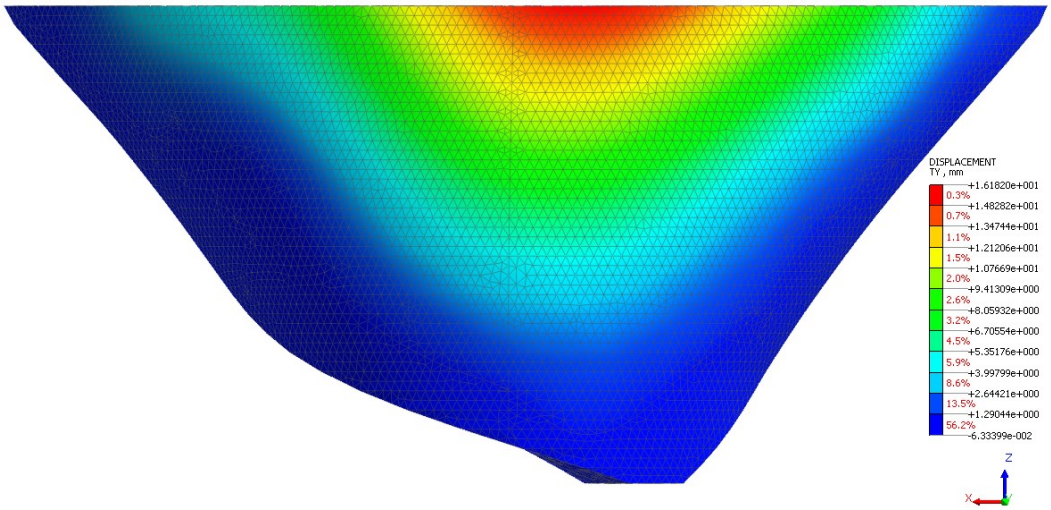

Figure 4.7.4.12: Maximum displacements along y – Upstream face – Test 4

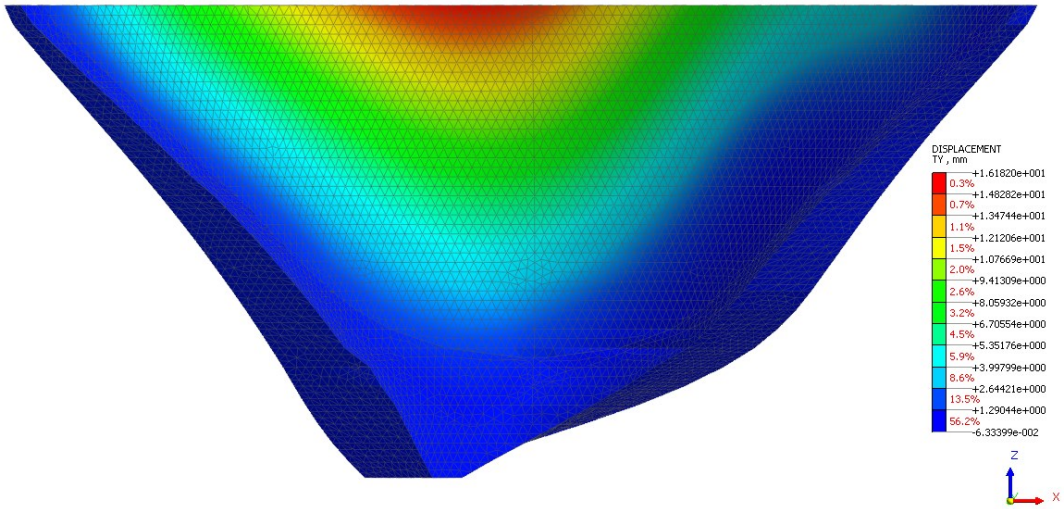

Figure 4.7.4.13: Maximum displacements along y – Downstream face – Test 4

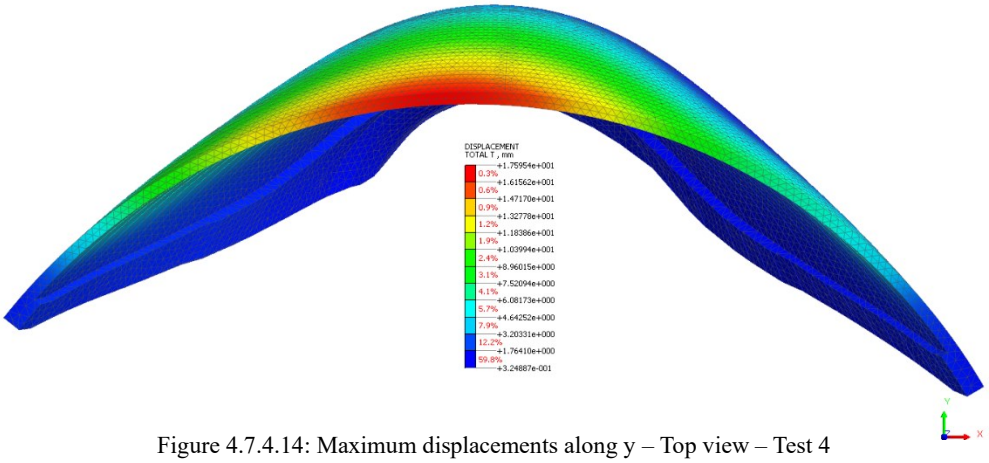

Figure 4.7.4.14: Maximum displacements along y – Top view – Test 4

The results shown above highlight how the model displacements are slightly asymmetric with respect to the dam body. From monitored data results a null average displacement in *x* direction of target M4, while the model develops displacements in the relative node of about 1 *mm*. The differences between data can be due to the positioning of the contact point between the terrain and the dam body that being asymmetric doesn't produce the same constraint effects on the structure. Differences can derive from the use of a too coarse DTM resolution, giving a certain degree of uncertainties starting from the input data of the model, from the positioning of topographic targets or from the rotation matrix applied to compare the displacements. Another source of uncertainty is the lack of information about the real position of the thermometers immersed in the concrete and the

availability of data being provided data from only 2 thermometers out of 18 installed. Surely the use of a static water level equal to the mean water level in the analysis period doesn't allow to develop the same variability of displacements as in reality.

The model analyzed in Test 4, however, considering these potential source of error, responds correctly to the applied thermal and piezometric stresses, providing displacement results consistent with those monitored, both in terms of direction and order of magnitude.

5. Critical Case analysis

Once the model has been calibrated both thermally and mechanically, we can state, with a certain degree of accuracy, that it responses correctly to the heat transfer and to the development of displacements induced by the water level and temperature fluctuations.

The application of the model to critical cases is fundamental because it allows us to understand if the calibration is valid only for average conditions or if it is valid also in stress conditions, producing consistent results.

The critical case studied, replicates the critical conditions of 2004 event for which increases in piezometric pressure were observed. The water table in that event reached 500.04 *m a.s.l.*, for this reason the water table level in the model is set to 500 *m a.s.l.* .
The analysis is carried out over an annual time period, with the day 0 of the analysis equal to the day 0 of the mechanical calibration analysis, being defined as the day representing the undeformed condition of the dam. The analysis period goes from 27/05/2021 to 26/05/2022, processing displacements and temperature data with averages every three days in order to streamline the computational burden.

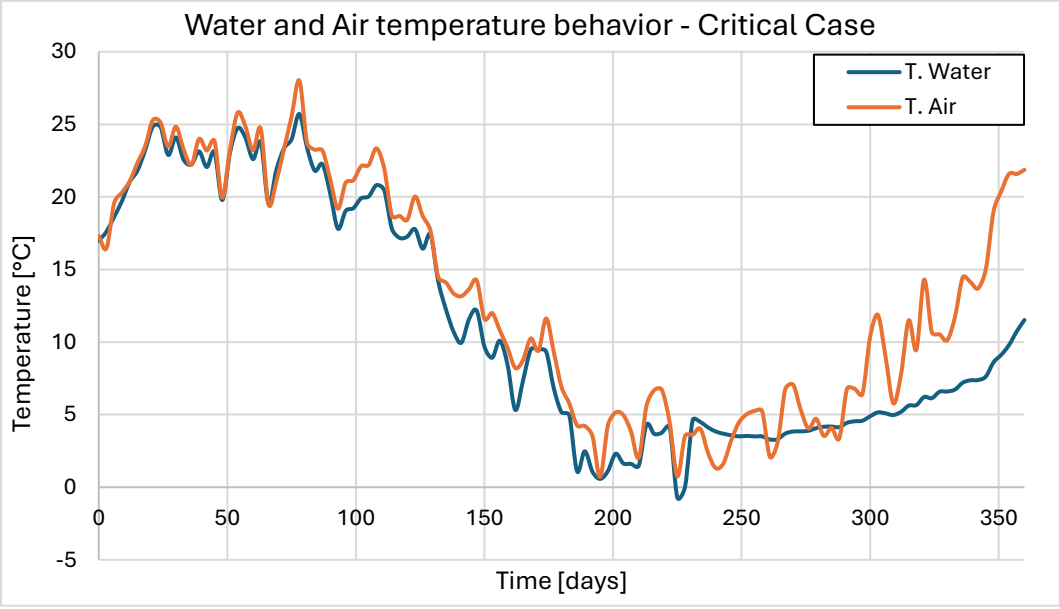

Figure 5.1: Water and air temperature behavior during the analysis period

In Figure 5.1, are shown the behaviors of temperature functions applied through *Convection* to the model, lasting 1 year and averaging every 3 days. It's possible to observe a cyclic trend of temperatures, that allows us to observe the consequences on the model induced by both cooling and heating phases.

Characteristics and properties of materials used in the model are summarized in the following Table 5.1, using mechanical and thermal parameters those defined through calibrations.

	Concrete	Soil
Elastic Modulus *[kN/m^2]*	$3 \cdot 10^7$	$4.4 \cdot 10^7$
Poisson's Ratio *[-]*	0.2	0.3
Unit Weight *[kN/m^3]*	25.8	27.6
Thermal Coefficient *[1/T]*	$8 \cdot 10^{-6}$	$2.2 \cdot 10^{-6}$
Conductivity *[W/(m · (T)]*	1.6	1.62
Specific Heat *[J/(ton · [T])]*	1080000	800000
Cohesion *[kN/m^2]*	-	600
Friction Angle *[°]*	-	40

Table 5.1 : Material parameters in critical model

In the following part, the results of critical case will be analyzed, considering the necessity to individuate the nodes that contribute in the best way to understand the displacements of the dam.

Displacements along *y* direction are studied, taking into account the node with the maximum positive displacement, identified with the ID 84128 and positioned slightly to the left of the center of the upstream side crown. Also, the node with the maximum absolute displacement is considered, represented by the ID 84127 and positioned close to the previous node. Due to the proximity of the two nodes the displacements produced are almost the same. In order to connect the critical case to reality, also the displacements in *y* direction of target M4 are studied.

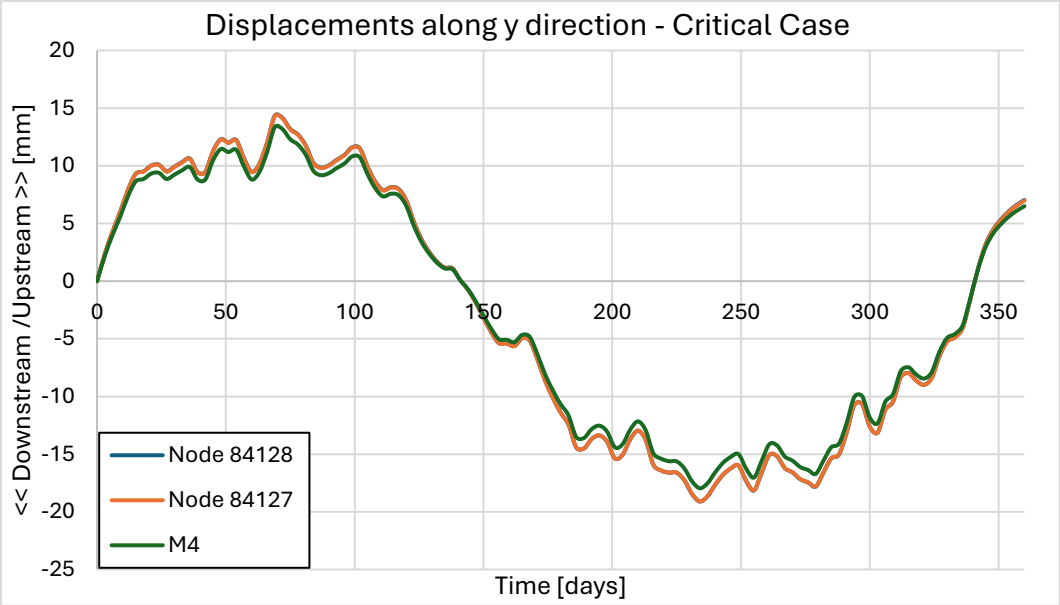

Figure 5.2: Displacements along y direction – Critical Case

In order to study the displacements in *x* direction, two nodes showing the maximum displacements are identified: one to the left side with ID 84154 and one on the right side with ID 84085 as compared to the center of the dam crown on the downstream side.

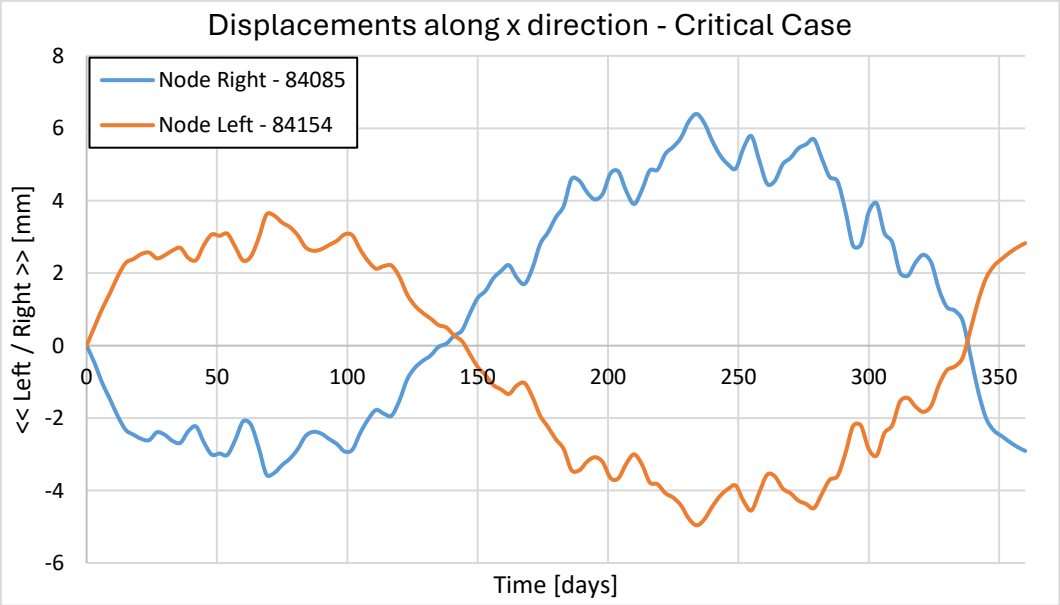

Figure 5.3: Displacements along x direction – Critical Case

The graph shows the maximum displacements trend to the right and left of the studied nodes. It is possible to observe how in the autumn period there is an inversion of the displacements from the right to the left and vice versa. The behavior suggests that the

model responds correctly to seasonal temperature variations following a cyclical trend and highlighting greater displacements in absolute terms in winter period, as found in the study of the displacements in the *y* direction.

In the following Table 5.2 are summarized all the critical conditions of the model in terms of displacements and temperatures.

	Value	Time *[day]*	Node ID
Max. Temperature *[°C]*	26.98	66	84056
Min. Temperature *[°C]*	-0.22	216	133988
Max. Y + upstream displacement *[mm]*	14.351	69	84128
Max. Y - downstream displacement *[mm]*	-19.087	234	84127
Max. X + right displacement *[mm]*	6.397	234	84085
Max. X - left displacement *[mm]*	-4.960	234	84154

Table 5.2 : Critical condition values

Looking at the outcomes, the displacement in the upstream direction results lower than the mechanical calibration case in the same analysis period May – July, due to the rise of the water level that acts in the opposite direction respect to the node displacement induced by temperature functions. Results show how the rising of the water level in the reservoir contributes to the development of displacements along the *y* direction in the winter period, when they develop towards the downstream direction.
This observation helps explain the development of greater absolute displacements during the winter period compared to the summer period.

It can be stated that the critical condition at a maximum level of the reservoir occurs in the winter period, in which both thermal and hydrostatic loads contribute to the development of displacements towards downstream, reaching a maximum displacement defined by the model, equal to approximately 19 *mm* in the *y* direction.

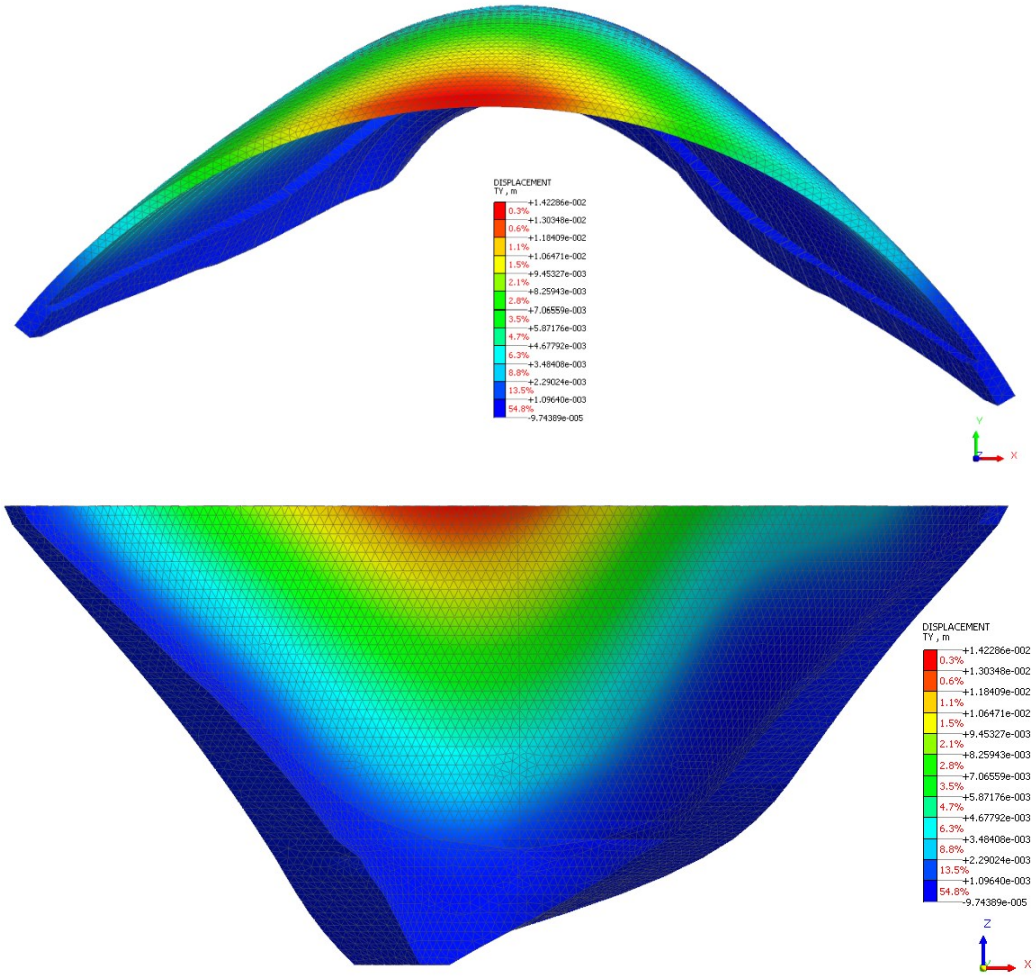

Figure 5.4: Displacements in y direction on day 69, summer period

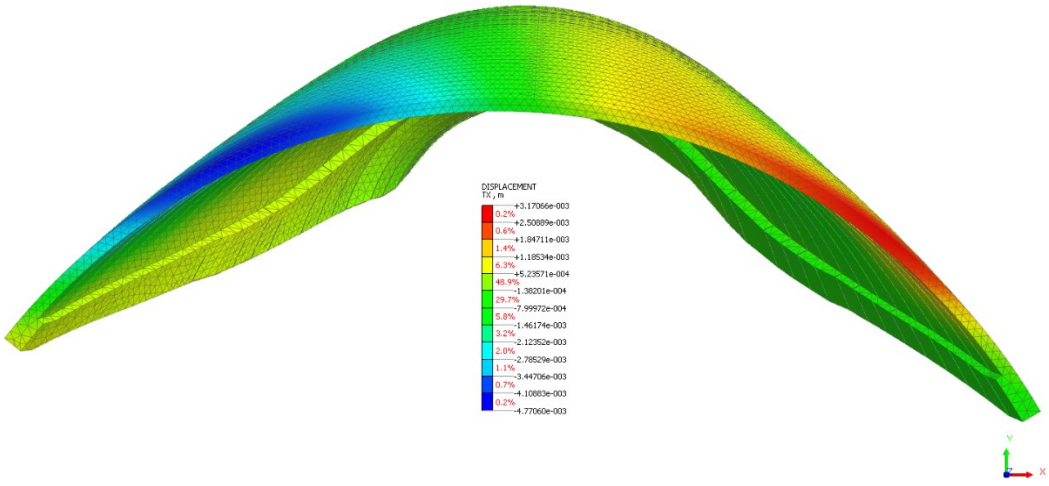

Figure 5.5: Displacements in x direction on day 69, summer period

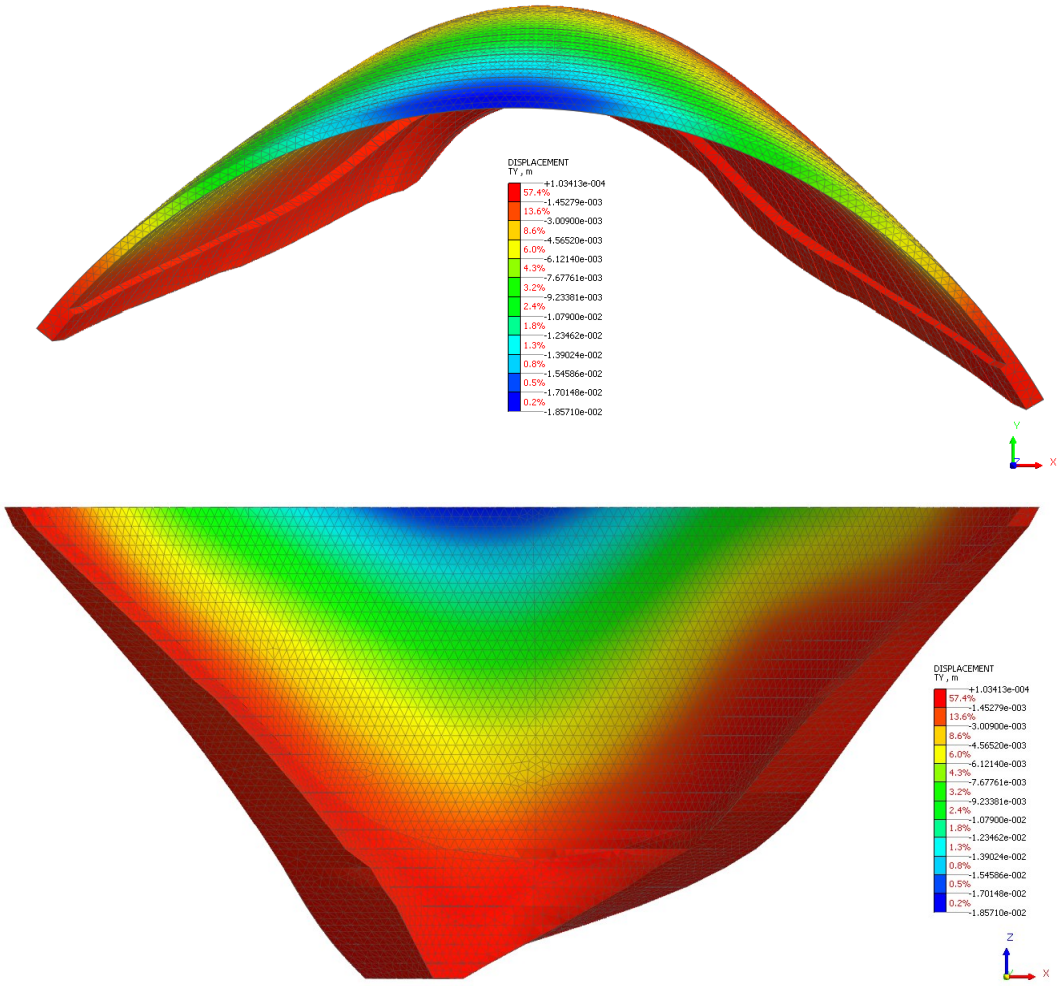

Figure 5.6: Displacements in y direction on day 234, winter period

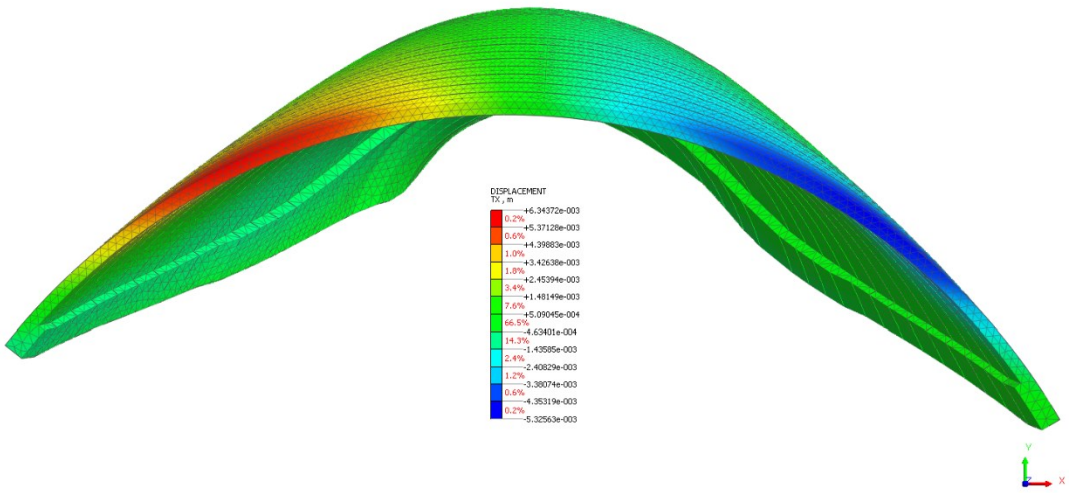

Figure 5.7: Displacements in x direction on day 234, winter period

In the end, the results of displacements of the critical case and the maximum displacements values of topographic targets are compared, considering the same period of analysis. The monitored data has been processed in order to individuate and delete the outliers that would have disturbed the determination of critical events. Once did it, all the data have been averaged with the same time scale used in the critical case, permitting to individuate the maximum displacements, in absolute terms, in the summer and winter months, defining the average water level in the reservoir in that period. As can be noted from the graph, there are discontinuities in the monitored displacements due to the unavailability of data from October 2021 to November 12, 2021, this doesn't affect the final considerations as it is a transition period between the summer and winter configuration subject to limited displacements.

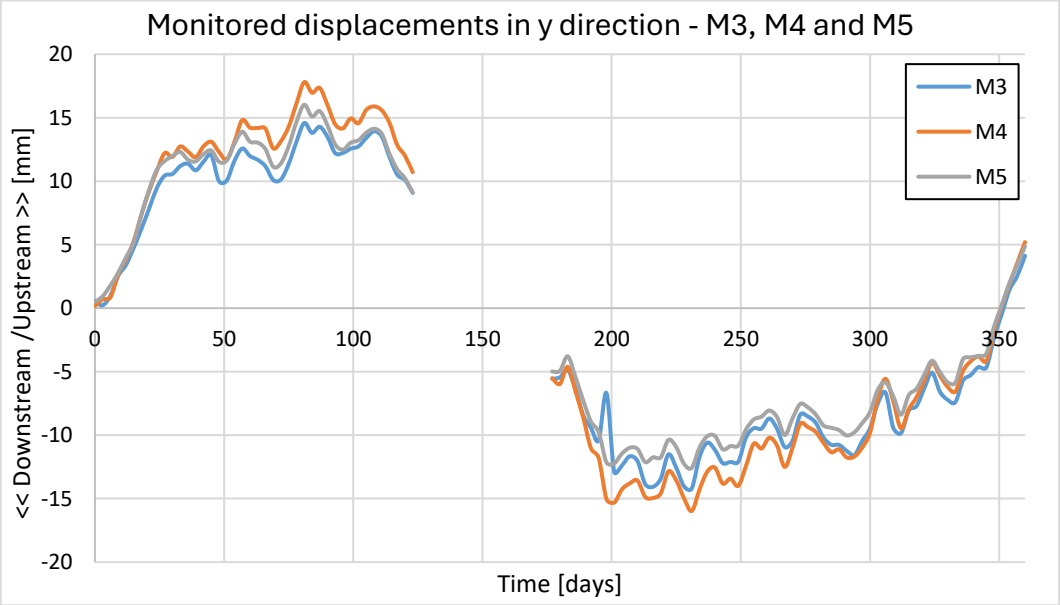

Figure 5.8: Monitored displacements in y direction, M3, M4 and M5 targets

	Maximum Abs. Displacements in y - M4 *[mm]*	Time Period	Water level *[m a.s.l.]*
Monitored - Upstream	17.802	16 Aug. 2021 – 18 Aug. 2021	466.82
Monitored - Downstream	15.976	10 Jan. 2022 – 12 Jan. 2022	463.13
Critical Model - Upstream	14.351	12 Aug. 21	500.00
Critical Model - Downstream	19.087	16 Jan. 22	500.00

Table 5.3 : Maximum absolute displacements in y directions

The maximum displacements in downstream and upstream direction are equal respectively to 15.976 *mm* and 17.802 *mm*, with a water level in the reservoir of 463.12 *m a.s.l.* and of 466.82 *m a.s.l.*. The temperatures applied to the model derive from air, water and concrete sensors, which allowed the application of real temperatures to the model, furthermore, through thermal calibration it was possible to make the model as similar as possible to reality in terms of temperature. Assuming that the imposed temperatures to the model in the critical case, are the same of the reality, it is possible to define the contribution given by the water level in the different period of the year.

The maximum displacements in upstream direction develop in the summer period, in which the mean temperature of water and air assume high values. The displacements recorded in the summer period are greater by 3.451 *mm* compared to those of critical case due to the maintenance of the water level in the reservoir at a level lower than 34 *m* compared to the critical case. In fact, with summer temperatures, the pressure load relative to the water level gives a contribution opposite to the thermal one, and at the same temperature, the displacements toward the upstream decreases as the water table increases.

The maximum displacements in downstream direction instead, develop during the winter period in which temperatures reach minimum recorded values and produce a contraction of the dam body compared to the undeformed condition. As can be seen from the difference in maximum displacements in the downstream direction, the development of them is directly proportional to the rise of the water level in the reservoir. The water level in the period of maximum displacement in downstream direction is equal to 463.13 *m a.s.l.*, with a relative displacement of 3.111 *mm* less than the critical case, characterized by a water level of 500 *m a.s.l.*.

6. Conclusions

The study of the preliminary models, in addition to understanding the correct application of the loads, allows to study temperature variability as a function of the average period. The results of the studied models identify a reduction in variability as the time scale used increases. The use of daily averaged data is justified by the need to limit computational demand, considering that the thermal conductivity of the concrete influences heat transfer throughout the material. This implies that using daily averaged data, the model does not lose accuracy since the concrete is hardly affected by limited thermal variations in a very small-time scale.

Thermal calibration allowed us to understand how to correctly set the temperature inside the model, obtaining an optimal calibration for the nodes located at the highest elevations where the thickness of the dam is reduced. The nodes located at lower elevations are affected by the thickening of the dam body, which influences the heat transfer, leading to a less accurate calibration but overall acceptable, as orders of magnitude. Differences are due to simplifications of the system, considering the lack of temperature data that would have allowed a greater understanding of temperature behavior in the real dam body.

The mechanical calibration allowed to verify the presence of symmetry in the displacements of nodes in the x direction, identifying as source of asymmetry for the central node corresponding to the M4 target, both the positioning of the reference system with respect to the monitored data, and a different configuration of the constraints due to the dam-soil union. Considering the distance between topographic targets, it cannot be ruled out that also in the reality the central target doesn't match to the maximum displacement point of the dam, although it is noted that the movements of the targets adjacent to the central one are overestimated compared to those monitored. Overall, mechanical calibration allowed to define the thermal expansion coefficient values which produces displacements of an order of magnitude similar to those monitored, also using the RMSE as statistic instrument to evaluate the most accurate test.

The critical case, analyzed by maintaining the water level in the reservoir equal to 500 *m a.s.l.* for a period of one year, allowed the identification of the periods of potential criticality of the dam, in which the thermal and hydrostatic pressure effects add up in the development of the displacements. The model results faithfully reproduce the initially predicted behavior, identifying a different contribution of the water table level in the displacements of the dam as a function of the environmental temperatures.

The model could be improved from several points of view:

- the use of a DTM with a higher resolution would allow a more precise dam-terrain connection, avoiding an overestimation of the applied constraints and an asymmetrical development of the results;

- the development of a subroutine to be implemented in Midas environment, able to consider automatically a dynamic water level in the reservoir and consequents changes in elements involved in thermal load and water pressure;

- the improvement of the mechanical calibration of the model by implementing the monitored data from optical fibers positioned at 503 *m a.s.l.* in the model;

- carry out an additional series of analysis to define the stratigraphy not only downstream the dam, but also in correspondence of the foundations, in order to improve the model, recreating the real stratigraphy of the terrain, actually considered as uniform.

Bibliographic References

Abdulrazeg, A. A., Noorzaei, J., Jaafar, M. S., Khanehzaei, P., & Mohamed, T. A. (2014). Thermal and structural analysis of RCC double-curvature arch dam. *Journal of Civil Engineering and Management, 20*(3), 434–445.

C. Martone (2021/2022). Thesis with title “Calibration of thermo-mechanical parameters for a FEM-based analysis of the deformations induced in a double-arched concrete dam by changes ambient temperature and reservoir water level”.

Decreto-Legge 8 agosto 1994, n. 507, ripubblicato e coordinato con la Legge di conversione 21 ottobre 1994, n. 584. Misure urgenti in materia di dighe. Gazzetta Ufficiale, Serie Generale, n. 195, 22 agosto 1994; n. 247, 21 ottobre 1994; n. 255, 31 ottobre 1994.

Nilipour, N., & Cekerevac, C. (n.d.). *Some examples of Z_Soil application to dam engineering*. Stucky Ltd.

Ribacchi, R. (1975). *Caratteristiche meccaniche della roccia di fondazione della diga di Ponte Cola e comportamento dell'opera nel corso dell'invaso del 1974 p.c.* [PDF]. ENEL - SOIC, Compartimento di Milano.

Pan, J., Liu, W., Wang, J., Jin, F., & Chi, F. (2022). A novel reconstruction method of temperature field for thermomechanical stress analysis of arch dams. *Measurement, 188*, 110585.

Excel sheet: “Calibrazione_termica.xlsx”
“Calibrazione_meccanica.xlsx”
“Spostamenti_mire.xlsx”
“Stazionetot.xlsx”
“PCola_temp_invaso_2021-2022.xlsx”

PDF: “Anidel_Ponte_cola.pdf”

“rl1020.pdf”

Webography

Dighe.eu. (n.d.). Information on dams. Retrieved [30 July 2024], from https://www.dighe.eu/documentazione/informazioni.htm#

Midas. (n.d.). *Heat of hydration analysis*. Midas Structure Blog. Retrieved [10 September 2024], from https://www.midasstructure.com/blog/en/blog/heat-of-hydration-analysis